RESUMEN

La ingeniería civil viene usando los modelos digitales de elevaciones (DEMs) y las ortofotos como material básico para poder redactar y ejecutar cualquier proyecto de ingeniería, así como para controlar la geometría de las construcciones de forma periódica.

Dentro de los medios técnicos posibles para obtener este tipo de información, los vehículos aéreos no tripulados (*Unmanned Aerial Vehicles UAVs*) están imponiendo, cada vez más, su uso debido a la reducción de costes, la flexibilidad y la mejora en la resolución obtenida. Este éxito se ha debido, en parte, a la evolución de la fotogrametría digital y al uso de algoritmos especiales como el *Structure-from-Motion* (SfM).

Muchos son los autores que desde hace varios años vienen estudiando las aplicaciones de la fotogrametría UAV y la influencia que determinados parámetros tienen en la precisión de los productos resultantes.

Esta Tesis Doctoral ha pretendido profundizar en el estudio de aplicaciones fotogramétricas desde UAVs para situaciones de topografía extrema, como pueden ser los deslizamientos de taludes de desmonte en obras lineales, así como analizar la influencia que la altura de vuelo, la morfología del terreno y el número de puntos de apoyo *Ground Control Points* (GCPs) tienen en la precisión de DEMs y ortoimágenes obtenidas mediante fotogrametría UAV a través de software basado en el algoritmo SfM.

Los resultados obtenidos han demostrado que la fotogrametría UAV constituye una técnica útil y adecuada para proyectos de ingeniería relacionados con la reparación y gestión de deslizamientos de taludes en desmontes de carreteras. Asimismo, se ha constatado que la morfología del terreno y la altura de vuelo tienen poca influencia sobre la precisión planimétrica alcanzada, debido principalmente al bajo rango de altura de vuelo en el que suelen operar los UAVs (50-120 m). También se ha corroborado, igual que otros estudios, que la precisión altimétrica disminuye conforme aumenta la altura, aportando esta Tesis Doctoral que esa consecuencia es más notable conforme disminuye el número de GCPs. Por último, se ha arrojado luz sobre la influencia que el número de GCPs tiene en la precisión final de los productos obtenidos, concluyéndose que el uso de un número alto de puntos de apoyo (15-20) optimiza los resultados, tanto en planimetría como en altimetría, llegando a permitir, incluso para alturas de 120 m y según las normas del ASPRS, la creación de mapas cartográficos a escala 1:150.

UNIVERSIDAD DE ALMERÍA

PATRICIO JESÚS MARTÍNEZ CARRICONDO

TÉCNICAS FOTOGRAMÉTRICAS DESDE VEHÍCULOS AÉREOS NO TRIPULADOS APLICADAS A LA OBTENCIÓN DE PRODUCTOS CARTOGRÁFICOS PARA LA INGENIERÍA CIVIL

2016 | TESIS DOCTORAL

TÉCNICAS FOTOGRAMÉTRICAS DESDE VEHÍCULOS AÉREOS NO TRIPULADOS APLICADAS A LA OBTENCIÓN DE PRODUCTOS CARTOGRÁFICOS PARA LA INGENIERÍA CIVIL

PHOTOGRAMMETRIC TECHNIQUES FROM UNMANNED AERIAL VEHICLES FOR MAPPING IN CIVIL ENGINEERING

PATRICIO JESÚS MARTÍNEZ CARRICONDO

Directores:
Dr. Francisco Agüera Vega
Dr. Fernando Carvajal Ramírez
Dr. Julián Sánchez-Hermosilla López

TESIS DOCTORAL

2016

DEPARTAMENTO DE INGENIERÍA

GRUPO DE INVESTIGACIÓN AGR-199

UNIVERSIDAD DE ALMERÍA

TÉCNICAS FOTOGRAMÉTRICAS DESDE VEHÍCULOS AÉREOS NO TRIPULADOS APLICADAS A LA OBTENCIÓN DE PRODUCTOS CARTOGRÁFICOS PARA LA INGENIERÍA CIVIL

PHOTOGRAMMETRIC TECHNIQUES FROM UNMANNED AERIAL VEHICLES FOR MAPPING IN CIVIL ENGINEERING

PATRICIO JESÚS MARTÍNEZ CARRICONDO

TESIS DOCTORAL

NOVIEMBRE 2.016

DIRECTORES:

DR. FRANCISCO AGÜERA VEGA

DR. FERNANDO CARVAJAL RAMÍREZ

DR. JULIÁN SÁNCHEZ-HERMOSILLA LÓPEZ

UNIVERSIDAD DE ALMERÍA
COMISIÓN PERMANENTE DEL COMITÉ DE DIRECCIÓN DE LA EIDUAL

AUTORIZACIÓN DEL DIRECTOR DE LA TESIS

Versión 17/03/15

TESIS DOCTORAL

Nombre Doctorando/a	Patricio Jesús Martínez Carricondo
NIF/NIE/Pasaporte	23.272.078-B
Título de la Tesis	TÉCNICAS FOTOGRAMÉTRICAS DESDE VEHÍCULOS AÉREOS NO TRIPULADOS APLICADAS A LA OBTENCIÓN DE PRODUCTOS CARTOGRÁFICOS PARA LA INGENIERÍA CIVIL.
Programa Doctorado	DOCTORADO EN TECNOLOGÍA DE INVERNADEROS E INGENIERÍA

01. DIRECTOR

*Documento de Identidad (*NIF / NIE / PSP)	30.495.297-B	Nacionalidad	Española
Apellidos, Nombre	Agüera Vega, Francisco		
Correo electrónico	faguera@ual.es		
Universidad/Centro	Universidad de Almería	*País*	España

02. CODIRECTOR

*Documento de Identidad (*NIF / NIE / PSP)	26.007.004-F	Nacionalidad	Española
Apellidos, Nombre	Carvajal Ramírez, Fernando		
Correo electrónico	Carvajal@ual.es		
Universidad/Centro	Universidad de Almería	*País*	España

03. CODIRECTOR

*Documento de Identidad (*NIF / NIE / PSP)	30.517.136-T	Nacionalidad	Española
Apellidos, Nombre	Sánchez-Hermosilla López, Julián		
Correo electrónico			
Universidad/Centro	Universidad de Almería	*País*	España

AUTORIZACION DEL DIRECTOR/ES DE LA TESIS

El/los Director/es de la Tesis arriba mencionada AUTORIZA el depósito y la presentación de la misma para su defensa.

El **Director/a**	El **Codirector/a**	El **Codirector/a**
Firma electrónica	Firma electrónica	Firma electrónica
Fdo.: Francisco Agüera Vega	Fdo.: Fernando Carvajal Ramírez	Fdo.: Julián Sánchez-Hermosilla López

INFORME DEL TUTOR DE LA TESIS SOBRE LA CALIFICACIÓN DEL ACTA DE TUTELA PREVIA AL DEPOSITO DE LA TESIS (Sólo aplicable a doctorados regulados por los RD 1393/2007 y 99/2011)

El tutor del doctorando, arriba indicado, informa que la calificación del acta de tutela previa al depósito de la tesis debe ser de: APTO, 10.

El **Tutor/a**

Firma electrónica

Fdo.: Francisco Agüera Vega

Y con esta fecha se remite la presente comunicación

Almería, a 28 de octubre de 2016

Dirigido a la:
COMISIÓN PERMANENTE DEL COMITÉ DE DIRECCIÓN DE LA EIDUAL

A mi familia

Los que se enamoran de la práctica sin la teoría son como los pilotos sin timón ni brújula, que nunca podrán saber a dónde van.

Leonardo Da Vinci (1452-1519)

AGRADECIMIENTOS

Cuando de pequeño me preguntaban qué quería ser de mayor, siempre respondía “piloto de aviones”. Pasaron los años y, cuando llegó el momento de iniciar el vuelo, decidí quedarme en tierra para estudiar Ingeniería de Caminos. Sin embargo, supongo que esas ideas se quedan en la cabeza de algún modo. Tras otros tantos años de profesión, inicié una nueva etapa en la Universidad de Almería donde he tenido la suerte de cruzarme con grandes personas. En primer lugar, quiero agradecer a mis directores, Paco, Fernando y Julián, su ayuda, apoyo constante y paciencia en la realización de esta Tesis. A Paco y Fernando, además, el haber puesto por primera vez en mis manos uno de estos drones que me han permitido volar con los pies en el suelo y complementar de forma innovadora mi profesión. Gracias por haber sido el timón y la brújula durante estos cuatro años de Doctorado, por todas las cosas que hemos hecho juntos hasta la fecha, y por todas aquellas que seguro compartiremos en el futuro.

Gracias a mis padres, Patricio y Anita, por haber sido siempre excepcionales, por todo el amor que he recibido en cada momento, por los consejos, por el apoyo y la comprensión en todas las decisiones que he ido tomando en mi vida, y en definitiva, por ser los mejores padres que cualquier hijo querría tener.

Gracias a mi hermano Antonio, por estar siempre pendiente de mí, por poder contar contigo para cualquier problema que tenga y por todos los años que hemos pasado juntos. Gracias también a mi cuñada, Mª Dolores, y a mis sobrinas, Paula y Patricia, entre todos hacemos nuestra familia más grande y unida.

Gracias a Laura, mi mujer, mi compañera de viaje desde hace ya más de once años. Juntos hemos pasado momentos inolvidables y juntos hemos apostado por esta nueva etapa que estamos viviendo, que pese a que esté teniendo sus momentos de sacrificio, seguro que se verá recompensada en el futuro. Gracias, sobre todo, por ser mi mejor apoyo cuando más lo necesito, y por tu labor y dedicación como madre cuando el trabajo no me permite estar con vosotros.

Gracias, por supuesto, a mis dos hijos, Patri y Carmen, que vinieron juntos a este mundo y nos trajeron el doble de alegría. Habéis sido el motor del cambio y el combustible para todo lo que hacemos. Gracias por entender que vuestro papá tenga que jugar tanto con los “avioncitos”. Una sonrisa, un beso o un abrazo vuestro recompensa cualquier esfuerzo.

Gracias a mis abuelos, que aunque ya no están con nosotros, dejaron unos recuerdos imborrables y les hubiera encantado disfrutar de este momento.

Gracias al resto de mi familia, mis tíos, mis primos, mi familia política, mis suegros,…a mis amigos de toda la vida y los “camineros”, a mis antiguos compañeros de trabajo, a los que han confiado en mí como profesional del sector de los drones, etc. Todos habéis participado de las cosas buenas que me han ido pasando a lo largo de estos años de Doctorado.

A la Universidad de Almería, y a todas esas personas y profesores que aquí he ido conociendo durante estos últimos años, mi más sincero agradecimiento.

A todos aquellos que por despiste me haya podido olvidar, perdón y muchas gracias.

Por último, gracias a la Junta de Andalucía, por haberme concedido una beca con cargo al proyecto P08-TEP-3870 co-financiado con fondos FEDER procedentes de la Unión Europea.

¡MUCHAS GRACIAS A TODOS!

ÍNDICE

RESUMEN

La ingeniería civil viene usando los modelos digitales de elevaciones (DEMs) y las ortofotos como material básico para poder redactar y ejecutar cualquier proyecto de ingeniería, así como para controlar la geometría de las construcciones de forma periódica.

Dentro de los medios técnicos posibles para obtener este tipo de información, los vehículos aéreos no tripulados (*unmanned aerial vehicles UAVs*) están imponiendo, cada vez más, su uso debido a la reducción de costes, la flexibilidad y la mejora en la resolución obtenida. Este éxito se ha debido, en parte, a la evolución de la fotogrametría digital y al uso de algoritmos especiales como el *Structure-from-Motion* (SfM).

Muchos son los autores que desde hace varios años vienen estudiando las aplicaciones de la fotogrametría UAV y la influencia que determinados parámetros tienen en la precisión de los productos resultantes.

Esta Tesis Doctoral ha pretendido profundizar en el estudio de aplicaciones fotogramétricas desde UAVs para situaciones de topografía extrema, como pueden ser los deslizamientos de taludes de desmonte en obras lineales, así como analizar la influencia que la altura de vuelo, la morfología del terreno y el número de puntos de apoyo *Ground Control Points* (GCPs) tienen en la precisión de DEMs y ortoimágenes obtenidas mediante fotogrametría UAV a través de software basado en el algoritmo SfM.

Los resultados obtenidos han demostrado que la fotogrametría UAV constituye una técnica útil y adecuada para proyectos de ingeniería relacionados con la reparación y gestión de deslizamientos de taludes en desmontes de carreteras. Asimismo, se ha constatado que la morfología del terreno y la altura de vuelo tienen poca influencia sobre la precisión planimétrica alcanzada, debido principalmente al bajo rango de altura de vuelo en el que suelen operar los UAVs (50-120 m). También se ha corroborado, igual que otros estudios, que la precisión altimétrica disminuye conforme aumenta la altura, aportando esta Tesis Doctoral que esa consecuencia es más notable conforme disminuye el número de GCPs. Por último, se ha arrojado luz sobre la influencia que el número de GCPs tiene en la precisión final de los productos obtenidos, concluyéndose que el uso de un

número alto de puntos de apoyo (15-20) optimiza los resultados, tanto en planimetría como en altimetría, llegando a permitir, incluso para alturas de 120 m y según las normas del ASPRS, la creación de mapas cartográficos a escala 1:150.

ABSTRACT

Civil engineering has been using digital elevation models (DEMs) and orthophotos as a basic tool to design and construct any engineering project, as well as to check the geometry of the construction site periodically.

Within the technical means possible to obtain this type of information, unmanned aerial vehicles (UAVs) are implemented, increasingly, due to reduction of costs, flexibility and the improvement in the resolution obtained. This success has been due, in part, to the evolution of digital photogrammetry and the use of special algorithms such as the Structure-from-Motion (SfM).

There are many authors that have been studying the photogrammetry UAV applications and the influence that certain parameters have in the accuracy of the resulting products for several years.

This thesis has sought to deepen the study of photogrammetric applications from UAVs for extreme topography situations, as can be the landslides of slopes in linear construction, as well as analyze the influence of flight altitude, the terrain morphology and the number of ground control points (GCPs) in the accuracy of DEMs, and orthoimages obtained through photogrammetry UAV using software based on the SfM algorithm.

The results obtained have shown that the photogrammetry UAV constitutes a useful and suitable technique for engineering projects related to the repair and management of roads cut slopes construction. Also, it has been found that the terrain morphology and flight altitude have little influence on the planimetric accuracy achieved, which is due mainly to the low altitude range of flight in which the UAVs usually operate (50-120 m).

It has also been corroborated that, like other studies, the altimetric accuracy decreases with altitude, providing this thesis that this consequence is more notable if the number of GCPs decreases.

Finally, it has shed light on the influence that the number of GCPs has in the accuracy of the final product obtained, and concluded that the use of a high number of GCPs (15-20) optimizes the results, both in planimetry and altimetry, arriving to allow, even for altitudes of 120 m and according to the rules of the ASPRS, creating cartographic maps at a scale of 1:150.

INTRODUCCIÓN

INTRODUCCIÓN

Introducción General

La disponibilidad de ortofotos y de información digitalizada de muy alta precisión sobre el terreno, resulta de especial importancia para todas las actividades que requieren datos topográficos de precisión (Hugenholtz et al. 2015; Mancini et al. 2013).

La ingeniería civil usa los modelos digitales de elevaciones (DEMs) y las ortofotos como material básico para poder redactar y ejecutar cualquier proyecto, así como para controlar la geometría de forma periódica, por lo que es necesario conocer la precisión que presentan y que ésta esté dentro de los límites admisibles (D'Oleire-Oltmanns et al. 2012; Nelson, Reuter, y Gessler 2009; Ruzgienė et al. 2015).

Con el fin de caracterizar todo tipo de superficies, existen varias técnicas que pueden utilizarse para obtener los DEMs, a saber, estaciones totales de topografía (TS), Sistemas Globales de Navegación por Satélite (GNSS), láser escáner terrestre (TLS) y sensores aerotransportados como LIDAR (Light Detection and Ranging) o cámaras fotogramétricas (Sallenger et al. 2003).

Especial mención pueden tener diferentes morfologías de terreno tales como los taludes de desmonte de carreteras, de grandes longitudes en comparación con la altura, así como de pendientes elevadas lo que facilita que surjan problemas de estabilidad que pueden dar lugar a deslizamientos y deformaciones superficiales de difícil accesibilidad (Ai et al. 2015; Rieke et al. 2011).

En tales casos o bajo condiciones extremas, los levantamientos topográficos con medios clásicos pueden estar limitados por el número de puntos medibles debido a problemas de accesibilidad. Además, los TLS requieren largas sesiones de trabajo en campo y tediosos cálculos en post-procesos, y tienen como inconveniente adicional la aparición de posibles zonas ocultas en la superficie. Asimismo, los sistemas LIDAR o cámaras fotogramétricas sobre plataformas aéreas convencionales con piloto a bordo son ideales para grandes superficies, pero con costes demasiado elevados fuera de estas condiciones, además de la imposibilidad de conseguir una alta resolución espacial y temporal.

La fotogrametría terrestre también podría ser usada; sin embargo, en determinadas ocasiones, y debido a las limitaciones del espacio de trabajo y de posicionamiento en altura, la orientación de las fotografías desde el punto de vista terrestre estaría lejos de ser la ideal respecto al objeto del estudio, lo que podría producir grandes aberraciones, además de la posible aparición de zonas ocultas.

El uso de vehículos aéreos no tripulados (UAVs) en la Ingeniería Civil

La fotogrametría a partir de imágenes tomadas desde vehículos aéreos no tripulados UAVs (unmanned aerial vehicles) ha sido acuñada como "fotogrametría UAV" (Eisenbeiß et al. 2009) y se basa en usar los UAVs como plataformas que actúan controladas remotamente, de forma total o parcialmente autónoma, sin piloto en su interior.

En los últimos años, el uso de UAVs con fines civiles se ha incrementado de manera notable. Desde que se utilizaron los primeros globos para transportar sensores fotogramétricos hasta la actualidad, el desarrollo de las plataformas aéreas y la tecnología asociada para este uso ha sido enorme. Esto se ha debido al desarrollo de los componentes electrónicos que los forman, los cuales han evolucionado reduciendo su tamaño y precio, y aumentando sus prestaciones técnicas (Rock, Ries, y Udelhoven 2011). Una descripción detallada de esta evolución y el estado del arte se puede encontrar en Colomina y Molina (2014).

El uso de UAVs equipados con cámaras digitales no métricas para conseguir este tipo de información se está investigando desde hace algunos años para superar las limitaciones que imponen las técnicas topográficas clásicas (Nex y Remondino 2014).

Los UAVs han supuesto claras ventajas frente a las aeronaves convencionales con piloto a bordo o los satélites, tales como el bajo coste económico, la flexibilidad en las operaciones, así como la mejora en las resoluciones obtenidas, tanto geométricas como temporales (Harwin y Lucieer 2012; Hugenholtz et al. 2013; Immerzeel et al. 2014; Laliberte et al. 2010).

El uso de cámaras no métricas y el software de bajo coste para procesar las imágenes, alcanzando precisiones adecuadas, son otros factores que influyen en la viabilidad económica de la fotogrametría UAV (Vallet et al. 2012).

Desde el punto de vista de las dimensiones de las zonas de trabajo y para la obtención de imágenes de alta resolución, donde no es rentable el uso de medios aéreos convencionales o el uso de imágenes de satélites, los UAVs también han terminado implantando su uso (Nex y Remondino 2014).

Además, los UAVs requieren de menos tiempo para la adquisición de datos lo que también reduce el coste económico comparado con los medios clásicos pilotados (Aber et al. 2010).

Según Eyndt y Volkmann (2013) la fotogrametría UAV se ha usado con éxito en la inspección de infraestructuras, geodesia, sistemas de información geográfica, cartografía, mapas topográficos, aplicaciones catastrales, emergencias, cambios por erosión, etc.

Varias obras manifiestan la idoneidad de la fotogrametría UAV para la vigilancia y mantenimiento de infraestructuras, y en concreto, para el análisis de deslizamientos (Metni y Hamel 2007; Wang, Wu, y Zhang 2009).

Una revisión de las aplicaciones de los UAVs a la ingeniería civil en general, y a la obtención de productos cartográficos en particular, puede encontrarse en Liu et al. (2014) y Nex y Remondino (2014).

El proceso fotogramétrico desde un UAV. El algoritmo SfM (Structure-from-Motion)

La fotogrametría UAV ha abierto un abanico de nuevas aplicaciones en el campo de la fotogrametría de objeto cercano al combinar técnicas de fotogrametría aérea y terrestre, lo que permite contar con las ventajas de ambas. Así, el campo de aplicación de la fotogrametría UAV en el ámbito de la ingeniería civil puede situarse entre aquellas que usan técnicas clásicas terrestres (estaciones totales, GPS, etc.) y las que se basan en fotogrametría a partir de imágenes tomadas desde aeronaves convencionales (aviones o satélites), al representar una alternativa económicamente viable.

En su origen, la fotogrametría surge como el resultado de la acción incansable del ser humano por representar las tres dimensiones. Es definida por el Manual de la Sociedad Americana de Fotogrametría como la ciencia, arte y tecnología de obtener información fiable de los objetos y su entorno mediante el registro, medida e interpretación de imágenes fotográficas y datos obtenidos a partir de energía electromagnética radiante y otros fenómenos.

Desde que en el siglo XIX se inventará el primer estereoscopio, y tras años de evolución, la fotogrametría ha pasado de complejos dispositivos mecánicos a intuitivas herramientas informáticas.

La aplicación de técnicas de visión computacional a la fotogrametría (Atkinson 2001; Hartley y Zisserman 2003) ha facilitado la posibilidad del uso de imágenes tomadas a diferentes alturas con diferentes orientaciones, dando flexibilidad y resultados de alta calidad (Fernández-Hernandez et al. 2015). Varios son los softwares de bajo coste que permiten, en la actualidad, la obtención, a partir de fotografías tomadas con cámaras convencionales, del modelado 3D de superficies así como el estudio geométrico de objetos cercanos. La mayoría de estos softwares basan su funcionamiento en la obtención de nubes de puntos mediante algoritmos especiales, tales como *Structure-from-Motion SfM* (Fonstad et al. 2013; Javernick, Brasington, y Caruso 2014; Westoby et al. 2012).

El algoritmo SfM opera bajo los mismos principios básicos que la fotogrametría estereoscópica, es decir, las estructuras 3D pueden resolverse a partir de series de solapamiento entre imágenes. Sin embargo, a diferencia de la fotogrametría clásica, la geometría de la escena, las posiciones de la cámara y la orientación, se resuelven automáticamente sin necesidad de especificar previamente una red de elementos con coordenadas tridimensionales conocidas (Furukawa y Ponce 2010; Snavely, Seitz, y Szeliski 2008; Vasuki et al. 2014; Westoby et al. 2012).

En contraposición a la fotogrametría clásica aérea que exigía planificaciones rigurosas de vuelos y la caracterización previa de las cámaras (Kamal y Samar 2008), el SfM aporta espontaneidad al proceso, no siendo necesaria una planificación exhaustiva ni calibraciones de cámaras, incluso siendo posible el uso de imágenes procedentes de diferentes cámaras fotográficas.

El resultado de un proceso de SfM es en primer lugar una nube de puntos discreta, la cual puede variar en densidad en función de las correspondencias detectadas entre imágenes. En los procesos tradicionales de ajuste manual de puntos comunes entre imágenes, estas nubes no estaban muy pobladas; sin embargo con el algoritmo SfM dichas nubes pueden llegar a tener miles de puntos. Dichos puntos pueden ser establecidos manualmente, o en el caso del SfM son detectados automáticamente mediante lo que se conoce como el algoritmo *SIFT (Scale Invariant Feature Transform).* Lowe (2004) y Snavely, Seitz, y Szeliski (2008) aplicaron este algoritmo para la detección de puntos clave en la generación de nubes de puntos 3D a partir de fotografías. Varios estudios han concluido que este algoritmo es uno de los más potentes para detectar puntos o características comunes entre pares de imágenes permitiendo cotejar un gran número de fotografías (Juan y Gwun 2009; Remondino y El-hakim 2006).

A diferencia de la fotogrametría tradicional, las posiciones de la cámara derivadas del algoritmo SfM, no cuentan con la escala y la orientación proporcionadas por las coordenadas de los puntos de apoyo. Consecuentemente, la nube de puntos 3D se genera en coordenadas relativas, referentes al sistema de coordenadas imagen. La georreferenciación de dicho modelo se lleva a cabo, generalmente, utilizando un reducido número de puntos de apoyo (*Ground Control Points, GCPs*) situados en elementos claramente visibles tanto en la nube de puntos como en el terreno y en cada una de las imágenes.

Aunque estas nubes discretas pueden arrojar información suficiente para la creación de DEMs, el paso final de los procesos de SfM suele ser una nube de puntos densa con millones de puntos que describen con más detalle las superficies y geometría de objetos, aportando coordenadas tridimensionales tipo XYZ y una descripción colorimétrica en el modelo RGB.

Todos estos avances han desembocado en un nuevo concepto: **la fotogrametría UAV-SfM**.

El control de calidad y la precisión obtenida

En aplicaciones para levantamientos topográficos, es primordial poder georreferenciar a un sistema concreto los datos generados en el proceso

fotogramétrico. Como ya se ha comentado, para ello se usan dianas de referencia con coordenadas conocidas y altamente precisas, claramente visibles en las imágenes y que se distribuyen de forma dispersa en el suelo antes de realizar el vuelo con el UAV. También es posible el uso de dianas naturales, a saber, postes de electricidad, esquinas de construcciones, tapas de pozos, etc. Las coordenadas de estos GCPs deben ser obtenidas con métodos precisos tales como GPS diferencial o estaciones totales. Según Rosnell et al. (2012) se necesitan al menos 3 GCPs para georreferenciar el proceso fotogramétrico, aunque es recomendable aumentar el número de estos puntos para alcanzar mejores precisiones. Tahar (2013) concluyó que diferentes configuraciones, distribuciones y número de GCPs contribuyen a obtener diferentes errores en el ajuste del bloque fotogramétrico.

La literatura ha recogido clásicamente el uso del estadístico *Root Mean Square Error RMSE* (error medio cuadrático) como el más común y válido para la evaluación de los productos obtenidos mediante fotogrametría UAV. Este estadístico se aplica sobre una serie de puntos de control (PC) que se disponen sobre las superficies de estudio a la vez que los GCPs, y a los que se miden sus coordenadas de forma precisa mediante GNSS o TS para su posterior comparación con las coordenadas estimadas a partir del DEM y la ortofoto.

El error medio cuadrático de las componentes X, Y y Z será calculado según las siguientes expresiones:

$$RMSE_x = \sqrt{\frac{1}{n}\sum_{i=1}^{n}\left(x_{PCm} - x_{PCe}\right)^2}$$

$$RMSE_y = \sqrt{\frac{1}{n}\sum_{i=1}^{n}\left(y_{PCm} - y_{PCe}\right)^2}$$

$$RMSE_z = \sqrt{\frac{1}{n}\sum_{i=1}^{n}\left(z_{PCm} - z_{PCe}\right)^2}$$

donde el subíndice *PCm* significa componente medida del punto de control, *PCe* significa componente estimada del punto de control, para las tres componentes X, Y y Z, y *n* es el número de puntos de control tenidos en cuenta.

Según el US National Standard for Spatial Data Accuracy (FGDC 1998) , si no existen errores sistemáticos en los datos, las precisiones vertical y horizontal (P_v, P_h, respectivamente) con un intervalo de confianza del 95% pueden ser computadas de la siguiente manera:

$$P_v = 1.9600 \times RMSE_z \qquad P_h = 1.7308 \times RMSE_h$$

donde $RMSE_h$, es el error medio cuadrático horizontal, dado por:

$$RMSE_h = \sqrt{(RMSE_x^2 + RMSE_y^2)}$$

Con estos valores, y teniendo en cuenta un valor de 0.2 mm como límite de percepción visual humana, se podrá estimar la mayor escala a la que se puede representar el terreno:

$$D_e \geq P_h/0.2$$

donde P_h está expresado en mm, y D_e representa el denominador de la escala.

En los últimos años se han abordado numerosos estudios para evaluar la precisión de los productos obtenidos mediante fotogrametría UAV. Harwin y Lucieer (2012) evaluaron la precisión de nubes de puntos generadas a partir de imágenes procedentes de UAVs para elaboración de cartografía de paisajes naturales, utilizando software de código abierto basado en el algoritmo SfM. Llegaron a obtener precisiones de 0.025-0.040 m con vuelos con un alto grado de solape entre imágenes y un suficiente número de GCPs distribuidos a lo largo del área de estudio.

Turner, Lucieer, y Watson (2012) usaron UAVs de ala rotaroria con una cámara digital réflex de longitud focal fija (DSLR) para generar ortomosaicos con alta precisión.

Anders et al. (2013) generaron modelos digitales de superficie (DSMs) usando UAVs de ala fija, y obteniendo, para alturas de 90 m errores absolutos de 0.350 m, y de 0.450 m para alturas de 180 m.

Mancini et al. (2013) estudiaron la validación de nubes de puntos y DSMs de un conjunto de dunas de playa usando imágenes procedentes de un UAV de ala rotatoria equipado con una cámara réflex digital. A su vez, compararon estos resultados con los obtenidos con un láser escáner terrestre demostrando que el uso de UAVs es sencillo y la precisión similar a la obtenida con la tecnología TLS.

Más recientemente, Lucieer et al. (2014) generaron DSM de musgos antárticos a partir de imágenes UAV y obtuvieron un RMSE de 0.420 m.

Immerzeel et al. (2014) aplicaron la metodología UAV para la monitorización de la dinámica glaciar. A tal fin, usaron un UAV de ala fija portando una cámara digital de bajo coste para generar DEMs y ortoimágenes con resultados satisfactorios, concluyendo que con esta metodología se alcanzaban resoluciones y precisiones que no podían ser alcanzadas a través de imágenes procedentes de satélites.

Lucieer, de Jong, y Turner (2014) también usaron imágenes UAV para la caracterización topográfica de deslizamientos, obteniendo ortoimágenes con 0.01 m de resolución y $RMSE_{XY}$ de 0.070 m y $RMSE_{Z}$ de 0.062 m.

Pierzchala et al. (2014) llevaron a cabo un estudio para generar, mediante fotogrametría UAV, el DSM de una superficie agrícola tras una cosecha y compararlo con el obtenido previamente a la cosecha mediante TLS, y evaluar, de esta manera, las variaciones del suelo. El RMSE del DSM obtenido a partir de las imágenes del UAV fue de 0.082 m.

Tonkin et al. (2014) usaron un UAV de ala rotatoria para obtener imágenes para realizar levantamientos topográficos y obtener DSMs. A su vez, llevaron a cabo una comparación entre los datos obtenidos a través de fotogrametría UAV-SfM y los obtenidos a través de una estación total de topografía, concluyendo que los datos generados a partir de las imágenes UAV estaban en consonancia con los obtenidos con la estación total en cuanto a precisión se refería.

Mesas-Carrascosa et al. (2014) estudiaron la calidad posicional de ortofotos obtenidas a partir de imagenes tomadas con un UAV de ala rotatoria y una cámara digital. Los resultados mostraron que las ortofotos pasaron las pruebas de calidad espaciales propuestas por diversos organismos nacionales de cartografía.

Eltner et al. (2015) midieron los cambios a corto plazo en superficies con eventos de erosión usando las imágenes procedentes de un UAV de ala rotatoria. A su vez, el DSM generado fue comparado con el obtenido a través de un TLS alcanzando precisiones de menos de 0.01 m y concluyendo que los DSMs generados con imágenes UAV suponen una técnica ventajosa para cuantificar y clasificar los cambios en la superficie del suelo.

Harwin, Lucieer, y Osborn (2015) investigaron la influencia del método de calibración de la cámara en la precisión obtenida en las nubes de puntos obtenidas mediante imágenes UAV, en concreto, para acantilados costeros. Concluyeron que es necesario desplegar un alto número de GCPs y combinar fotografías tanto verticales como oblicuas para que la precalibración o la calibración automática de la cámara produzcan modelos fiables.

Uysal, Toprak, y Polat (2015) llevaron a cabo un estudio de precisiones de DSMs generados mediante fotogrametría UAV concluyendo que se puede usar esta metodología para obtener levantamientos topográficos y cartografía para aplicaciones de ingeniería, todo ello con metodologías de bajo coste y minimizando tiempos de trabajo en campo.

Ruzgienė et al. (2015) han estudiado la calidad de DSMs generados usando fotogrametría UAV y la influencia que tienen los GCPs en la precisión obtenida.

A la vista de todos estos resultados, significativos por su heterogeneidad, se puede deducir que es necesario llevar a cabo un intenso trabajo que de luz sobre la puesta a punto de la metodología y las precisiones que se pueden alcanzar en los DEMs y ortofotos obtenidos a partir de fotogrametría UAV, en función de los factores más significativos que intervienen en el proceso, como por ejemplo la altura de vuelo, la orografía del terreno, la resolución de las imágenes, o el tipo de UAV.

Referencias

Aber, James S., Irene Marzolff, Johannes B. Ries, y Small-format Aerial Photography. 2010. Small-Format Aerial Photography *Small-Format Aerial Photography*.

Ai, Mingyao et al. 2015. «A robust photogrammetric processing method of low-altitude UAV images». *Remote Sensing* 7(3): 2302-33.

Anders, Niels, Rens Masselink, Saskia Keesstra, y Juha Suomalainen. 2013. «High-Res Digital Surface Modeling using Fixed-Wing UAV-based Photogrammetry». *Geomorphometry 2013*: 2-5.

Atkinson, K. B. 2001. Whittles Publishing *Close range photogrammetry and machine vision*.

Colomina, I., y P. Molina. 2014. «Unmanned aerial systems for photogrammetry and remote sensing: A review». *ISPRS Journal of Photogrammetry and Remote Sensing* 92: 79-97.

D'Oleire-Oltmanns, Sebastian, Irene Marzolff, Klaus Daniel Peter, y Johannes B. Ries. 2012. «Unmanned aerial vehicle (UAV) for monitoring soil erosion in Morocco». *Remote Sensing* 4(11): 3390-3416.

Eisenbeiß, Henri, E T H Zurich, Henri Eisenbeiß, y Eidgenössischen Technischen Hochschule Zürich. 2009. Institute of Photogrammetry and Remote Sensing *UAV photogrammetry*.

Eltner, Anette, Philipp Baumgart, Hans Gerd Maas, y Dominik Faust. 2015. «Multi-temporal UAV data for automatic measurement of rill and interrill erosion on loess soil». *Earth Surface Processes and Landforms* 40(6): 741-55.

Eyndt, Tom Op t, y Walter Volkmann. 2013. «UAS as a tool for surveyors: From tripods and trucks to virtual surveying». *GIM International* 27(4).

Fernández-Hernandez, J., D. González-Aguilera, P. Rodríguez-Gonzálvez, y J. Mancera-Taboada. 2015. «Image-Based Modelling from Unmanned Aerial Vehicle (UAV) Photogrammetry: An Effective, Low-Cost Tool for Archaeological Applications». *Archaeometry* 57(1): 128-45.

FGDC. 1998. «National Standard for Spatial Data Accuracy». En *Geospatial Positioning Accuracy Standards*, , 28.

Fonstad, Mark A. et al. 2013. «Topographic structure from motion: A new development in photogrammetric measurement». *Earth Surface Processes and Landforms* 38(4): 421-30.

Furukawa, Yasutaka, y Jean Ponce. 2010. «Accurate, dense, and robust multiview stereopsis». *IEEE Transactions on Pattern Analysis and Machine Intelligence*

32(8): 1362-76.

Hartley, Richard, y Andrew Zisserman. 2003. 53 Cambridge University Press *Multiple View Geometry in Computer Vision.2nd*.

Harwin, Steve, y Arko Lucieer. 2012. «Assessing the accuracy of georeferenced point clouds produced via multi-view stereopsis from Unmanned Aerial Vehicle (UAV) imagery». *Remote Sensing* 4(6): 1573-99.

Harwin, Steve, Arko Lucieer, y Jon Osborn. 2015. «The impact of the calibration method on the accuracy of point clouds derived using unmanned aerial vehicle multi-view stereopsis». *Remote Sensing* 7(9): 11933-53.

Hugenholtz, Chris H. et al. 2013. «Geomorphological mapping with a small unmanned aircraft system (sUAS): Feature detection and accuracy assessment of a photogrammetrically-derived digital terrain model». *Geomorphology* 194: 16-24.

Hugenholtz, Chris H., Jordan Walker, Owen Brown, y Steve Myshak. 2015. «Earthwork Volumetrics with an Unmanned Aerial Vehicle and Softcopy Photogrammetry». *Journal of Surveying Engineering* 141(1): 6014003.

Immerzeel, W. W. et al. 2014. «High-resolution monitoring of Himalayan glacier dynamics using unmanned aerial vehicles». *Remote Sensing of Environment* 150: 93-103.

Javernick, L., J. Brasington, y B. Caruso. 2014. «Modeling the topography of shallow braided rivers using Structure-from-Motion photogrammetry». *Geomorphology* 213: 166-82.

Juan, Luo, y O Gwun. 2009. «A comparison of sift, pca-sift and surf». *International Journal of Image Processing (IJIP)* 3(4): 143-52.

Kamal, W. A., y R. Samar. 2008. «A mission planning approach for UAV applications». En *Proceedings of the IEEE Conference on Decision and Control*, , 3101-6.

Laliberte, Andrea S, Jeffrey E Herrick, Albert Rango, y Craig Winters. 2010. «Acquisition, Orthorectification, and Object-based Classification of Unmanned Aerial Vehicle (UAV) Imagery for Rangeland Monitoring». *Photogrammetric Engineering Remote Sensing* 76(6): 661-72.

Liu, Peter et al. 2014. «A review of rotorcraft Unmanned Aerial Vehicle (UAV) developments and applications in civil engineering». *Smart Structures and Systems* 13(6): 1065-94.

Lowe, David G. 2004. «Distinctive image features from scale-invariant keypoints». *International Journal of Computer Vision* 60(2): 91-110.

Lucieer, Arko, Steven M. de Jong, y Darren Turner. 2014. «Mapping landslide displacements using Structure from Motion (SfM) and image correlation of multi-temporal UAV photography». *Progress in Physical Geograph* 38(1): 97-116.

Lucieer, Arko, Darren Turner, Diana H. King, y Sharon A. Robinson. 2014. «Using an unmanned aerial vehicle (UAV) to capture micro-topography of antarctic moss beds». *International Journal of Applied Earth Observation and Geoinformation* 27(PARTA): 53-62.

Mancini, Francesco et al. 2013. «Using unmanned aerial vehicles (UAV) for high-resolution reconstruction of topography: The structure from motion approach on coastal environments». *Remote Sensing* 5(12): 6880-98.

Mesas-Carrascosa, Francisco Javier, Inmaculada Clavero Rumbao, Juan Alberto Barrera Berrocal, y Alfonso García Ferrer Porras. 2014. «Positional quality assessment of orthophotos obtained from sensors onboard multi-rotor UAV platforms». *Sensors (Switzerland)* 14(12): 22394-407.

Metni, Najib, y Tarek Hamel. 2007. «A UAV for bridge inspection: Visual servoing control law with orientation limits». *Automation in Construction* 17(1): 3-10.

Nelson, A., H. I. Reuter, y P. Gessler. 2009. 33 Developments in Soil Science *Dem Production methods and sources*.

Nex, Francesco, y Fabio Remondino. 2014. «UAV for 3D mapping applications: A review». *Applied Geomatics* 6(1): 1-15.

Pierzchala, M., Talbot, B., and Astrup, R. 2014. «Estimating soil displacement from timber extraction trails in steep terrain: Application of an unmanned aircraft for 3D modelling». *Forest*, 5(6), 1212–1223.

Remondino, Fabio, y Sabry El-hakim. 2006. «Image-based 3D modelling: A review». *Photogrammetric Record* 21(115): 269-91.

Rieke, M, T Foerster, J Geipel, y T Prinz. 2011. «High-precision positioning and real-time data processing of UAV systems». *International Archives of the Photogrammetry, Remote Sensing and Spatial Information Sciences* 28(C22): 6.

Rock, G., J. B. Ries, y T. Udelhoven. 2011. «Sensitivity Analysis of Uav-Photogrammetry for Creating Digital Elevation Models (Dem)». *ISPRS - International Archives of the Photogrammetry, Remote Sensing and Spatial Information Sciences* XXXVIII-1/: 69-73.

Ruzgienė, Birutė et al. 2015. «The surface modelling based on UAV Photogrammetry and qualitative estimation». *Measurement* 73: 619-27.

Sallenger, Asbury H et al. 2003. «Evaluation of airborne topographic lidar for

quantifying beach changes». *Journal of Coastal Research* 19(1): 125-33.

Snavely, Noah, Steven M. Seitz, y Richard Szeliski. 2008. «Modeling the world from Internet photo collections». *International Journal of Computer Vision* 80(2): 189-210.

Tahar, K.N. 2013. «An evaluation on different number of ground control points in unmanned aerial vehicle photogrammetric block». I*nternational Archives of the Photogrammetry, Remote Sensing and Spatial Information Sciences*, Vol. XL-2/W2, ISPRS. 8th 3DGeoInfo Conference & WG II/2 Whorkshop, 27-29 November 2013, Istambul, Turkey.

Tonkin, T. N., N. G. Midgley, D. J. Graham, y J. C. Labadz. 2014. «The potential of small unmanned aircraft systems and structure-from-motion for topographic surveys: A test of emerging integrated approaches at Cwm Idwal, North Wales». *Geomorphology* 226: 35-43.

Turner, Darren, Arko Lucieer, y Christopher Watson. 2012. «An automated technique for generating georectified mosaics from ultra-high resolution Unmanned Aerial Vehicle (UAV) imagery, based on Structure from Motion (SFM) point clouds». *Remote Sensing* 4(5): 1392-1410.

Uysal, M., A. S. Toprak, y N. Polat. 2015. «DEM generation with UAV Photogrammetry and accuracy analysis in Sahitler hill». *Measurement: Journal of the International Measurement Confederation* 73: 539-43.

Vallet, J., F. Panissod, C. Strecha, y M. Tracol. 2012. «Photogrammetric Performance of an Ultra Light Weight Swinglet "Uav"». *ISPRS - International Archives of the Photogrammetry, Remote Sensing and Spatial Information Sciences* XXXVIII-1/(September): 253-58.

Vasuki, Yathunanthan, Eun Jung Holden, Peter Kovesi, y Steven Micklethwaite. 2014. «Semi-automatic mapping of geological Structures using UAV-based photogrammetric data: An image analysis approach». *Computers and Geosciences* 69: 22-32.

Wang, Feng, Yundong Wu, y Qiang Zhang. 2009. «UAV borne real-time road mapping system». En *2009 Joint Urban Remote Sensing Event*,.

Westoby, M. J. et al. 2012. «"Structure-from-Motion" photogrammetry: A low-cost, effective tool for geoscience applications». *Geomorphology* 179: 300-314.

HIPÓTESIS Y OBJETIVOS

HIPÓTESIS Y OBJETIVOS

Como hipótesis común a los tres capítulos expuestos en esta Tesis Doctoral, y en pos de la puesta a punto de la metodología y la optimización de la precisión en la obtención de DEMs y ortoimágenes, se han usado UAVs de ala rotatoria, en detrimento de los de ala fija, ya que proporcionan imágenes más estables y con mayor control de la posición desde la que son tomadas, lo que a priori se supone debe favorecer la obtención de mejores resultados. Sin embargo, los de ala fija tienen una mayor autonomía de vuelo y pueden ser más adecuados cuando se trabaja con superficies extensas.

El objetivo principal del Capítulo 1 es el desarrollo de una metodología útil para la caracterización topográfica de determinados tipos de superficies con altos grados de inclinación, como pueden ser los deslizamientos producidos en los desmontes de carreteras, mediante fotogrametría UAV a partir de software no basado en el algoritmo SfM.

Para ello, se establecen una serie de hipótesis acerca de la influencia de la orientación del eje de la fotografía respecto a la superficie bajo estudio sobre la calidad de los productos obtenidos en el proceso fotogramétrico. En este sentido, el objetivo que se persigue es comparar los resultados obtenidos con imágenes tomadas con el eje perpendicular a la superficie objeto de estudio, y otras realizadas clásicamente de forma cenital.

Debido a la inaccesibilidad de este tipo de superficies, se establece como segundo objetivo del Capítulo 1 la evaluación de la ubicación idónea de cada uno de los 3 GCPs, número mínimo necesario para poder realizar la georreferenciación absoluta del ajuste fotogramétrico.

Aunque la literatura está aumentando paulatinamente los estudios relativos a la precisión obtenida en DSMs y ortofotos a partir de fotogrametría UAV y la influencia que diferentes parámetros como la altura de vuelo, la distancia focal, la morfología del terreno, el número de GCPs, etc. tienen en la precisión, es necesario llegar a una profunda comprensión de la influencia de estos parámetros para la mejora de las precisiones obtenidas en todos los productos derivados de fotogrametría UAV.

Con tal fin, el objetivo del artículo que constituye el Capítulo 2 es analizar la influencia de la altura de vuelo, la morfología del terreno y el número de

GCPs en la precisión de DEMs y ortoimágenes obtenidas a través de fotogrametría UAV a partir de software basado en el algoritmo SfM.

Asimismo, el objetivo del Capítulo 3 es profundizar en el conocimiento de la influencia que el número de GCPs tiene sobre la precisión de DSMs y ortofotos obtenidos mediante fotogrametría UAV a partir de software basado en el algoritmo SfM.

CAPÍTULO 1:

EFFECTS OF IMAGE ORIENTATION AND GROUND CONTROL POINTS DISTRIBUTION ON UNMANNED AERIAL VEHICLE PHOTOGRAMMETRY PROJECTS ON A ROAD CUT SLOPE

Publicado como:

Fernando Carvajal-Ramírez, Francisco Agüera-Vega, Patricio J. Martínez-Carricondo, "Effects of image orientation and ground control points distribution on unmanned aerial vehicle photogrammetry projects on a road cut slope," J. Appl. Remote Sens. 10(3), 034004 (2016), doi: 10.1117/1.JRS.10.034004.

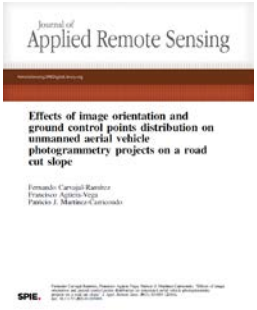

CAPÍTULO 1. EFFECTS OF IMAGE ORIENTATION AND GROUND CONTROL POINTS DISTRIBUTION ON UNMANNED AERIAL VEHICLE PHOTOGRAMMETRY PROJECTS ON A ROAD CUT SLOPE

ABSTRACT

The morphology of road cut slopes, such as length and high slopes, is one of the most prevalent causes of landslides and terrain stability troubles. Digital elevation models (DEMs) and orthoimages are used for land management purposes. Two flights with different orientations with respect to the target surface were planned, and four photogrammetric projects were carried out during these flights to study the image orientation effects. Orthogonal images oriented to the cut slope with only sidelaps were compared to the classical vertical orientation, with sidelapping, endlapping, and both types of overlapping simultaneously. DEM and orthoimages obtained from the orthogonal project showed smaller errors than those obtained from the other three photo- grammetric projects, with the first one being much easier to manage. One additional flight and six photogrammetric projects were used to establish an objective criterion to locate the three ground control points for georeferencing and rectification DEMs and orthoimages. All possible sources of errors were evaluated in the DEMs and orthoimages.

Keywords: Unmanned Aerial Vehicle Photogrammetry, Digital Elevation Model, Orthoimage, Cut slope, Images Orientation, GCP distribution

1. INTRODUCTION

For Engineering and Architecture projects, graphical data is a necessity. The object to be transformed in the project has to be geometrically defined in the previous state, including the terrain where any project activities will be carried out[1]. To control and manage different projects, terrain measurements must be carried out. Additionally, during the course of the project, the geometry has to be periodically controlled and corrected. One of the best tools to carry this out is Digital Elevation Models (DEMs) with a high spatial resolution and vertical accuracy[2,3] and orthoimages with high planimetric accuracy[4]. Other studies[5-7] have been carried out to validate measurements

with robust processing methods to ensure quality. Road cut slopes are generally characterized by large lengths compared to widths, and high slopes. This morphology, combined with other factors, can produce stability problems, which can result in landslides and surface deformations. According to Ayala et al.,[8] a complete characterization of landslide cut slopes should include geometric and morphological data (e.g., profiles, DEMs and orthoimages), geological and geotechnical characteristics, hydrogeological features, and any other external causes. Once again, high resolution DEMs are critical to design controls and correction actions.

Several techniques can be used to obtain DEMs of cut slope surfaces, including the use of surveying devices, such as receivers of surveying accuracy quality based on Global Navigation Satellite Systems (GNSS), Terrestrial Laser Scanning (TLS) or Total Stations (TS)[9], and airborne sensors such as LIDAR (Light Detection and Ranging) or photogrammetric cameras[10]. In general, surveying techniques are very workforce intensive[11]. At extreme topography conditions, surveying can be limited by the number of measurable points that can be done due to accessibility troubles. TLS requires long surveying sessions and consumes significant computing time during post-process assessments to avoid hidden parts of the surface. TS is especially labour demanding and is limited in the amount of possible measured data[12, 13] that can be gathered. However, both LIDAR and photogrammetric cameras mounted to conventional aerial platforms are suitable for covering large extension areas. However, the costs associated with these methods are high and the measurement data are not as accurate as those obtained from TLS and GNSS[14]. Terrestrial photogrammetry could be used to characterize road cut slopes, but the associated errors may be excessive due to the aberrant orientation of the cut slope surface with respect to the terrestrial point of view. Orthogonal orientation toward the cut slope can improve the results if hidden parts of the surface are minimized.

Unmanned Aerial Vehicles (UAVs) have been used as aerial platforms for remote sensing purposes in several areas, including agriculture,[15-17] archaeology,[18, 19] and environmental studies.[3,20] An extensive overview of UAV applications may be found in Ref.[21]. Unmanned Aerial Vehicle Photogrammetry (UAV-Ph) is a versatile technique[22, 23], that can be used to geometrically and morphologically characterize a landslide cut slope due to

its high flexibility at adopting the necessary scale to reach high accuracy cartographic products, and the possibility to orient the axes of the images orthogonally to the surface cut slopes, which are generally characterized by high slopes. The main aim of UAV-Ph is to achieve similar or higher accuracies than are obtained when using airborne-based systems[24-27]. According to Mesas-Carrascosa et al.[6] and Eyndt and W. Volkmann[28], UAV-Ph has been successfully performed for infrastructure inspection, geodesy, geographic information system, cartography, topographic mapping, cadastral applications, mapping for emergencies, erosion, and change detection or measuring the area of lands plots for land policies.

Several works are found in the bibliography that relate to the monitoring and maintenance of road infrastructure[29-30], which shows that UAV-Ph is an efficient technique for road cut slope control.

In this work, classical photogrammetric techniques[31] are adapted to obtain high resolution DEMs and orthoimages from images taken by a nonmetric compact digital camera mounted on a UAV. The main objective of this work was to evaluate the possibility of orienting the axes of the images orthogonally to the target mean surface, the road cut slope, and comparing the images used in classical photogrammetry, oriented orthogonally to the horizontal reference plane, versus oblique images obtained from UAV-Ph projects.

Once the images are taken, postprocessing UAV-Ph can be adapted to its scale level. The relative and absolute orientation process using classical close range photogrammetry workflow implies the use of blocks of images to assess the coordinates of Ground Control Points (GCPs) located within the overlapping image areas[32]. In these cases, rigorous flight planning and a surveying campaign to collect the GCPs are carried out prior to any flights[33].

Alternatively, point-clouds can be obtained by specially indicated algorithms for the UAV-Ph data, such as Structure from Motion (SfM)[34-36] or autocorrelation. This significantly reduces the surveying campaign, the absolute orientation process,[37, 38] the postprocess labor needs and the computing time.

To obtain accurate results, one of the critical steps in DEM and orthoimage assessment is the absolute orientation process, which is also known as registering or assignment of the reference system to the photogrammetric block adjusted by the relative orientation process.[39]

If nonlinear distortions over the road cut slope are assumed to be insignificant, a rigorous spatial Helmert three-dimensional (3-D) transformation[40] can be applied to perform the registration process, which includes seven unknowns, that is, three translation components, three rotation angles and a scale change factor. The minimum data to achieve the characterization of Helmert 3-D transformation is the knowledge of the three GCP coordinates, which generates three equations per each GCP. It was not of interest in this work to calculate how the accuracy of the registration process improves through increasing the redundancy, thus only three GCPs were considered.

The secondary objective of this work was to evaluate where the three GCPs need to be located over the road cut slope to ensure the accuracy of the DEM and orthoimages. This includes taking into account that the accessibility troubles force the use of only the top of the images and the cut slope surface and carrying out a rigorous geometric validation of the resulting DEMs and orthoimages from several sets of three different GCPs.

2. STUDIED CUT SLOPE

The studied cut slope is located at the A92, a dual carriageway between the Almeria and Granada provinces in southeast Spain, with geographic coordinates of 37°9'2.09"N latitude and 2°45'58.61"W longitude. The cut slope is nearly 100 m long and the elevation difference between the ditch and the top of the cut slope is 20 m.

Kilometric point 339 is within the municipality of Abla, Almeria. The instability of the terrain was confirmed quickly after the beginning of servicing on the road. It was necessary to install a small retaining wall made of stones. Some months after, a new landslide appeared (Fig. 1). No significant vegetation was present at the cut slope, thus it was not necessary for some removal process.

3. MATERIALS AND METHODS

The chosen UAV platform was a Microdrones md4-200[41] (Fig. 2), which is a vertical takeoff and landing small aircraft that can carry a load of up 200 g. It was equipped with several navigation devices and remotely controlled by flight routes programmed from GPS waypoints. Signals from the navigation devices are transmitted to the base station via radio and are saved on the onboard flight microSD card, including inertial data at shut positions, which can be used for exterior orientation processing. A stabilized platform supported a 12 megapixel Pentax Optio A40 digital camera. The camera orientation and shutting actions can also be remotely controlled and programmed.

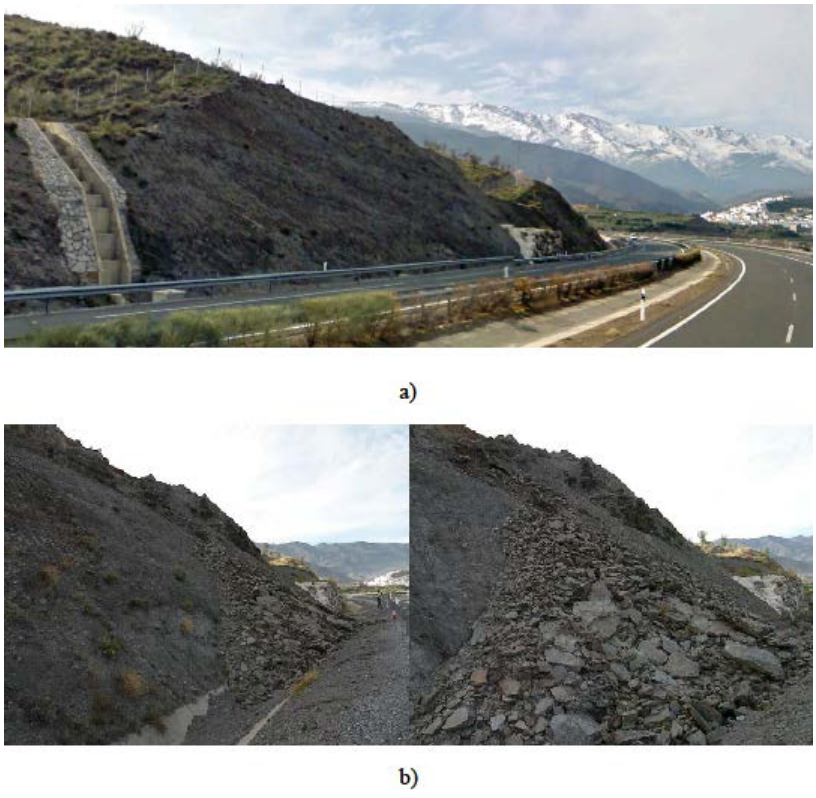

FIG. 1. Studied area: (a) kilometric point 339 of A92, a dual carriageway located between the Almeria and Granada provinces, shown prior to the landslide in 2010 and (b) the same kilometric point after the landslide.

All the photogrammetric operations were carried out with the Photomodeler Scanner V2012[42], a low-cost multi-application software, which can be used for both convergent and parallel photogrammetric operations[22].

FIG. 2. UAV Microdrones model md4-200, base station and hand held remote control transmitter. Both the flight routes and flight controls were planned and programmed, respectively, using the md-Cockpit Standard Edition V2.8.0.6 software package, which is compatible with the Microdrones UAV.

The coordinates of the GCP were measured using a Trimble R6 GPS Receiver[43] in the Real Time Kinematic (RTK) Mode, and applying a postprocess operation using time data corrections saved to the Calar Alto station, and belonging to the Positioning Andalusian Network (RAP),[44] which is 20.8 km from the study area. To determine the statistics to estimate any errors and perform quality control on the photogrammetric operations, 33 check points were measured with the same method. Both the GCP and check points marked on the terrain using A4-format target points (Fig. 3).

FIG. 3. Target points detail from one of the photogrammetric project image.

3.1. ORIENTATION OF THE IMAGES AXIS AND OVERLAPS

To evaluate the benefits of the photogrammetric projects based on orthogonal images to target ground surfaces, two flights were programmed to cover the entire cut slope. The first flight was planned using conventional maps of the cut slope and included 11 transversal profiles to the main direction of the cut slope, which were overlapped to determine the average slope (Fig. 4). The altitude of the flight was ~50 m with respect to the road level and image axis was tilted 35 deg from vertical.

The horizontal projection of the route path was parallel to the centerline of the road. Only nine images, with 75% overlapping, were sufficient to cover the cut slope surface.

The second flight was composed of three paths parallel to each other and to the centerline of the road. There were a total of 36 vertical axis images, with a 75% overlap in both the sidelap and endlap directions.

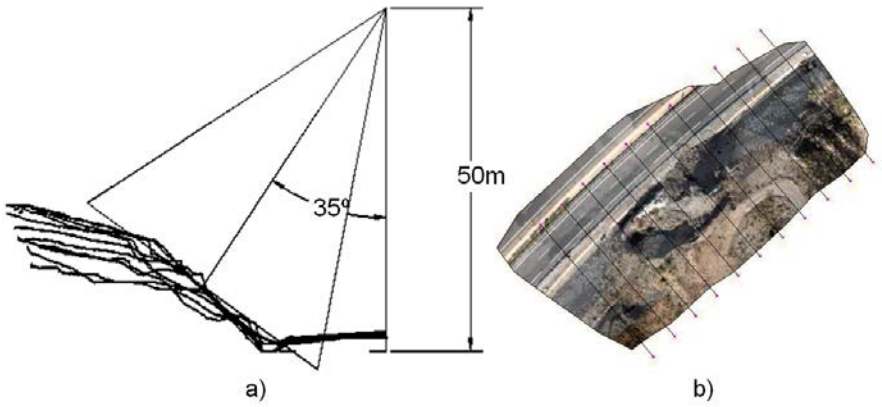

FIG. 4. (a) Overlapping transversal profiles to obtain the average slope of the cut slope and the altitude of the flight and (b) Horizontal projections of the 11 transversal profiles.

From both flights, four photogrammetric operations were arranged following the same workflow:

A1. Orthogonal axis images to the cut slope surface with sidelapping.

A2. Vertical axis images with sidelapping.

A3. Vertical axis images with sidelapping and endlapping.

A4. Vertical axis images with endlapping.

3.1.1. SEQUENTIAL WORKFLOW USED TO OBTAIN DEM AND ORTHOIMAGES

Geometric errors introduced by the camera lens into the images were characterized by a lab calibration process and then a field calibration process was conducted prior to the flights to correct any variations due to instability of the camera calibration parameters, which was based on a set of 60 target points with known coordinates. The height of the programmed calibration flights was the same as the height of flights carried out in this work.

The lab and field calibration quality values obtained included an overall residual root mean square (RMS) of 0.375 mm, a maximum residual of 1.510 mm and photo coverage of 82%.

The calibrated camera parameters included the focal length, format size of the CCD camera sensor, location of the principal point, two radial distortion function coefficients and two decentering distortion function coefficients[45]. All the images from the photogrammetric projects were resampled using the distortion functions obtained from the calibration process (Table 1).

Focal length (mm)	8.1841	
Format size (micro-m)	7.4853 x 5.6132	
Principal point (micro-m)	3.7223, 2.6773	
Radial distortion function parameters	K1	2.820e-003
	K2	-1.526e-005
Decentering distortion function parameters	P1	5.139e-005
	P2	-4.462e-004

TABLE 1. Calibration report of Pentax Optio A40 camera after lab pre-calibration and field calibration post-process.

The relative orientation process[45] was carried out based on an autocorrelation algorithm[37], which identified sets of common points in each of the overlapped pairs of images, known as tie points. An overall error estimation of the block adjustment and the root squared mean error (RMSE) relative to each tie point was obtained.

All the flights included in this work were carried out in very similar light conditions due to short-time consumption by the UAV system for completing each of missions. That was the reason why by-default parameters of a correlator algorithm were used, taking into account that a previous visual inspection of images did not show dramatic shadow troubles nor histograms significant differences.

The absolute orientation process[45] was applied using a Helmert 3D transformation, which uses translation, rotation and scale changing, based on the coordinates of three measured points following the criteria explained in Location of the GCPs for the absolute orientation process section. The

photogrammetric block was fit to the Universal Endlap Mercator UTM coordinate system, northern hemisphere and zone number 30, with the European Terrestrial Reference System 1989, the official datum in Spain, and the geoidal model Ibergeo.

Once the photogrammetric block is adjusted and re-projected to the reference system, a three-dimensional point cloud is built through the unique block generated. After editing and noise filtering, a triangulated surface is derived from the point cloud. Due to grid DEMs being more frequently used to define the terrain morphology than triangular DEMs, DEMs with a new grid scheme were obtained, with one point each 0.5 m being interpolated by the radial basis function method[45, 46].

The DEM and the adjusted mosaic of images are the input data to the orthorectification process, consisting on two steps: a reprojection of the mosaic based on the morphology of DEM, then an interpolation process applying the nearest neighbour algorithm[47] to fill all possible gaps in the orthoimages. The spatial resolution of the obtained orthoimages from all the photogrammetric projects was 0.01 m/pixel.

3.1.2. QUALITY CONTROL

To control the accuracy of the obtained DEMs and orthoimages by including all possible sources of errors, a rigorous statistical study was applied to all the photogrammetric projects that were performed. The well-known RMSE value[48, 49] was calculated by comparing the true coordinates of the check points, which were measured using a high precision GPS device, and the obtained coordinates from both the cartographic products at the same check points. Therefore, the number and spatial distribution of the statistical sample of the check points were designed taking into account the accessibility limits of the cut slope and the statistical criteria to arrive at a quality control metric based on a representative sample of the surface morphology at a certain confidence level. Furthermore, the RMSE value is used in this paper to establish an objective criterion to compare the relative accuracy between different photogrammetric projects.

Orthoimages contain only planimetric information, whereas DEMs contain both planimetry and altimetry. Therefore, planimetric and altimetric statistics

were estimated separately and designated as RMSExy and RMSEz, respectively. See equation (1) and equation (2):

$$RMSE_{xy} = \sqrt{RMSE_x^2 + RMSE_y^2} = \sqrt{\frac{(Ex_1^2 + \ldots + Ex_{N-3}^2) + (Ey_1^2 + \ldots + Ey_{N-3}^2)}{N-3}} \quad (1)$$

where RMSEx and RMSEy represent the RMSEs for both the X and Y axes, respectively, Ex_i and Ey_i are the differences between the true X and Y coordinates measured using GPS and the X and Y coordinates obtained from the orthoimages at the *i*-order control point, respectively, and N is the total number of target points registered during the surveying campaign. Three of the target points are reserved for use as GCPs in the absolute orientation process:

$$RMSE_z = \sqrt{\frac{(Ez_1^2 + \ldots + Ez_{N-3}^2)}{N-3}} \quad (2)$$

where RMSEz represents the RMSE for the Z axis and Ez_i is the difference between the true Z coordinates measured using the GPS and the Z coordinates obtained from the DEM at the *i*-order check point.

Because the targets points were not always perfectly visible in the orthoimages due to sunlight reflections, the corresponding Ex_i and Ey_i were weighted based on the following criterion: high confidence identified points were given a weight factor of $w_i = 0.7$ and low confidence identified points were given a weight factor of $w_i = 0.3$. In these cases, equation (1) is reformulated to become equation (3):

$$RMSE_{xy} = \sqrt{\frac{(Ex_1^2 w_1 + \ldots + Ex_{N-3}^2 w_{N-3}) + (Ey_1^2 w_1 + \ldots + Ey_{N-3}^2 w_{N-3})}{(w_1 + \ldots + w_{N-3})}} \quad (3)$$

3.2. LOCATION OF THE GCPS FOR THE ABSOLUTE ORIENTATION PROCESS

Once the relative orientation of the photogrammetric blocks is completed, the assignment of absolute coordinates must be performed to register the project over an official projection system for Spain. The absolute orientation in this work was carried out by a rigorous Helmert 3-D transformation, which implies the solution of a transformation system of equations with seven unknowns: three translation vector components, three rotation angles and a scale factor. To determine the transformation system, the 3-D coordinates of the three GCPs must be known, which use X, Y and Z coordinates for two of them and a Z coordinate for the third one, reaching the same number of equations and unknowns.

The Helmert algorithm relies on a linear procedure. Hence, nonlinear distortions are considered over the cut slope surface. This is assumed due to the small size of the target surface and the relative uniformity of its slope.

Nevertheless, this hypothesis must be confirmed via quality control. The three GCPs must be located to try to represent as well as possible the variability in X, Y and Z at the site of the study. However, accessibility troubles can make arriving at the optimal location difficult. Therefore, a specific flight was designed to examine the same cut slope, which consisted of three flight paths with 54 images with 80% sidelap overlap and 60% endlapping at an altitude of 50 m to study the influence that the three GCP locations have on the final cartographic product quality.

A set of 35 well-spaced targets points, located at the top or the bottom of the cut slope, were measured with a high precision GPS device.

Then, the photogrammetric block obtained from the relative orientation was absolutely oriented using six sets of three GCPs selected from the 35 target points to obtain six photogrammetric projects, designated L1 to L6 (Fig. 5), with their corresponding orthoimages and DEMs. Once again, the selected GCPs used to carry out the absolute orientation were excluded from the quality control assessment. The remaining 33 target points were used as check points for quality control carried out for each of the six projects and followed the same method described in quality control section.

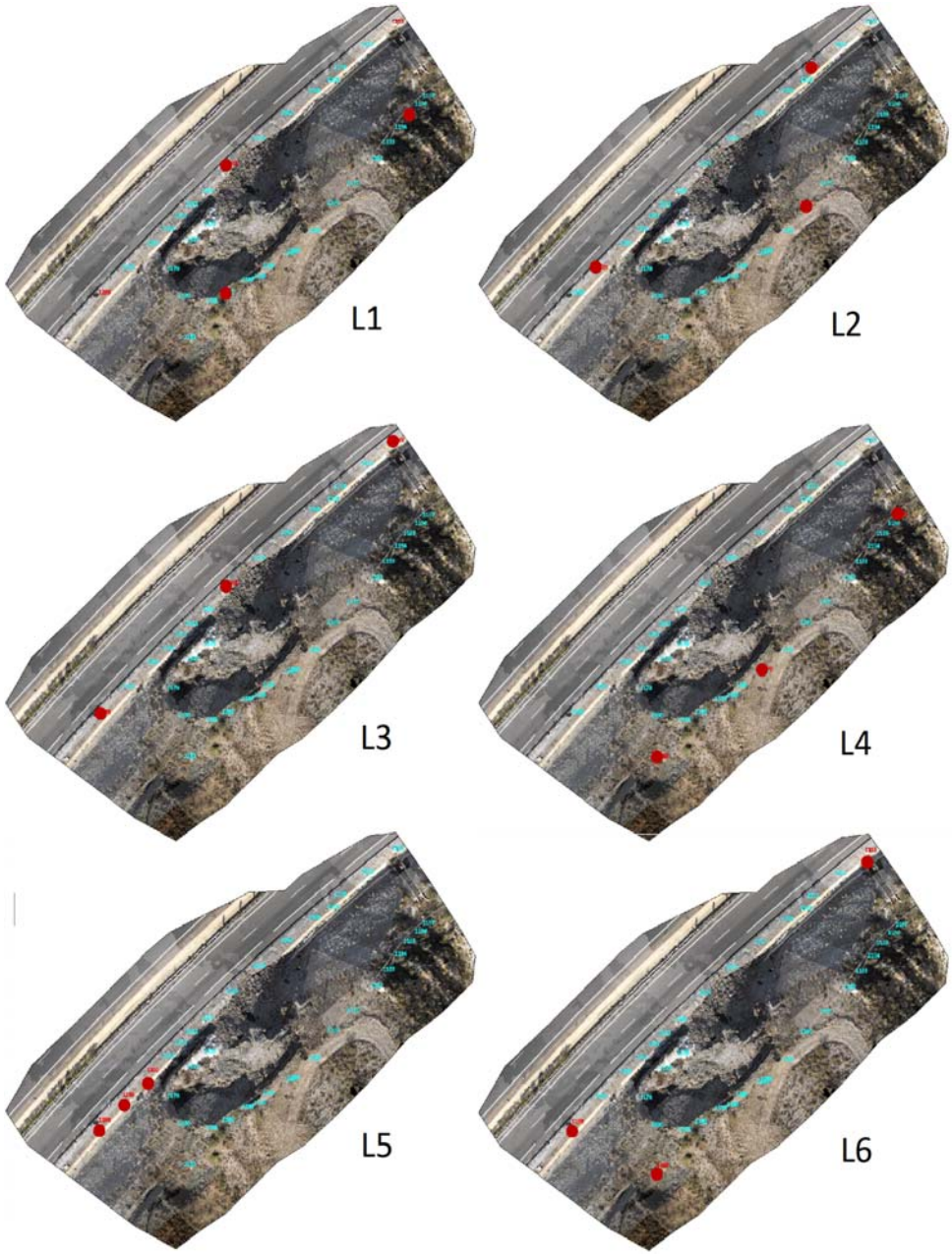

FIG. 5. Distribution of the 35 target points over the cut slope surface. Projects L1 to L6 show the six sets of the chosen three GCPs used to generate the six photogrammetric projects.

4. RESULTS AND DISCUSSION

4.1. SAMPLE SIZE

Orthoimages obtained from the photogrammetric projects contain 14,000x14,000 pixels, which may be considered infinite for the purposes of the sample size estimation. The number of check points N to distribute in an orthoimage to achieve a statistically representative sample is estimated using equation (4):

$$N = \frac{Z^2 \sigma^2}{e^2} \quad (4)$$

where Z is a statistic reliability parameter that measures the reliability and depends on the confidence level, σ^2 is the variance of the population and e is the acceptable sample error.

The variance of population relative to the RMSE associated with the check points is unknown *a priori*. Therefore, σ=0.05 obtained from Ref.[50] under similar conditions is used here. Table 2 shows the sample sizes obtained at different confidence levels and acceptable sample errors.

		e (%)			
Confidence level (%)	Z	1	2	3	4
90	1.65	68	17	8	4
95	1.96	96	24	11	6
98	2.24	125	31	14	8
99	2.58	166	41	18	10

TABLE 2. Sample size defined by the number of check points depending on the confidence level and acceptable sample error, e.

A total number of 64 check points were measured over the four photogrammetric projects designed to study axis image orientation. The results imply that we can achieve a sample error of < 2% with a confidence of 99%. However, 32 check points were measured and designated to be used to

study the influence of the Helmert GCP location, which implies a sample error of less than 2% with a confidence of 98%.

The total error obtained after correcting the differential data recorded by the GPS device was estimated through a total RMS of 0.0124 m at a 95% level of confidence.

4.2. EFFECTS THAT THE THREE GCP LOCATIONS USED IN ABSOLUTE ORIENTATION HAVE ON THE QUALITY OF THE DEMS AND ORTHOIMAGES

The planned flight for this purpose covered the entire extension of the cut slope with three parallel strips of 18 images each. All the images were taken on the vertical axis, using 85% and 60% sidelap and endlapp, respectively.

Although image distortion introduced by the camera lens was corrected analytically by the photogrammetric software, the deformations were geometrically checked. Figure 6 shows how the straight lines are rectified after the distortion correction process.

FIG. 6. (a) One of the original images taken in the flight (b) the same image after distortion error correction.

The relative orientation process was carried out by identifying sets of common tie points in each overlapping pair of images. A total number of 8,451 tie points were automatically identified during the relative orientation process using 54 images, which was sufficient to cover the entire target surface. A total of 41 main overlaps were identified between the images.

Relative orientation is carried out using an iterative method, which calculates the overall error estimation of the block adjustment. The RMSE relative to each tie point is used. After the fourth iteration, the system converged. The overall error was 0.607 pixels, and the maximum RMSE was 0.832 pixels.

Six photogrammetric projects were derived from the adjusted block by processing the absolute orientation based on the GCPs represented in Fig. 5, and designated L1 to L6. Each was processed following the same workflow. The 3-D point clouds were generated by autocorrelation and well-distributed over the model (Fig. 7).

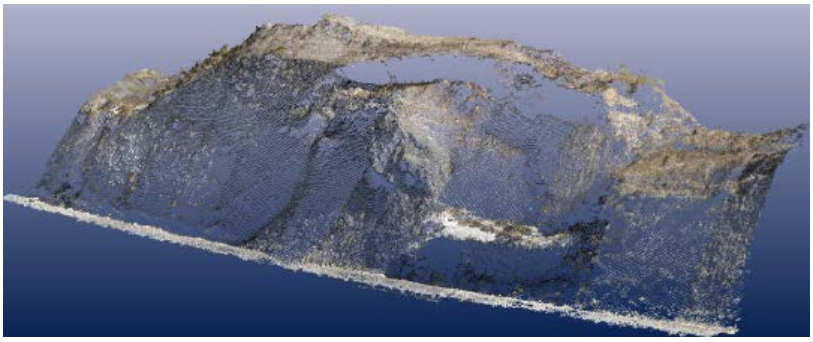

FIG. 7. Point cloud covering the entire cut slope obtained by the autocorrelation algorithm and following the normal distribution function.

After editing and noise filtering over the point clouds, a triangulated surface with ~150,000 triangles was derived from ~78,000 mesh points over the six projects. Then a DEM from each of the six projects was extracted with 234 rows and 286 columns. Therefore, six corresponding orthoimages were obtained, using one interpolated point for each 0.5 m interval and by registering and resampling the images from these DEMs.

Quality control was applied to each of the DEMs and orthoimages. The X, Y and Z residuals are adjusted to a normal distribution over the six projects by the Kolmogorov-Smirnov test[51].

Figure 8 shows the photogrammetric projects for which absolute orientation was carried out using three aligned GCPs in the bottom of the cut slope, such as L3 and L5, which exhibited high RMSEs. In contrast, L1, L2, L4 and L6 have at least one GCP in the top of the cut slope, dramatically reducing both the RMSEs.

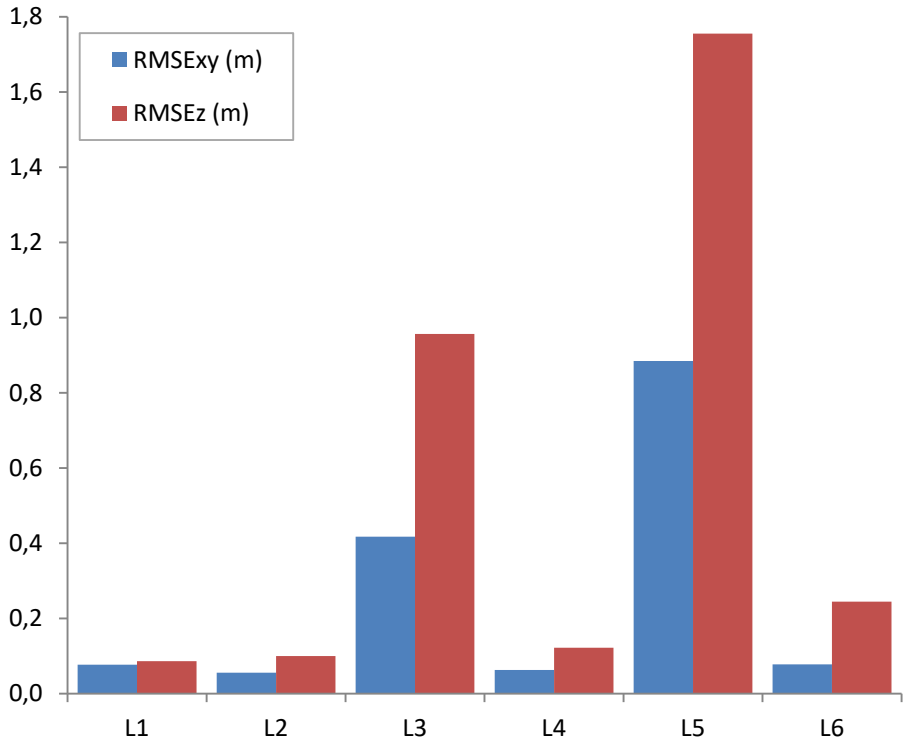

FIG. 8. Planimetric and altimetric RMSE (m), obtained from the six photogrammetric projects L1 to L6.

In this subgroup of projects (L1, L2, L4 and L6), L6 exhibits the highest RMSE due to the GCPs being located at the bottom of the cut slope and not well centered. This is followed by L4, which has no GCP at the bottom of the cut slope. This fact suggests that the GCP has to be centered and distributed between the top and bottom, which was only observed for L1 and L2.

Project L2 exhibits three small advantages with respect to L1: the vector sum of the planimetric and altimetric RMSEs is lower than L1, its corresponding orthoimage has fewer errors, and its GCP accessibilities are better than L1's.

4.3. ORTHOGONAL AXIS ORIENTATION TO THE CUT SLOPE VS. VERTICAL AXIS PHOTOGRAMMETRIC PROJECTS

Two photogrammetric flights were carried out for comparison proposes. One had the orthogonal axis pointed at the cut slope for only one path with nine images containing a 75% overlap and the other had the vertical axis pointed

at the cut slope with two paths and 36 images containing 75% sidelapping and endlapping. In both photogrammetric flights, the front part of the drone and the camera support were orthogonal to flight direction for better angle camera control and for achieving the orthogonally of the images with respect to the cut slope. Thus, sidelapping was established along the flight direction.

A photogrammetric project was processed from the orthogonal flight, following the previously described workflow, and designated as A1. Three projects were extracted from the vertical flight that considered the sidelap, endlap and both types of overlaps, respectively, and designated A2, A3 and A4. The locations of the GCPs used for absolute orientation in the four projects matches that used on the L2 project.

Table 3 summarizes some characteristics of photogrammetric projects A1 to A4, including the number of overlaps that were used to extract point clouds covering the entire cut slope.

Project	Axis orientation	Paths	Images	% Overlap	Type of overlaps	Number of overlaps
A1	Orthogonal	1	9	75	Sidelap	8
A2	Vertical	2	18	75	Sidelap	34
A3	Vertical	2	18	75	Sidelap and Endlap	52
A4	Vertical	2	18	75	Endlap	18

TABLE 3. Characteristics of photogrammetric projects A1 to A4.

The point cloud density has a suitable accuracy of ~5,000 points per overlap. In this sense, A1 covers the target surface with fewer points and, consequently, fewer interpolated triangles, ~86,000, are used to represent the surface. This is in opposition to A3, which uses 52 overlaps and delivers 125,000 triangular surfaces. Projects A2 and A4 are in an intermediate position between A1 and A3. Due to the orthogonal orientation to the target surface in A1, this project is the most efficiently designed and reaches the

desired accuracy using less data. Furthermore, fewer computational resources are required.

Applying the radial basis function algorithm, the regular 0.5 m/pixel DEMs were interpolated from A1 to A4. This was always performed after the filtering and editing processes to produce four 0.01 m/pixel orthoimages (Fig. 9).

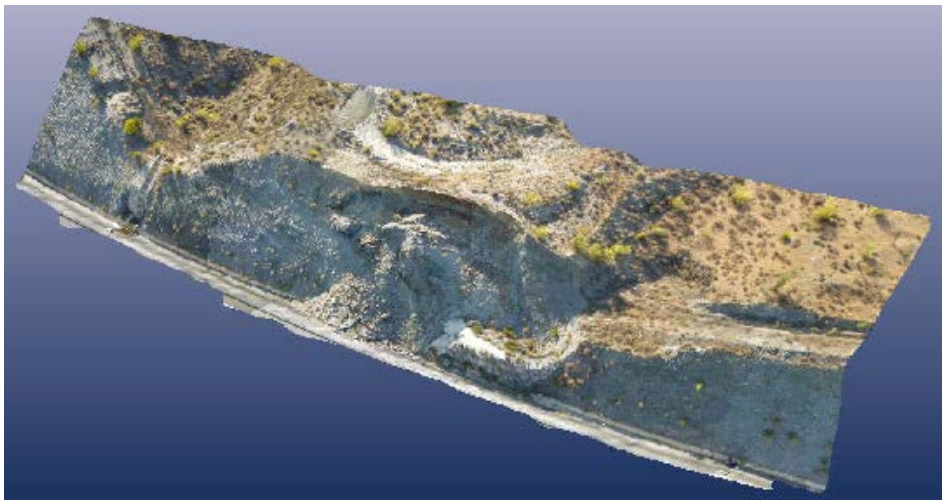

FIG. 9. Perspective view of the MDS of the A1 photogrammetric project, draped with the texture obtained from the corresponding orthoimage.

For quality control, a small set of GCPs caused visibility troubles in the orthoimages, due to unpredictable reflections of the target points. This was solved by weighting the residuals in the RMSE calculations. Table 4 shows the planimetric and altimetric RMSEs for the four projects.

	A1	A2	A3	A4
RMSExy	0.058	0.064	0.071	0.079
RMSEz	0.100	0.100	0.172	0.181

TABLE 4. Planimetric and altimetric RMSEs of photogrammetric projects A1 to A4, expressed in m.

In photogrammetric projects in which endlapping existed were used, such as A3 and A4, the errors were higher. The reason for this is that lateral areas of the images exhibit higher distortion errors due to increased distance from the centre of the image.

Comparing A1 and A2, the altimetric errors are practically the same, whereas the planimetric errors are similar. Even A1 is somewhat smaller, which is quite remarkable since the management of the orthogonal axis is much simpler, both for outdoor campaigns and postprocessing, resulting in fewer errors than vertical orientation of principal axis versus oblique orientation.

5. CONCLUSIONS

Two conclusions were derived from this work and corresponded to the established objectives. For the location of the GCPs to assign absolute coordinates to a photogrammetric project and in the context of a landslide cut slope, the three GCPs do not have to be aligned. One GCP has to be well centred in the cut slope, and the other two GCPs have to be far from each other and on the bottom of the cut slope. Summarizing, the triangle formed by GCPs needs to have as large an area as possible, with a vertex in the centre of the top line of the cut slope and the other two vertices on both ends of the bottom of the cut slope. This configuration is very convenient for this type of surface for which accessibility is complicated.

With respect to the orientation of the image axes, the new UAV-Ph technique can be applied in a landslide cut slope context, and orienting the images axes orthogonal to the target surface avoids endlapping.

Finally, planimetric and altimetric errors of 0.058 and 0.100 m, respectively, are suitable for engineering projects related to the repair and management of landslides in road cut slopes.

ACKNOWLEDGMENTS

This work was supported by the grant P08-TEP-3870 from CICE-Junta de Andalucía (Spain), and co-financed with FEDER funds from the European Union.

REFERENCES

1. C. Hugenholtz et al., "Earthwork volumetrics with an unmanned aerial vehicle and softcopy photogrammetry," J. Surv. Eng. 141, 06014003 (2015).

2. A. Nelson, H. I. Reuter, and P. Gessler, "DEM production methods and sources," in Geomorphometry Concepts, Software, Applications, T. Hengl and H. I. Reuter, Eds., pp. 65–85, Elsevier, Amsterdam, The Netherlands (2009).

3. S. D'Oleire-Oltmanns et al., "Unmanned aerial vehicle (UAV) for monitoring soil erosion in Morocco," Remote Sens. 4, 3390–3416 (2012).

4. D. Turner, A. Lucieer, and C. Watson, "An automated technique for generating georectified mosaics from ultra-high resolution unmanned aerial vehicle (UAV) imagery, based on struc- ture from motion (SfM) point clouds," Remote Sens. 4, 1392–1410 (2012).

5. M. Rieke et al., "High-precision positioning and real-time data processing of UAV-Systems," in Conf. on Unmanned Aerial Vehicle in Geomatics Int. Archives of the Photogrammetry, Remote Sensing and Spatial Information Sciences, Zurich, Switzerland, Vol. XXXVIII-1/C22, p. 6 (2011).

6. F. J. Mesas-Carrascosa et al., "Positional quality assessment of orthophotos obtained from sensors onboard multi-rotor UAV platforms," Sensors 14, 22394–22407 (2014).

7. M. Ai et al., "A robust photogrammetric processing method of low-altitude UAV images," Remote Sens. 7, 2302–2333 (2015).

8. F. J. Ayala et al., "Manual de taludes," in Serie Geotecnia, Instituto Geográfico y Minero de España Madrid, España, Spain (1987).

9. N. Brodu and D. Lague, "3D terrestrial lidar data classification of complex natural scenes using a multi-scale dimensionality criterion: applications in geomorphology," ISPRS J. Photogramm. Remote Sens. 68, 121–134 (2012).

10. A. H. Sallenger et al., "Evaluation of airborne topographic lidar for quantifying beach changes," J. Coastal Res. 19(1), 125–133 (2003).

11. J. M. Wheaton et al., “Accounting for uncertainty in DEMs from repeat topographic surveys: Improved sediment budgets,” Earth Surf. Processes Landforms 35, 136–156 (2010).

12. I. Colomina and P. Molina, “Unmanned aerial systems for photogrammetry and remote sensing: a review,” ISPRS J. Photogramm. Remote Sens. 92, 79–97 (2014).

13. J. Kim et al., “UAV photogrammetry for topographic monitoring of coastal areas,” ISPRS J. Photogramm. Remote Sens. 104, 101–111 (2015).

14. F. Mancini et al., “Using unmanned aerial vehicles (UAV) for high-resolution reconstruction of topography: the structure from motion approach on coastal environments,” Remote Sens. 5, 6880–6898 (2013).

15. F. Agüera et al., “Multi-temporal imaging using an unmanned aerial vehicle for monitoring a sunflower crop,” Biosyst. Eng. 132, 19–27 (2015).

16. A. Mathews and J. Jensen, “Visualizing and quantifying vineyard canopy LAI using an unmanned aerial vehicle (UAV) collected high density structure from motion point cloud,” Remote Sens. 5, 2164–2183 (2013).

17. E. Hunt et al., “Acquisition of NIR-green-blue digital photographs from unmanned aircraft for crop monitoring,” Remote Sens. 2, 290–305 (2010).

18. G. Verhoeven, “Providing an archaeological bird’s eye view—An overall picture of ground- based means to execute low-altitude aerial photography (LAAP) in archaeology,” Archaeol. Prospect. 16, 233–249 (2009).

19. G. Verhoeven et al., “Helikite aerial photography (HAP)—a versatile means of unmanned, radiocontrolled, low-altitude aerial archaeology,” Archaeol. Prospect. 16, 125–138 (2009).

20. A. Rango et al., “Unmanned aerial vehicle-based remote sensing for rangeland assessment, monitoring, and management,” J. Appl. Remote Sens. 3, 033542 (2009).

21. G. Pajares, “Overview and current status of remote sensing applications based on unmanned aerial vehicles (UAVs),” Photogramm. Eng. Remote Sens. 81, 281–330 (2015).

22. H. Eisenbeis, "UAV photogrammetry," PhD Doctor, Institut für Geodäsie und Photogrammetrie, Zürich, Switzerland (2009).

23. C. H. Hugenholtz et al., "Geomorphological mapping with a small unmanned aircraft sys- tem (sUAS): Feature detection and accuracy assessment of a photogrammetrically-derived digital terrain model," Geomorphology 194, 16–24 (2013).

24. N. Haala et al., "Performance test on UAV-based photogrammetric data collection, international archives of the photogrammetry," Remote Sens. Spat. Inf. Sci. 38, 7–12 (2011).

25. F. Remondino et al., "UAV photogrammetry for mapping and 3D modeling– current status and future perspectives, international archives of the photogrammetry," Remote Sens. Spat. Inf. Sci. 38(1/C22), 25–31 (2011).

26. C. Strecha, "Automated photogrammetric techniques on ultralight UAV imagery," in Proc. of the 53rd Photogrammetric Week, Institut für Photogrammetrie, Universität Stuttgart, pp. 289–294 (2011).

27. Q. Liu et al., "A new approach to fast mosaic UAV images, ISPRS International Archives of the Photogrammetry," Remote Sens. Spat. Inf. Sci. 38, 271–276 (2011).

28. T. Eyndt and W. Volkmann, UAS as a tool for surveyors: from tripods and trucks to virtual surveying, GIM Int. 27, 20–25 (2013).

29. W. Feng, W. Yundong, and Z. Qiang, "UAV borne real-time road mapping system," in Joint Urban Remote Sensing Event, pp. 1–7 (2009).

30. N. Metni and T. Hamel, "A UAV for bridge inspection: visual servoing control law with orientation limits," Autom. Constr. 17, 3–10 (2007).

31. T. Rosnell and E. Honkavaara, "Point cloud generation from aerial image data acquired by a quadrocopter type micro unmanned aerial vehicle and a digital still camera," Sensors 12, 453–480 (2012).

32. M. A. R. Cooper and S. Robson, "Theory of close range photogrammetry," in Close Range Photogrammetry and Machine Vision, 1st ed., K. B. Atkinson,

Eds., pp. 9–50, Whittles Publishing, Caithness, Scotland, United Kingdom (1996).

33. W. A. Kamal and R. Samar, “A mission planning approach for UAV applications,” in 47th IEEE Conf. Decision and Control, pp. 3101–3106 (2008).

34. M. J. Westoby et al., “Structure-from-motion’ photogrammetry: a low-cost, effective tool for geoscience applications,” Geomorphology 179, 300–314 (2012).

35. L. Javernick, J. Brasington, and B. Carusoa, “Modeling the topography of shallow braided rivers using structure-from-motion photogrammetry,” Geomorphology 213, 166–182 (2014).

36. M. A. Fonstad et al., “Topographic structure from motion: a new development in photogrammetric measurement,” Earth Surf. Processes Landforms 38, 421–430 (2013).

37. F. Ackermann, “Digital image correlation: performance and potential application in photogrammetry,” Photogramm. Rec. 11, 429–439 (1984).

38. E. Baltsavias et al., “High-quality image matching and automated generation of 3D tree models,” Int. J. Remote Sens. 29, 1243–1259 (2008).

39. C. Heipke, “Automation of interior, relative, and absolute orientation,” ISPRS J. Photogramm. Remote Sens. 52, 1–19 (1979).

40. A. Fusiello and F. Crosilla, “Solving bundle block adjustment by generalized anisotropicProcrustes analysis,” ISPRS J. Photogramm. Remote Sens. 102, 209–221 (2015).

41. Microdrones GmbH, “UAV case studies: over 1000 satisfied microdrones customers,” 2011, http://www.microdrones.com/ (13 April 2015).

42. Photomodeler, Measuring and Modeling the Real World, “Mesauring and modeling the realworld,” http://www.photomodeler.com/ (13 April 2015).

43. Trimble website, Transforming the way the world works, “Transforming the way the world works,” http://www.trimble.com/ (13 April 2015).

44. Red Andaluza de Posicionamiento, Portal de Posicionamiento de Andalucía, "Portal de posicionamiento de andalucía," http://www.ideandalucia.es/portal/web/portal-posicionamiento/ rap (13 April 2015).

45. P. R. Wolf, Elements of Photogrammetry, McGraw Hill, New York (1983).

46. R. Webster and M. A. Oliver, Statistical Methods in Soil and Land Resource Survey, Oxford University, Oxford, United Kingdom (1990).

47. J. A. Richards and X. Jia, Remote Sensing Digital Image Analysis, 3rd ed., Springer-Verlag, Berlin, Germany (1999).

48. S. Harwin and A. Lucieer, "Assessing the accuracy of georeferenced point clouds produced via multi-view stereopsis from unmanned aerial vehicle (UAV) imagery," Remote Sens. 4, 1573–1599 (2012).

49. E. Rupnik et al., "Aerial multi-camera systems: accuracy and block triangulation issues," ISPRS J. Photogramm. Remote Sens. 101, 233–246 (2015).

50. F. Carvajal, F. Agüera, and M. Pérez, "Surveying a landslide in a road cut slope using unmanned aerial vehicle photogrammetry," in Proc. of the ISPRS ICWG I/V UAV-g (Unmanned Aerial Vehicle in Geomatics) Conf. Int. Archives of the Photogrammetry, Remote Sensing and Spatial Information Sciences, Zurich, Switzerland (2011).

51. J. P. Royston, "Expected normal order statistics (exact and approximate)," Appl. Stat. 31, 161–165 (1982).

CAPÍTULO 2:

ACCURACY OF DIGITAL SURFACE MODELS AND ORTHOPHOTOS DERIVED FROM UNMANNED AERIAL VEHICLE PHOTOGRAMMETRY

Publicado como:

Agüera-Vega, F., Carvajal-Ramírez, F., and Martínez-Carricondo, P. (2016). "Accuracy of Digital Surface Models and Orthophotos Derived from Unmanned Aerial Vehicle Photogrammetry." J. Surv. Eng. , 10.1061/(ASCE)SU.1943-5428.0000206 , 04016025.

CAPÍTULO 2. ACCURACY OF DIGITAL SURFACE MODELS AND ORTHOPHOTOS DERIVED FROM UNMANNED AERIAL VEHICLE PHOTOGRAMMETRY

ABSTRACT

This paper explores the influence of flight altitude, terrain morphology and the number of Ground Control Points (GCPs) on Digital Surface Model (DSM) and orthoimage accuracies obtained with Unmanned Aerial Vehicle (UAV) photogrammetry. For this study, 60 photogrammetric projects were carried out, considering five terrain morphologies, four flight altitudes (i.e. 50, 80, 100 and 120 m) and three different numbers of GCPs (i.e. 3, 5 and 10). The UAV was a rotatory wing platform with eight motors and the sensor was a non-metric mirrorless reflex camera. The Root Mean Square Error (RMSE) was used to assess the accuracy of the DSM (Z component) and orthophotos (X, Y and XY components $RMSE_X$, $RMSE_Y$ and $RMSE_{XY}$, respectively).

The results show that $RMSE_X$, $RMSE_Y$ and $RMSE_{XY}$ were not influenced by flight altitude or terrain morphology. For horizontal accuracy, differences between terrain morphologies were observed only for 5 or 10 GCPs were used, whick were the best accuracies for the flattest morphologies. Nevertheless, the number of GCPs influenced the horizontal accuracy; as the number of GCPs increased, the accuracy improved. Vertical accuracy was not influenced by terrain morphology, but both flight altitude and the number of GCPs had significant influence on $RMSE_Z$; as the number of GCPs increased, the accuracy improved. Regarding flight altitude, vertical accuracy decreased as flight altitude increased. The most accurate combination of flight altitude and number of GCPs was 50 m and 10 GCPs, respectively, which yielded $RMSE_X$, $RMSE_Y$, $RMSE_{XY}$ and $RMSE_Z$ values equal to 0.038, 0.035, 0.053 and 0.049 m, respectively.

In view of these results, the map scale according to the legacy American Society for Photogrammetry and Remote Sensing (ASPRS) map standard of 1990 will be approximately 1:150, and an equivalent contour interval of 0.150 m is sufficient for most civil engineering projects.

Keywords: Unmanned Aerial Vehicle (UAV), photogrammetry, Digital Surface Model (DSM), orthophoto

1. INTRODUCTION

The availability of digital terrain information and orthoimages at high spatial and temporal resolution and accuracy is of increasing importance for all activities that require accurate topographic data sets (Mancini et al., 2013; Hugenholtz et al., 2015). The use of Unmanned Aerial Vehicles (UAVs) with non-metric digital cameras to recover this information is being investigated to overcome the limitations of classical techniques (Nex and Remondino, 2014). UAVs are a relatively new type of remote sensing platform that has distinct advantages over conventional piloted aircrafts and satellites, especially their low cost, operational flexibility and better spatial and temporal resolution (Laliberte et al., 2010; Harwin and Lucieer, 2012; Hugenholtz et al., 2013). From the point of view of the scene dimensions, there is a gap between conventional airborne and very-high-resolution satellite imagery mapping applications that can be filled by UAVs (Nex and Remondino, 2014). In such cases, UAVs require less time in data acquisition and therefore reduce the cost compared to that for classical manned aircraft (Aber et al., 2010). Furthermore, the capital value of UAVs is much lower than manned aircraft, and so the per-hour cost is also lower.

Moreover, UAV imagery provides results at resolution and accuracy that cannot currently be met by satellite-derived products (Immerzeel et al., 2014); more important is that the spatial resolution from UAV imagery is better than that which manned aircraft sensors can achieve. The significant development of these systems in recent years and the miniaturization of sensors have increased the civil applications of UAVs (Lambers et al., 2007). From the time at which the first balloons were used to carry photogrammetric sensors until now, the development of aerial platforms and associated technology for this use has been huge. A detailed description of this evolution and the state-of-the-art can be found in Colomina and Molina (2014). Furthermore, a review of the applications of UAV in civil engineering in general and in three-dimensional (3D) mapping applications in particular can be found in Liu et al. (2014) and Nex and Remondino (2014), respectively.

The integration of photogrammetry and computer vision (Atkinson, 1996; Hartley and Zisserman, 2003) has provided advances in automation as a result of the possibility of collecting images from different heights and in different

directions, greater flexibility and high-quality results (Fernández et al., 2015). As a result of these developments, the Structure-from-Motion (SfM) technique is widely applied. SfM is a photogrammetric technique that automatically solves the geometry of the scene, the camera positions, and the orientation without requiring a priori specification of a network of targets that have known 3D positions (Snavely et al., 2007; Westoby et al., 2012, Vasuki et al., 2014). SfM incorporates multi-view stereopsis (MSV) techniques (Furukawa and Ponce, 2007), which derive the 3D structure from overlapping photography acquired from multiple locations and angles. Lowe (2004) and Snavely et al. (2007) applied the Scal-Invariant-Feature-Transform (SIFT) operator for key-point detection for generating 3D point clouds from photographs. Certain studies concluded that this operator is one of the most robust to large image variations (Remondino and El-Hakim, 2006; Juan and Gwun, 2009). Recently, research was carried out using UAV imagery and SfM techniques with geomorphologic and terrain mapping purposes; Harwin and Lucieer (2012) evaluated the accuracy of the point cloud generated from UAV imagery for natural landscape mapping using open source software that uses the SfM technique. They found accuracies of 0.025–0.040 m when the flight planning ensured a high degree of overlap (70–95%) between images and a clearly visible sufficient number of Ground Control Points (GCPs) were distributed evenly throughout the study area. Turner et al. (2012) used a rotary wing UAV with a digital single lens reflex (DSLR) camera to generate georectified mosaics with accurate results. Anders et al. (2013) produced Digital Surface Models (DSMs) using imagery taken from a fixed-wing UAV. For images taken 90 m above ground level (AGL), the absolute deviation achieved in the DSM was 0.350 m; with images taken at 180 m, the absolute deviation was 0.450 m. Lucieer et al. (2013) generated a high-resolution DSM of Antarctic moss beds from UAV imagery and obtained an overall root mean square error (RMSE) of 0.420 m. Mancini et al. (2013) studied the creation and validation of point clouds and DSM of a beach dune system using images taken by a rotary-wing UAV equipped with a DSLR camera. They also compared their results to those from a Terrestrial Laser Scanner (TLS) survey. The UAV-based approach was demonstrated to be straightforward, and the accuracy of the vertical data set was comparable to that obtained by TLS technology. More recently, Immerzeel et al. (2014) applied the UAV methodology to monitor glacier dynamics. To that end, they used a fixed-

wing UAV carrying a low-cost digital camera attached to generate Digital Elevation Models (DEMs) and orthoimages with satisfactory results, and they concluded that UAV imagery provides resolution and accuracy that cannot currently be met by satellite-derived products. Lucieer et al. (2014) used UAV imagery for mapping landslide displacements. DEMs and orthoimages were exported at 1 cm resolution, resulting in a $RMSE_{XY}$ of 0.070 m and a $RMSE_Z$ of 0.062 m. Pierzchala et al. (2014) carried out a study to generate a detailed postharvest surface model using UAV photogrammetry and compared it to a preharvest surface model that was made by using airborne laser scanning to measure soil displacement. The total RMSE of the DSM produced from the UAV images was 0.082 m. Tonkin et al. (2014) used a rotary wing UAV to recover images for topographic surveys. The images were used to produce a DSM of moraines. They carried out a direct comparison between total station-based data acquisition and the UAV-SfM method. They concluded that the DSM produced from the UAV imagery was in good agreement with that from the total station survey points. Eltner et al. (2015) measured surface changes of short-term erosion events by using images taken from a rotary-wing UAV. The DSM generated from the UAV imagery was compared to a DSM produced with TLS data. They pointed out that DSMs have an accuracy of less than 1 cm; hence, the use of UAV imagery to generate DSM is an advantageous technique fot quantifying and qualifying soil surface changes at field scales. Harwin et al. (2015) investigated the impact of camera calibration method on the accuracy of derived point clouds using UAV Multiview stereopsis of a coastal cliff. They found that if a dense array of high-accuracy GCPs is deployed, and the UAV photography includes both vertical and oblique images, then camera precalibration or an on-the-job self-calibration will yield reliable models. However, the accuracy of these models decreased when the accuracy of the GCPs was degraded and when the density of the points was reduced.

Therefore, although in the literature there are increasing data comparing the accuracy of derived DSMs and orthophotos, there is still a lack of data regarding the influence of terrain morphology, flight altitude and the number of GCPs on the accuracy that can be achieved in the production of DSM and orthoimages with UAV photogrammetry.

The aim of this study was to analyze the influence of flight altitude, terrain morphology and number of GCPs on the accuracy of DSMs and orthoimages obtained with UAV photogrammetry.

2. MATERIALS AND METHODS

2.1 STUDY SITE

The study area was located in Campo de Níjar (Almería), southeast Spain (Fig. 1). This area has a semi-arid climate and an average annual rainfall of 260 mm. Nevertheless, the field dedicated to horticultural crops, including tomato, cucumber, or watermelon growing in plastic greenhouses, is growing rapidly, being currently the most dynamic zone in the province in terms of greenhouse spreading, with approximately 10000 ha concentrated in an area of 18000 ha. The water for irrigation comes from wells or a desalination station located in Carboneras, 25 km away. In both cases, the water is distributed through a network of pipes. Furthermore, many industries are represented in the area, including crop processing, plastics, greenhouses, industrial buildings, and road building. All this infrastructure requires a knowledge of the morphology of the land to carry out construction projects.

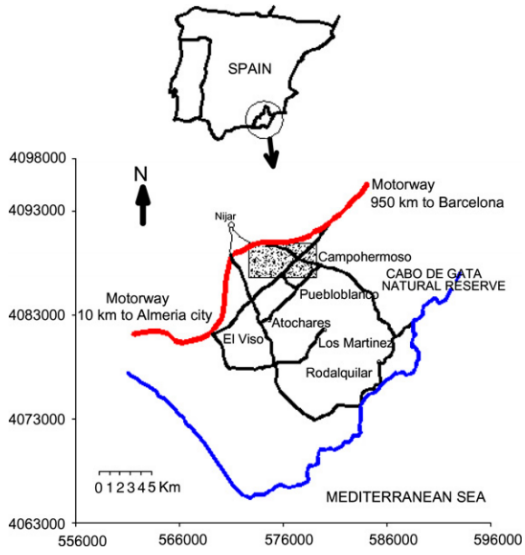

Figure 1. Location of the study area (rectangle), where main villages and roads are located. Coordinates are UTM meters (Zone 30, ETRS89).

To cover varying terrain morphologies, data used in this study were collected from five experimental surfaces in Campo de Níjar, with different topographies. Table 1 shows the southwest and the northeast coordinates of each experimental area and summarizes some relief features that are closely connected to the terrain's variability, such as standard deviation of slope, mean slope, or standard deviation of normalized normal vectors perpendicular to the topographic surface (SDUV). These parameters were calculated from a pre-existing 2 m resolution DSM by using orthometric elevations, map projection Universal Transverse Mercator (UTM) Zone 30, and European Datum 1950. The experimental surfaces were named T_1, T_2, T_3, T_4 and T_5, and were ordered from highest to lowest SDUV. Vegetation present in all these terrains is scarce and limited only to low scrub.

Table 1. Location (UTM, zone 30N, ETRS89) and general characteristics of the topographic surfaces studied.

Terrain descriptor	T_1	T_2	T_3	T_4	T_5
Minimum elevation (m)	189.90	194.57	192.82	218.37	217.95
Maximum elevation (m)	213.52	234.46	228.43	249.13	226.10
Average elevation (m)	199.67	216.89	214.05	231.31	222.47
Elevation coefficient of variation (%)	0.027	0.029	0.021	0.011	0.006
Average slope (%)	29.72	27.32	26.06	25.33	19.01
Standard deviation of slope (degrees)	18.70	19.49	18.57	17.60	17.05
Standard deviation of unitary vectors (SDUV)	0.257	0.200	0.169	0.105	0.047
X minimum	582741	582202	582606	582244	582021
Y minimum	4093462	4092827	4093477	4093452	4093939
X maximum	582889	582545	582722	582416	582165
Y maximum	4093608	4092965	4093605	4093585	4094077
Area (m^2)	21608	47334	14848	22876	19872

To obtain a better understanding of the morphology of every studied surface, Fig. 2 shows a perspective block diagram.

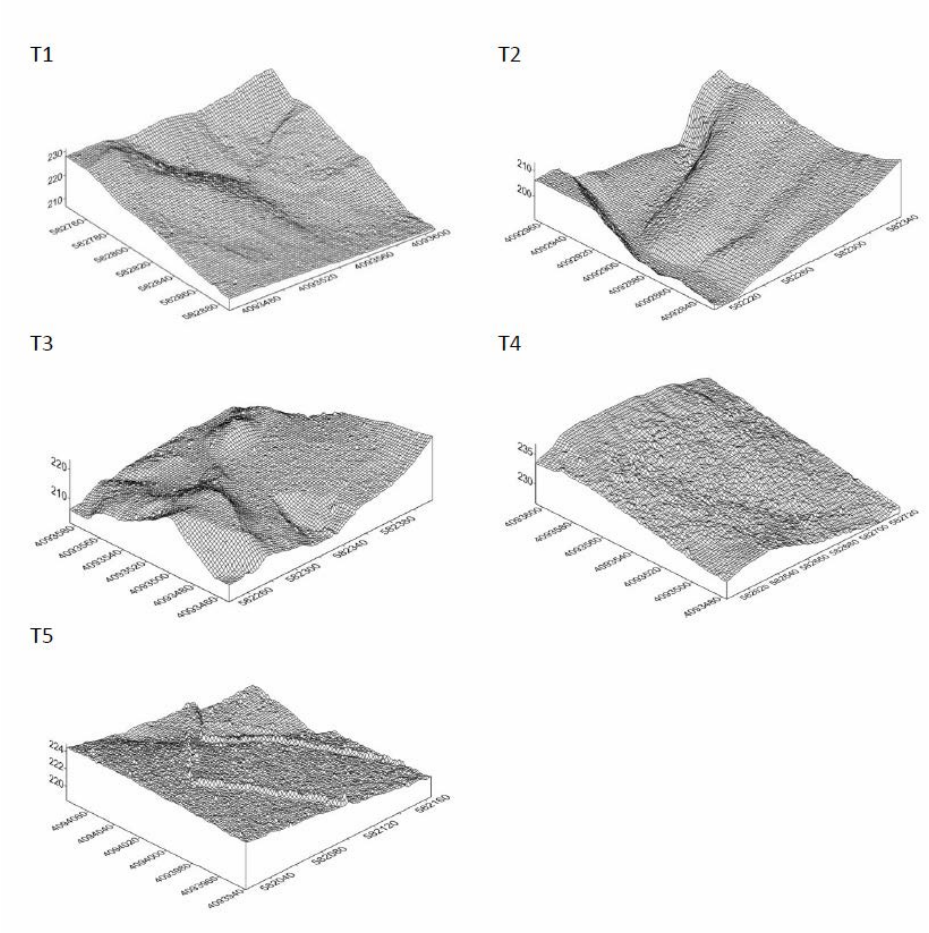

Figure 2. Perspective block diagram of every one of the five topographic surfaces studied, ordered from higher (T1) to lower (T5) standard deviation of unitary vectors.

2.2 IMAGE COLLECTION

The images used in this work were taken from a rotatory wing UAV with eight rotors and MikroKopter (Moormerland, Germany) electronic boards and motors. It has a payload of approximately 2.5 kg and is equipped with a motion-compensated gimbal for the sensor. In this case, the sensor was a Sony (Tokyo) Nex 7 digital camera with a lens of 16 mm fixed focal length. This camera had a Complementary metal-oxide semiconductor (CMOS)

sensor of 24.3 effective Megapixels, with a size of 366.6 mm^2 (23.5 mm x 15.6 mm). Fig. 3 shows the entire system.

Figure 3. UAV oktokopter used as a photogrammetric platform.

To determine the influence of flight altitude on the accuracy of DSMs and orthophotos produced, four photogrammetric projects per surface were carried out, differing in flight altitude (50, 80, 100 and 120 m). Table 2 summarizes some photogrammetric flight characteristics for each flight altitude: surfaces covered per image and ground sample distance (GSD).

Table 2. Area covered per image and GSD for every flight altitude

Flight altitude (m)	Terrain covered per image (m×m)	GSD ($m \times pixel^{-1}$)
50	72 × 49	0.012
80	115 × 78	0.019
100	143 × 98	0.024
120	172 × 117	0.029

The flight projects were carried out in navigation mode which means that the UAV flew following a previously programmed and loaded path, via the MikroKopter-Tool software. The camera was triggered every 2 seconds by a controller on the UAV, and the flight speed was set to obtain forward and side overlaps of 90% and 80%, respectively.

Before image acquisition, several targets were scattered on every studied surface for georeferencing (Ground Control Points, GCPs) and assessing the accuracy of the DSM and orthophoto (Check Points, CPs).

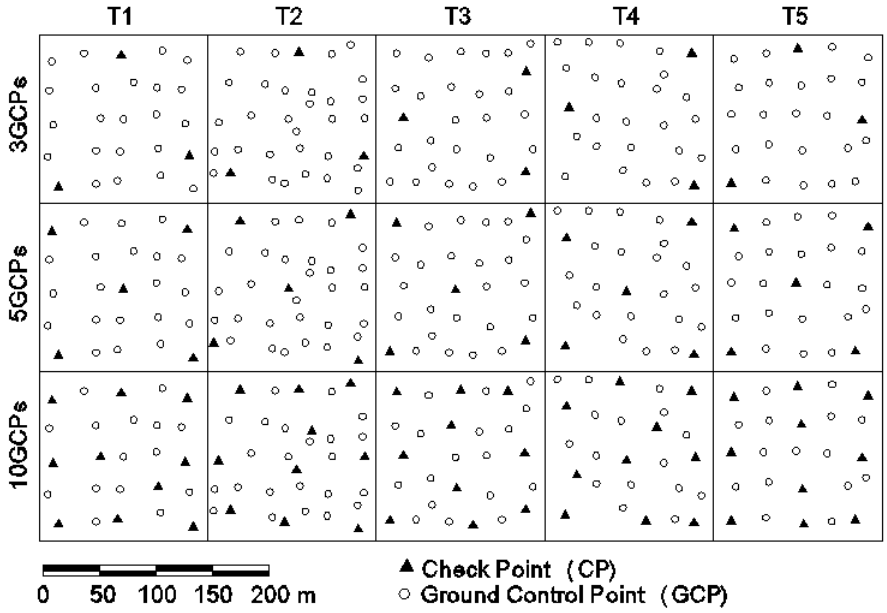

Figure 4. GCP and CP configuration for photogrammetric block, considering 3, 5 and 10 GCPs and every studied terrain. The number of CP varied depended on the case.

Fig. 4 shows the GCP and CP configuration for the photogrammetric block, considering 3, 5 and 10 GCPs, and every studied terrain. These configurations were the same for all the flights. For any combination of GCP number, the strategy in this study was to spread these points uniformly over the entirety of every experimental surface: the largest equilateral triangle inscribed (3 GCPs), 1 GCP at each corner and 1 in the middle (5 GCP), and 1 GCP at each corner and 1 at each midpoint of the sides, plus 2 GCPs around the middle. The number of targets in each terrain was 25 for T1 and T5, 33 for T2, 28 for T3, and 26 for T4. Of these amounts, 3, 5 or 10 were taken as GCPs, and the rest were taken as CPs. The 3D coordinates of these points were measured using Global Navigation Satellite Systems (GNSSs) working with differential corrections in real-time kinematic (RTK) mode, with the base station on a geodesic pillar located closer than 1 km from the studied surfaces. The 3D coordinates of the geodesic pillar, named Cerro Gordo II (Instituto Geográfico Nacional, 2015), by the Spanish National Geographic Institute are

582.655,945 m, 4.093.630,095 m and 240,883 m, respectively. The horizontal coordinates are referred to as UTM Zone 30N (European Terrestrial Reference System 1989, ETRS89) and the elevation is referred to as the mean sea level, using the EGM08 geoid model. Both rover and base GNSS receivers were Trimble R6s. For the RTK measurements, these dual-frequency geodetic instruments, which track the GPS and Global Navigation Satellite System (GLONASS) signals simultaneously, have a manufacturer's stated accuracy specification of ±8 mm+1 ppm RMS horizontal, and ±15 mm+1 ppm RSM vertical. Therefore, the maximum horizontal and vertical RMS was ±9 mm and ±16 mm, respectively.

2.3 IMAGE PROCESSING

Image processing was performed using the software package AgisoftPhotoScan Professional, version 1.0.4 (Agisoft 2013). The SfM procedure of SfM routines incorporated in PhotoScan and commonly used parameters are described in Verhoeven (2011). The workflow of this software is a three-step process. The first step is the alignment of the images by feature identification and feature matching. This task was carried out with the PhotoScan accuracy set to high. Imagery were not geotagged. The result of this step is the camera position corresponding to each picture, the internal calibration parameters and the 3D coordinates of a sparse point cloud of the terrain. In the second step, a densification of the point cloud is achieved by using the height field method that is based on pairwise depth-map computation (Agisoft, 2013), which resulted in a more detailed 3D model that could be used to identify the GCPs and CPs. The third step applies a texture to the mesh obtained in the previous step, and the point cloud is referenced to a local coordinate system (ETRS89 and frames in the UTM, in the case of this study). The bundle adjustment can be carried out using three GCPs at least, but higher accuracy results are obtained if more GCPs are used, and the recommendation is to use more than three to obtain optimal accuracy (Rosnell and Honkavaara, 2012). Taking into account this and the results of Tahar (2013), who observed that accuracy increased when the number of GCPs varied from four to nine, to study the influence of the number of GCPs used in the bundle adjustment on the accuracy of the results, this task was repeated using 3, 5 and 10 GCPs uniformly sparse on every surface, for every photogrammetric project, as described in the previous section.

Finally, the orthophoto is exported and a grid DSM can be generated from the point cloud.

2.4 ACCURACY ASSESSMENT

Taking into account all combinations of studied surfaces, flight altitude and number of GCPs used for georeferencing gives a total of 5 × 4 × 3 = 60 photogrammetric projects.

For every photogrammetric project, the accuracy assessment in easting (X), northing (Y), horizontal (XY) and height (Z), were carried out on the surveyed points that had not been used for georeferencing (CPs). Although identification of GCPs and CPs in the AgisoftPhotoScan software is performed in the imagery before running the final bundle adjustment once the photo locations have been taken out of these points and before point cloud densification and orthophoto production, the accuracy assessment was carried out from the point of view of an end-user of the products. In this way, the CPs were identified in the orthoimages and their coordinates were compared to the surveyed GNSS coordinates, resulting in $RMSE_X$, $RMSE_Y$ and $RMSE_{XY}$ horizontal accuracy measures:

$$RMSE_X = \sqrt{\frac{\sum_{i=1}^{n}(X_{Oi}-X_{GNSSi})^2}{n}} \quad (1)$$

$$RMSE_Y = \sqrt{\frac{\sum_{i=1}^{n}(Y_{Oi}-Y_{GNSSi})^2}{n}} \quad (2)$$

$$RMSE_{XY} = \sqrt{\frac{\sum_{i=1}^{n}[(X_{Oi}-X_{GNSSi})^2+(Y_{Oi}-Y_{GNSSi})^2]}{n}} \quad (3)$$

where n: number of CPs tested for this project; X_{Oi}, Y_{Oi}: X and Y coordinates, respectively, measured in the orthophoto for the i^{th} CP; and X_{GNSSi}, Y_{GNSSi}: X and Y coordinates, respectively, measured with GNSS for the i^{th} CP.

Vertical accuracy was derived in two different ways. In the first method, the height value was derived from the grid DSM for the X and Y coordinates of

the CPs on the orthoimage, and it was also compared to the GNSS observations, producing an $RMSE_{ZO}$ accuracy measure for the Z direction:

$$RMSE_{ZO} = \sqrt{\frac{\sum_{i=1}^{n}(Z_{Oi} - Z_{GNSSi})^2}{n}} \qquad (4)$$

where Z_{Oi} is the height in the i[th] CP, derived from DSM, taking into account its X and Y coordinates, measured on the orthophoto; and Z_{GNSSi}: Z coordinate of the i[th] CP measured with GNSS.

This method was followed as it would be the way that a user would determine the Z component of a point identified on the orthophoto. Nevertheless, this method, to some degree, removes the effect of the horizontal error from the process. Therefore, the second way to assess the vertical accuracy was to compute the difference between the DSM and GNSS measured CPs. Then, the RMSE was calculated as follows:

$$RMSE_{ZD} = \sqrt{\frac{\sum_{i=1}^{n}(Z_{Di} - Z_{GNSSi})^2}{n}} \qquad (5)$$

where Z_{Di} is the height in the i[th] CP, derived from DSM, taking into account its X and Y coordinates, measured with GNSS; and Z_{GNSSi}: Z coordinate of the i[th] CP measured with GNSS.

For each photogrammetric project, the orthophoto and DSM were generated at a resolution equal to its own ground pixel size. The DSM was derived from the generated point clouds by using the inverse distance to square power, taking into account the eight nearest points. Then, the distance from the interpolated grid point to the eight nearest points used for interpolation was less than 15 cm. In this way, the generated DSM fit with the points cloud.

3. RESULTS AND DISCUSSION

Fig. 5 shows $RMSE_X$, $RMSE_Y$ and $RMSE_{XY}$ for every terrain morphology studied, the number of GCPs and the flight altitudes. In Fig. 5, solid lines represent mean values considering the five terrain morphologies. In general, for every number of GCPs, the values of $RMSE_X$ and $RMSE_Y$ were quite similarly independent of flight altitude, which had no significant influence on the accuracy of X and Y. For $RMSE_X$, the ranges of variation were 0.135–0.224 m

for 3 GCPs (0.089 m), 0.036–0.088 m for 5 GCPs (0.052 m), and 0.018–0.059 m for 10 GCPs (0.041 m). For $RMSE_Y$, the ranges of variation were 0.118–0.195 m for 3 GCPs (0.077 m), 0.025–0.081 m for 5 GCPs (0.056 m), and 0.022–0.063 m for 10 GCPs (0.041 m). For $RMSE_{XY}$, the ranges of variation were 0.183–0.286 m for 3 GCPs (0.103 m), 0.046–0.108 m for 5 GCPs (0.062 m), and 0.028–0.081 m for 10 GCPs (0.053 m). For easting and northing components and 3 GCPs, all values were aproximately 0.150 m; for 5 GCPs these values were around 0.05 m, and for 10 GCPs practically all values were under 0.050 m. For 3 GCPs, $RMSE_{XY}$ was around 0.225 m, aproximately 0.075 m for 5 GCPs and aproximately 0.050 m for 10 GCPs. These ranges are summarized in Table 3. In all cases, the maximum RMSE values were found for 3 GCPs, whereas minimum values were observed for 10 GCPs. Furthermore, the ranges' amplitude decreased as the number of GCPs increased; values for the X and Y components were quite similar for each given GCP number.

Table 3. Ranges of RMSE (m) values for X, Y and XY components, taking into account the five studied surfaces and considering then GCPs number.

Number of GCP	$RMSE_x$			$RMSE_Y$			$RMSE_{XY}$		
	Min.	Max.	Range	Min.	Max.	Range	Min.	Max.	Range
3 GCPs	0.135	0.224	0.089	0.118	0.195	0.077	0.183	0.286	0.103
5 GCPs	0.036	0.088	0.052	0.025	0.081	0.062	0.046	0.108	0.062
10 GCPs	0.018	0.059	0.041	0.028	0.081	0.053	0.022	0.028	0.006

For all morphologies studied, horizontal accuracy improved as the number of GCPs increased. The horizontal accuracy increment (RMSE decrement) was higher from 3 to 5 GCPs than for 5 to 10 GCPs; these increments were similar for all terrains and flight altitudes. Taking into account all terrains and flight altitudes, the mean RMSE increments of horizontal components from 3 to 5 GCPs were -0.107 m, -0.109 m and -0.152 m for X, Y and XY components respectively, whereas the RMSE increments of these components from 5 to 10 GCPs were -0.019 m, -0.013 m and -0.023 m for X, Y and XY components respectively.

In general, when the GSD increases because the flight altitude increases, horizontal accuracy tends to decrease. Nevertheless, the results of this study show that horizontal accuracy was not influenced by flight altitude. In this case, the increment of GSD went from 1.2 cm, for 50 m flight altitude to 2.9 cm for 120 m flight altitude (Table 2), which was insufficient to yield differences in horizontal accuracy.

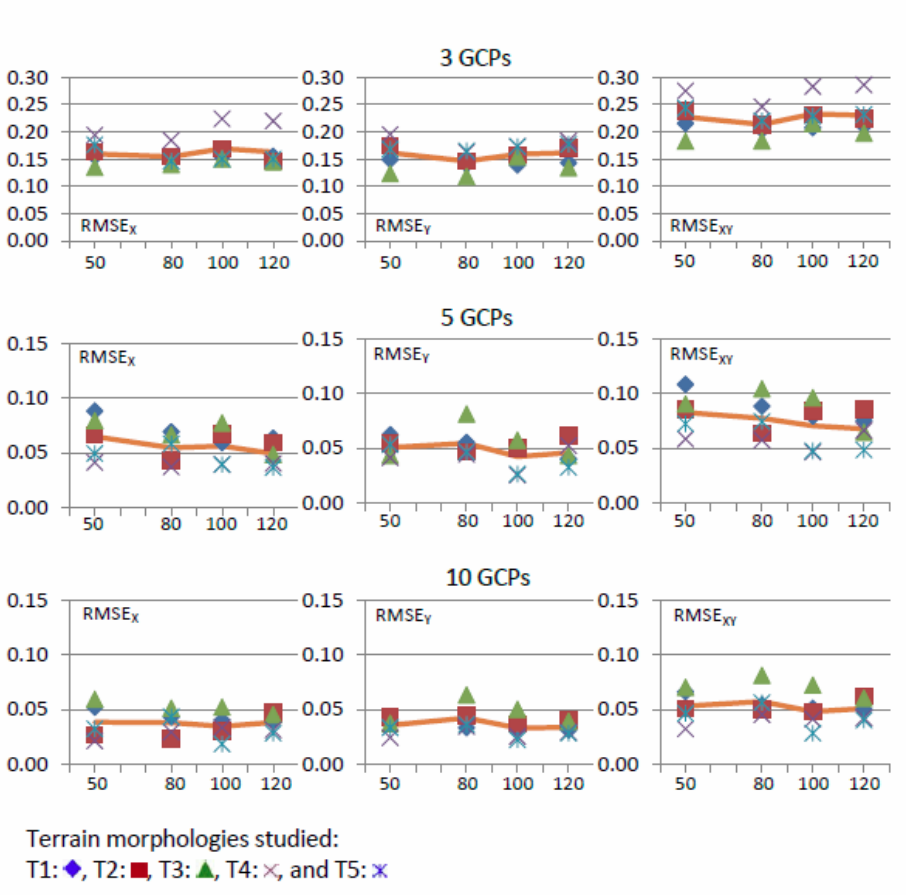

Figure 5. $RMSE_X$, $RMSE_Y$ and $RMSE_{XY}$ (m) for every terrain morphology studied, number of GCPs and flight altitude (m). Solid lines represent mean values considering the five terrain morphologies studied.

Furthermore, for a given number of GCPs, Fig. 5 does not show any significant horizontal accuracy differences between the studied morphologies: these differences were smaller as the number of GCPs increased. Very small horizontal accuracy differences between morphologies were observed for only for 5 and 10 GCPs between the flattest terrains (T4 and T5, lowest

horizontal RMSE values) and the rest. If the terrain complexity differences had been higher, the differences between the horizontal accuracies would have been higher, too.

Fig. 6 shows $RMSE_{ZO}$ and $RMSE_{ZD}$ calculated with Eqs. (4) and (5), respectively, for each flight altitude and terrain. In Fig. 6, solid lines represent mean values considering the five terrain morphologies. The ranges of variation for $RMSE_{ZD}$ were 0.072–0.176 m for 3 GCPs (0.104 m), 0.052–0.170 m for 5 GCPs (0.118 m), and 0.032–0.080 m for 10 GCPs (0.049 m). $RMSE_{ZO}$ values were 0.043–0.160 m for 3 GCPs (0.117 m), 0.010–0.170 m for 5 GCPs (0.160 m), and 0.025–0.080 m for 10 GCPs (0.055 m). Fig. 7 shows $RMSE_{ZO}$ versus $RMSE_{ZD}$ values for all photogrammetric projects. In all cases for a given project, $RMSE_{ZO}$ was lower than $RMSE_{ZD}$.

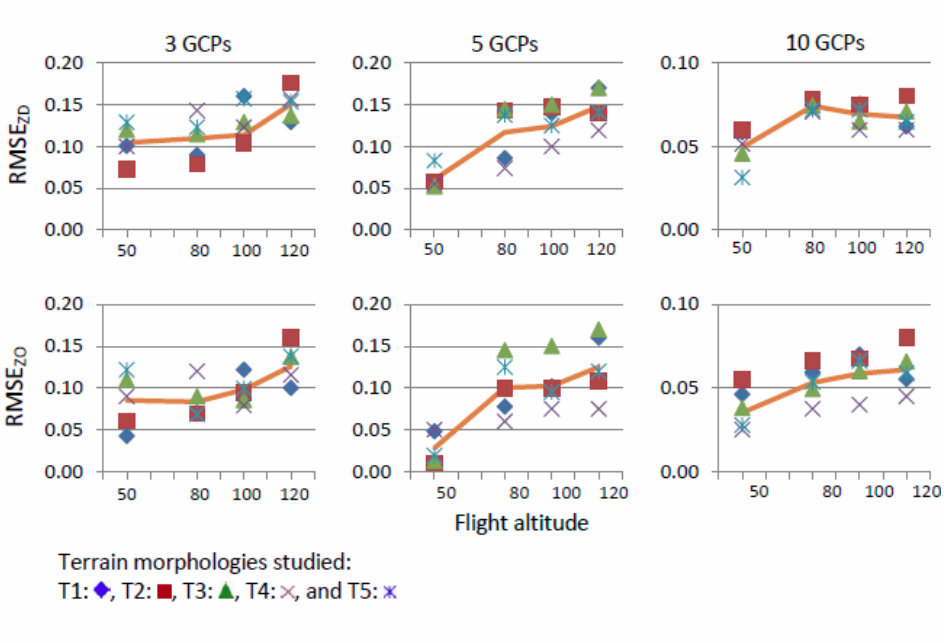

Figure 6. $RMSE_{ZD}$ and $RMSE_{ZO}$ (m) versus flight altitude (m), for every terrain morphology studied and number of GCPs. Solid lines represent mean values considering the five terrain morphologies studied.

For all studied terrains, the lowest values were found for 50 m flight altitude and 10 GCPs. For 3 and 5 GCPs, the $RMSE_{ZO}$ and $RMSE_{ZD}$ trends were to increase when the flight altitude increased: taking into account the five studied terrains, the average $RMSE_{ZD}$ for 50, 80, 100 and 120 m flight altitude

was 0.104 m, 0.110 m, 0.114 m and 0.151 m, respectively, for 3 GCPs, and 0.060 m, 0.117 m, 0.120 m and 0.148 m, respectively, for 5 GCPs. For 10 GCPs, the $RMSE_{ZD}$ value for the 50 m flight altitude (0.049 m) increased to 0.074 m for the 80 m flight altitude and to 0.069 for the 80 to 100 m altitude, maintaining practically the same value from the 100 m to the 120 m flight altitude (0.068 m). For the 50, 80, 100 and 120 m flight altitude, the equivalent values for $RMSE_{ZO}$ were 0.085 m, 0.084 m, 0.098 m and 0.126 m, respectively, for 3 GCPs, and 0.028 m, 0.100 m, 0.102 m and 0.125 m, respectively, for 5 GCPs. For 10 GCPs, the $RMSE_{ZO}$ increased from the 50 m (0.035 m) to the 80 m flight altitude (0.053 m), maintaining the same value for the 100 m (0.059 m) and 120 m flight altitudes (0.061 m). In all cases, $RMSE_{ZO}$ values were lower than their equivalents $RMSE_{ZD}$ values. This is, as has been explained before, because the method for calculating $RMSE_{ZO}$ removes the effect of the horizontal error from the process. If the Z coordinate of a point identified on the orthophoto is to be calculated, $RMSE_{ZO}$ will be the correct accuracy.

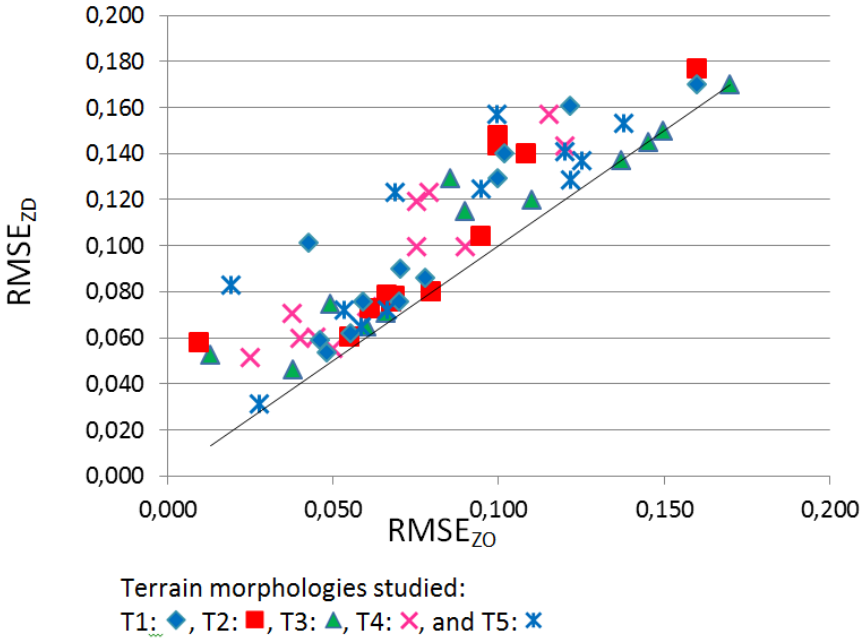

Figure 7. $RMSE_{ZO}$ versus $RMSE_{ZD}$, (m), for every photogrammetric project studied. Straight line represents 1:1 line.

If $RMSE_{ZD}$ values for 10 GCPs are studied separately according to flight altitude, a significant linear correlation can be observed between the average slope of every terrain (Table 1) and its corresponding $RMSE_{ZD}$ (r=0.918), for the 50 m flight altitude. This trend was similar for the other flight altitudes, but the correlation coefficients were not significant (0.579, 0.151, 0.148 for the 80 m, 100 m and 120 m flight altitude, respectively). Correlation coefficients were similar when the studied relation was SDUV versus $RMSE_{ZD}$. Therefore, when the conditions were optimal for higher vertical accuracy (i.e. 50 m flight altitude and 10 GCPs), there was a relationship between vertical accuracy and terrain complexity: more complex terrain was associated with a higher $RMSE_{ZD}$. The minimum $RMSE_{ZD}$ (0.032 m)was found for the flattest terrain (T5), and the maximum $RMSE_{ZD}$ (0.059 m) was found for the more complex terrain (T1). In view of these results, it can be concluded that both flight altitude and number of GCPs influence the vertical accuracy in all studied cases.

Regarding the number of GCPs, there are few studies that were concerned with the influence on the accuracy results of photogrammetric projects from UAVs. Most of them only reported the number of GCPs that were used. Tahar (2013) concluded that different configurations in distribution and number of GCPs (from 4 to 9) contributed different errors in the photogrammetric block. This work concluded that the most accurate results are reached from 8 GCPs. Although the number of GCPs used was different, the results of this study showed the same trend. Niethammer et al. (2012) generated a digital terrain model from a quad-rotor UAV-based image data set taken between 100 and 200 m as the flight altitude (0.030–0.080 m GSD), using 16 GCPs with VMS close range photogrammetry software (VMS, 2010) and an image-matching algorithm from University College London, on an area of 850 x 250 m. They found a mean horizontal error equal to 0.5 m and in the vertical direction an RMSE equal to 0.310 m. In an Antarctic environment site of approximately 200 x 100 m, Lucieer et al. (2014) used a fixed number of 12 GCPs in a UAV photogrammetric project with an altitude of 50 m above ground level. They used the Agisoft Photoscan Professional (0.85) software for the 3D reconstruction of terrain features.They also observed a geometric accuracy of 0.060 m in planimetry and 0.044 m in the Z component, which are both similar to the results presented here for a combination of 10 GCPs and 50 m flight altitude: the mean values, considering the five morphologies, of $RMSE_X$,

$RMSE_Y$, $RMSE_{XY}$ and $RMSE_Z$ were 0.038 m, 0.033 m, 0.051 m and 0.049 m respectively. Turner et al. (2012), working in similar conditions to those of Lucieer et al. (2014), found accuracies of 0.100 m and 0.150 m in the XY and Z components, respectively.

Mancini et al. (2013), worked with the same software, a flight altitude of 40 m and 10 GCPs. In their conclusions, they supposed that a reduction in the number of GCPs will not influence the accuracy, and will reduce the effort for acquiring ground-based references for the georeferencing of SfM products. This conclusion disagrees with the results shown in Figs. 5 and 6, which indicate that values of horizontal and vertical RMSEs decreased when the number of GCPs increased from 5 to 10. Hugenholtz et al. (2015), with a rotatory-wing UAV, 10 GCPs and 100 m flying height, performed two aerial surveys of a stockpile before and after a portion of this pile was excavated and reported vertical RMSE values of 0.106 m and 0.097 m, respectively. These results are worse than all results observed in any of the terrains studied here, taking into account 10 GCPs and 100 m flight altitude, which ranged from 0.060 m to 0.075 m. This poorer accuracy might be associated with the GCP distribution, which was positioned around the stockpile and was not uniformly sparse. Cryderman et al. (2014) carried out a study on a stockpile, too, by using a fixed-wing UAV with a flight altitude of 118 m and taking into account 11 GCPs. They yielded values of $RMSE_{XY}$ equal to 0.039 m, which agrees with the results observed in this study. Nevertheless, the value of $RMSE_Z$ reached by Cryderman et al. (2014) was 0.049 m, whereas the equivalent $RMSE_{ZD}$ value in the present study (120 m flight altitude and 10 GCPs) was 0.068 m; it was necessary to fly at 50 m to reach an accuracy of 0.049 m. Udin and Ahmad (2014) used an UAV system for large-scale stream mapping, and compared the accuracies of the orthophotos and DSMs by using the horizontal and vertical RMSE values at several flight altitudes (i.e. 40, 60, 80 and 100 m), which were associated with GSDs ranging from 1.5 to 3.6 cm. They worked with 23 GCPs on only one terrain. Their results showed that $RMSE_{XY}$ values had no clear trend when the flight altitude varied, which is similar to the results obtained in the present study. Furthermore, $RMSE_Z$ values increased with flight altitude, in agreement with the trend of vertical RMSE observed in the present study.

4. CONCLUSIONS

In this study, several kinds of terrain morphologies, flight altitudes and number of GCPs for a georeferencing task were taken into account to evaluate the accuracy of DSMs and orthophotos produced from images taken from a mirroless reflex camera mounted on a rotatory wing UAV.

The results obtained demonstrate that neither the studied terrain morphologies nor flight altitude have a significant bearing on the accuracy of X, Y or XY. For the size and resolution of the camera sensor used in this work and the range of flight altitudes covered (50–120 m), the GSD ranged from 1.2 cm to 2.7 cm and did not influence the horizontal accuracy. For horizontal accuracy, very small differences between terrain morphologies were observed only when 5 or 10 GCPs were used, which were the best accuracies fot the flattest morphologies (T4 and T5).

The number of GCPs has a significant influence on the accuracy of X, Y and XY; the highest values are obtained with 10 GCPs. Furthermore, differences between terrain morphologies in horizontal accuracy decrease as the number of GCPs increases.

Regarding the Z accuracy, terrain morphology has a significant bearing on this component only for optimal conditions (i.e., 50 m flight altitude and 10 GCPs). In this case, higher accuracies are obtained for the flattest terrains. A similar trend is observed for other flight altitudes studies, although the relationship was not as evident as that observed under optimal conditions.

For the studied flight altitudes, Z accuracy decreases when flight altitude increases. Both $RMSE_{ZO}$ and $RMSE_{ZD}$ increases with flight altitude are more notable for 3 and 5 GCPs than for 10 GCPs. For 10 GCPs, $RMSE_Z$ increases at 50 to 80 m flight altitudes; at altitudes from 80 to120 m, it is almost constant.

The most accurate combination of flight altitude and number of GCPs studied in this work is 50 m and 10 GCPs, which yields mean $RMSE_X$, $RMSE_Y$, $RMSE_{XY,}$ $RMSE_{ZD}$ and $RMSE_{ZO}$ values equal to 0.038 m, 0.035 m, 0.053m, 0.049 m and 0.035 m, respectively. For 10 GCPs and 80, 100 or 120 m flight altitude, horizontal accuracy values are quite similar to those found for 50 m flight altitude, and $RMSE_{ZD}$ increases to 0.074 m, 0.069 m and 0.068 m for 80, 100 and 120 m flight altitude, respectively.

According to the American Society for Photogrammetry and Remote Sensing (ASPRS) positional accuracy standards for digital geospatial data (ASPRS, 2015) and taking into account the mean $RMSE_X$ (0.038 m), $RMSE_Y$ (0.035 m), $RMSE_{XY}$ (0.053 m) and $RMSE_Z$ (0.049 m) values for 10 GCPs and 50 m flight altitude, the horizontal and vertical accuracies at the 95% confidence level are equal to 0.092 m and 0.096 m respectively. The equivalent map scale according to the legacy ASPRS map standard of 1990 (ASPRS, 1990) will be approximately 1:150, and an equivalent contour interval is 0.150 m.

The results of this study come from experiments carried out under a wide range of conditions (viz. terrain morphologies, flight altitudes and number of ground control points), and support the findings of other researchers with respect to the accuracy and mapping suitability of UAV photogrammetry.

ACKNOWLEDGMENTS

This work was supported by grant P08-TEP-3870 from CICE-Junta de Andalucía (Spain) and was co-financed with European Union FEDER funds.

REFERENCES

Aber, J. S., Marzolff, I., and Ries, J. B. (2010). Small-format aerial photography: Principles, techniques and geoscience applications, Elsevier, Amsterdam, the Netherlands.

Agisoft (2013). Agisoft PhotoScan user manual: Professional edition, versión 1.0.0, Agisoft, St. Petersburg, Russia.

Anders, N.,Masselink, R., Keesstra, S., and Suomalainen, J. (2013). "High- Res digital surface modeling using fixed-wing UAV-based photogrammetry." http://geomorphometry.org/Anders2013 (June 6, 2016).

ASPRS (American Society for Photogrammetry and Remote Sensing). (2015). "ASPRS positional accuracy standards for digital geospatial data." Photogramm. Eng. Remote Sens., 81(3), A1–A26.

ASPRS (American Society for Photogrammetry and Remote Sensing). (1990). "ASPRS accuracy standards for large-scale maps."

http://www.asprs.org/a/society/committees/standards/1990_jul_1068-1070.pdf (Jan. 22, 2015).

Atkinson, K. (1996). Close range photogrammetry and machine vision, Whittles Publishing, Caithness, Scottland.

Colomina, I., and Molina, P. (2014). "Unmanned aerial systems for photogrammetry and remote sensing: A review." ISPRS J. Photogramm. Remote Sens., 92(Jun), 79–97.

Cryderman, C., Mah, S. B., and Shufletoski, A. (2014). "Evaluation of a UAV photogrammetric accuracy for mapping and earthworks computation." Geomatica, 68(4), 309–317.

Eltner, A., Baumgart, P., Maas, H., and Faust, D. (2015). "Multi-temporal data for automatic measurement of rill and interrill erosion on loess soil." Earth Surf. Processes Landforms, 40(6), 741–755.

Fernández, J., González, D., Rodríguez, P., and Mancera, J. (2015). "Image-based modelling from unmanned aerial vehicle (UAV) photogrammetry: An effective, low-cost tool for archaeological applications." Archaeometry, 57(1), 128–145.

Furukawa, Y., and Ponce, J. (2007). "Accurate, dense, and robust multiview stereopsis." Proc., 2007 IEEE Conf. on Computer Vision and Pattern Recognition, Vol. 1, IEEE, Piscataway, NJ, 1–8.

Hartley, R., and Zisserman, A. (2003). Multiple view geometry in computer vision, Cambridge University Press, New York.

Harwin, S., and Lucieer, A. (2012). "Assessing the accuracy of georeferenced point clouds produced via multi-view stereopsis from unmanned aerial vehicle (UAV) imagery." Remote Sens., 4(6), 1573–1599.

Harwin, S., Lucieer, A., and Osborn, J. (2015). "The impact of the calibration method on the accuracy of point clouds derived using unmanned aerial vehicle multi-view stereopsis." Remote Sens., 7(9), 11933–11953.

Hugenholtz, C. H., Walker, J., Brown, O., and Myshak, S. (2015). "Earthwork volumetrics with an unmanned aerial vehicle and softcopy photogrammetry." J. Surv. Eng., 10.1061/(ASCE)SU.1943-5428.0000138, 06014003.

Hugenholtz, C. H., et al. (2013). "Geomorphological mapping with a small unmanned aircraft system (sUAS): Feature detection and accuracy assessment of a photogrammetrically-derived digital terrain model." Geomorphology, 194, 16–24.

Immerzeel, W. W., et al. (2014). "High-resolution monitoring of Himalayan glacier dynamics using unmanned aerial vehicles." Remote Sens. Environ., 150, 93–103.

Instituto Geográfico Nacional. (2015). Centro Nacional de Información Geográfica. ftp://ftp.geodesia.ign.es/Red_Geodesica/Hoja1046/104639.pdf (Aug. 15, 2015).

Juan, L., and Gwun, O. (2009). "A comparison of SIFT, PCA-SIFT and SURF." Int. J. Image Process, 3(4), 143–152.

Laliberte, A. S., Herrick, J. E., Rango, A., and Winters, C. (2010). "Acquisition, orthorectification, and object-based classification of unmanned aerial vehicle (UAV) imagery for rangeland monitoring." Photogramm. Eng. Remote Sens., 76(6), 661–672.

Lambers, K., et al. (2007). "Combining photogrammetry and laser scanning for the recording and modelling of the Late Intermediate Period site of Pinchango Alto, Palpa, Peru." J. Archaeolog. Sci., 34(10), 1702–1712.

Liu, P., et al. (2014). "A review of rotorcraft unmanned aerial vehicle (UAV) developments and applications in civil engineering." Smart Struct. Syst., 13(6), 1065–1094.

Lowe, D. G. (2004). "Distinctive image features from scale-invariant keypoints." Int. J. Comput. Vis., 60(2), 91–110.

Lucieer, A., Turner, D., King, D. H., and Robinson, S. A. (2013). "Using an unmanned aerial vehicle (UAV) to capture micro-topography of Antarctic moss beds." Int. J. Appl. Earth Obs. Geoinf., 27(part A), 53–62.

Lucieer, A., de Jong, S. M., and Turner, D. (2014). "Mapping landslide displacements using structure from motion (SfM) and image correlation of multi-temporal UAV photography." Prog. Phys. Geogr., 38(1), 97–116.

Mancini, F., et al. (2013). “Using unmanned aerial vehicles (UAV) for high-resolution reconstruction of topography: The structure from motion approach on coastal environments.” Remote Sens., 5(12), 6880–6898.

MikroKopter-Tool [Computer software]. MikroKopter, Moormerland, Germany.

Nex, F., and Remondino, F. (2014). “UAV for 3D mapping applications: A review.” Appl. Geomatics, 6(1), 1–15.

Niethammer, U., James, M. R., Rothmund, S., Travelletti, J., and Joswig, M. (2012). “UAV-based remote sensing of the Super-Sauze landslide: Evaluation and results.” Eng. Geol., 128, 2–11.

Pierzchala, M., Talbot, B., and Astrup, R. (2014). “Estimating soil displacement from timber extraction trails in steep terrain: Application of an unmanned aircraft for 3D modelling.” Forest, 5(6), 1212–1223.

Remondino, F., and El-Hakim, S. (2006). “Image-based 3D modelling: A review.” Photogramm. Rec., 21(115), 269–291.

Rosnell, T., and Honkavaara, E. (2012). “Point cloud generation from aerial image data acquired by a quadrocopter type micro unmanned aerial vehicle and a digital still camera.” Sensors, 12(1), 453–480.

Snavely, N., Seitz, S. M., and Szeliski, R. (2007). “Modeling the world frominternet photo collections.” Int. J. Comput. Vision, 80(2), 189–210.

Tahar, K. N. (2013). “An evaluation on different number of ground control points in unmanned aerial vehicle photogrammetric block.” Int. Arch. Photogramm. Remote Sens. Spatial Inf. Sci., XL-2/W2, 93–98.

Tonkin, T. N., Midgley, N. G., Graham, D. J., and Labadz, J. C. (2014). “The potential of small unmanned aircraft systems and structure-frommotion for topographic surveys: A test of emerging integrated approaches at Cwm Idwal, North Wales.” Geomorphology, 226, 35–43.

Turner, D., Lucieer, A., and Watson, C. (2012). “An automated technique for generating georectified mosaics from ultra-high resolution unmanned aerial vehicle (UAV) imagery, based on structure from motion (SfM) point clouds.” Remote Sens., 4(125), 1392–1410.

Udin, W. S., and Ahmad, A. (2014). "Assessment of photogrammetric mapping accuracy based on variation flying altitude using unmanned aerial vehicle." IOP Conf. Ser. Earth Environ. Sci., 18(1), 012027.

Vasuki, Y., Holden, E. J., Kovesi, P., and Micklethwaite, S. (2014). "Semiautomatic mapping of geological structures using UAV-based photogrammetric data: An image analysis approach." Comput. Geosci., 69(Aug), 22–32.

Verhoeven, G. J. (2011). "Taking computer vision aloft—Archaeological three-dimensional reconstructions from aerial photographs with Photoscan." Archaeol. Prospect., 18(1), 67–73.

VMS [Computer software]. Geomsoft, Coburg, Australia.

Westoby, M. J., Brasington, J., Glasser, N. F., Hambrey, M. J., and Reynolds, J. M. (2012). "Structure from motion photogrammetry: A low cost, effective tool for geoscience applications." Geomorphology, 179, 300–314.

CAPÍTULO 3:

ASSESSMENT OF PHOTOGRAMMETRIC MAPPING ACCURACY BASED ON VARIATION GROUND CONTROL POINTS NUMBER USING UNMANNED AERIAL VEHICLE

Enviado a revisión como:

Agüera-Vega, F., Carvajal-Ramírez, F., and Martínez-Carricondo, P. (2016). "Assessment of Photogrammetric Mapping Accuracy Based on Variation Ground Control Points Number Using Unmanned Aerial Vehicle". Measurement.

CAPÍTULO 3. ASSESSMENT OF PHOTOGRAMMETRIC MAPPING ACCURACY BASED ON VARIATION GROUND CONTROL POINTS NUMBER USING UNMANNED AERIAL VEHICLE

ABSTRACT

Digital Surface Models and orthoimages at high spatial and temporal resolution and accuracy are of increasing importance for many applications. From several years ago photogrammetry-UAV is being used to produce these topographic products. The aim of this study is to analyse the influence of the number of Ground Control Points used for georeferencing on Digital Surface Model and orthoimage accuracies obtained with UAV-photogrammetry. In this purpose, 160 images were taken on a 17.64 ha surface at 120 m altitude above ground level, and five replications of photogrammetric projects taking into account 4, 5, 6, 7, 8, 9, 10, 15, and 20 GCPs were made. Root Mean Square Error (RMSE) was used as accuracy measurement.

Optimal results for $RMSE_X$, $RMSE_Y$ and $RMSE_{XY}$ mean±standard deviation values were reached for 15 GCPs: 3.3±0.346, 3.2±0.441, 4.6±0.340 and 4.5±0.169 cm respectively. Similar conclusion was derived for vertical accuracy: lower $RMSE_Z$ mean±standard deviation values were reached for 15 and 20 GCPs: 5.8±1.21 cm and 4.7±0.860 cm respectively.

In view of these results maps at 1:150 scale and contour interval of 15 cm can be obtained from UAV-photogrammetry.

Keywords: UAV, Photogrammetry, Georeferencing, Orthophoto, Accuracy evaluation.

1. INTRODUCTION

Digital Surface Models (DSM) and orthoimages at high spatial and temporal resolution and accuracy is of increasing importance for many applications [1,2]. From several years ago, Unmanned Aerial Vehicles (UAVs) with non-metric digital cameras are being used to produce these topographic products because they have distinct advantages over conventional piloted aircrafts and satellites, especially their low cost, operational flexibility and better spatial and temporal resolution [3,4,5,6]. UAVs require less time in data acquisition therefore reduce the cost in comparison with classical manned aircraft [7].

The great development of these systems in recent years and the miniaturization of sensors have increased the civil applications of UAVs [8]. A detailed description of UAV evolution and applications can be found in [9]. Furthermore, a review of the applications of UAV in civil engineering in general is made in [10], and a review of UAV applications in 3D mapping can be found in [11].

As a result of the integration of photogrammetry and computer vision [12,13], the Structure from Motion (SfM) technique is widely being applied because this integration allows the possibility of collecting images from different heights and in different directions, greater flexibility and high quality results [14]. SfM is a photogrammetric technique which solves automatically the geometry of the scene, the camera positions and orientation, without the need to specify a priori a network of targets which have known 3-D positions [15, 16, 17]. SfM incorporates multi-view stereopsis (MSV) techniques [18], which derives 3D structure from overlapping photography acquired from multiples angles. In [19] and [15], the Scale Invariant Feature Transform (SIFT) operator was applied for key-point detection for generating 3D point clouds from photographs. There are works concluding that this operator is one of the most robust to large image variations [20, 21]. All these developments have led to a new concept: UAV-photogrammetry.

In surveying applications is essential to geo-reference generated data in the photogrammetric process, which can be applied by measuring reference targets clearly visible in the images that were scattered on the ground before the flight or other objects as base of electricity poles, building corners, well's covers, etc. 3D coordinates of these Ground Control Points (GCPs), must be surveyed with a suitable survey method, as differential GPS or tachymetry. At least three GCPs are needed for this process, but it is recommended to use significantly more to reach better accuracies.

Recently, some works have been carried out using UAV imagery and SfM techniques with geomorphologic and terrain mapping purposes: in [4], the accuracy of the point cloud generated from UAV imagery of a natural landscape mapping using an open source software that uses SfM technique is evaluated. They found accuracies of 2.5-4.0 cm when the flight planning ensured a high degree of overlap (70%–95%) between images and clearly

visible sufficient number of Ground Control Points (GCPs) were evenly distributed throughout the study area. In [22], a study was carried out employing a rotary wing UAV with a digital single lens reflex (DSLR) camera in order to generate georectified mosaics with accurate results. In [23], high resolution DSM of Antartic moss beds was generated from UAV imagery obtaining an overall root mean square error (RMSE) of 4.2 cm. In [24], author used UAV imagery for mapping landslide displacements. DSMs and orthoimages were exported at 1 cm resolution resulting $RMSE_{XY}$ of 7.0 cm and $RMSE_Z$ of 6.2 cm. In [25], a rotary wing UAV was used to recover images for topographic surveys. The images were used to produce a DSM of moraines. In this work, authors carried out a direct comparison between a total station base data acquisition and the UAV-SfM method. They concluded that the DSM produced from the UAV imagery was in good agreement with the total station survey points. In [26], changes of short term erosion events were measured using images taken from a rotary-wing UAV. In this work, the DSM generated from the UAV imagery was compared to a DSM produced with terrestrial laser scanning data. They pointed out that DSMs have an accuracy of less than one centimetre; hence the use of UAV imagery to generate DSM is an advantageous technique to quantify and qualify soil surface changes at field scales. Uysal et al. [27], carried out an accuracy analysis of DSMs generated with UAV photogrammetry and they concluded that is possible to use this methodology as map producing, surveying and some other engineering applications with the advantages on classical methodologies of low-cost, time conservation, and minimum field work. In [28], combinations of several terrain morphologies, flight altitudes and number of GCP were used to study their influence on DSM and orthophoto accuracy. The work of Mesas-Carrascosa et al. [29], had the purpose of using the UAV remote multispectral images for spectral discrimination of bare soil and vegetation (crop and weeds). They studied the effect of combination of flight altitude, flight mode (stop and cruising modes) and GCPs configuration on weeds detection an concluded that a balance between spatial resolution and spectral discrimination is need to optimize the weed detection .Ruzgiene et al. [30], studied the quality of DSMs generated using UAV photogrammetry techniques and the influence of the number of GCPs on the accuracy. In [31], the positional quality of orthophotos obtained from images taken from a multi-rotor UAV and standard camera were studied. Results showed that the

orthophotos passed the spatial quality tests proposed by various national mapping agencies. So, although in the literature there are increasing data relative on the accuracy of derived DSMs and orthophotos and the influence of some parameters (flight altitude, camera focal length, terrain morphology, number of GCPs, etc) on the accuracy, it is necessary to deepen the understanding of the influence of these parameters to achieve better accuracies in the products derived from UAV photogrammetry.

The aim of this study is to analyse the influence of the number of GCPs on DSM and orthoimage accuracies obtained with UAV photogrammetry.

2. MATERIALS AND METHODS

2.1 STUDY SITE

The study area is located in Campo de Níjar (Almería), Southeast Spain (figure 1). The south-west and the north-east coordinates UTM (Zone 30, ETRS89) of this area are (581915, 4094210) and (582335, 4094630), respectively. So, its dimension was 420x420 m, which covers an area of 17.64 ha. The selection of the study area was based on its morphology, which includes a wide range of slope values. The elevation range is about 60 m, varying from 187 m to 247 m above mean sea level.

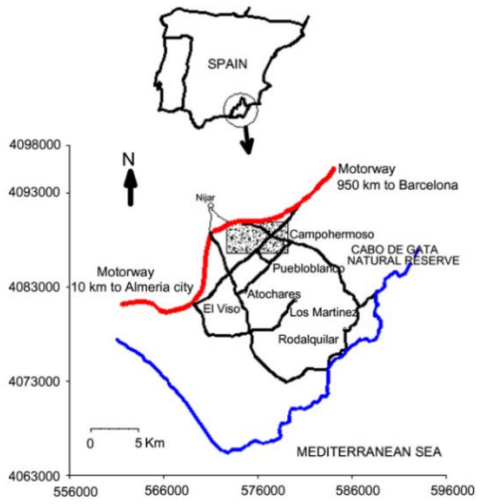

Figure 1. Location of the study area (shadow rectangle), where main villages and roads have been located.

Coordinates are UTM (Zone 30, ETRS89).

2.2 IMAGE COLLECTION

Images used in this work were taken from a rotatory wing UAV with eight rotors and MikroKopter electronic boards and motors [32]. It has a payload of 2.5 kg approximately and is equipped with a motion compensated gimbal for the sensor. In this case, the sensor was a Nikon D-3100 digital reflex camera with a lens of 16 mm fixed focal length. Figure 2 shows the entire system.

Figure 2. The UAV oktokopter used in this work as photogrammetric platform.

The flight projects were carried out in navigation mode. This means the UAV flies following a previously programmed and loaded path, via the MikroKopter-Tool software. The camera was triggered every two seconds by a controller on the UAV and the flight speed was set to get forward and side overlaps of 90% and 80% respectively. Flight altitude was 120 m above ground level which implies a surface of 190x113.75 m^2 covered by every photo and an equivalent ground sample distance of 3.291 cm.

Previous to the images acquisition, 72 targets were scattered on the studied surface for georreferencing (Ground Control Points, GCPs) and assessing the accuracy of DSM and orthophoto (Check Points, CPs) purposes. Location of these targets is showed in figure 3. 3D coordinates of these points were measured with a GPS receptor working in RTK mode, with the base station on a geodesic pillar located closer than one kilometer of the studied surfaces. 3D coordinates of the geodesic pillar, named Cerro Gordo II [33], by the Spanish National Geographic Institute are 582655.945 m, 4093630.095 m and 240.883

m, respectively. Horizontal coordinates are referred to UTM Zone 30N (European Terrestrial Reference System 1989, ETRS89) and the elevation is referred to the mean sea level, using the EGM08 geoid model. Both rover and base GPS receivers were Trimble R6. For RTK measurements, these dual-frequency geodetic instruments have a manufacturer's stated accuracy specification of ±1 cm+1 ppm RMS horizontal, and ±2 cm+1 ppm RSM vertical. As distance between base station and study area was 670 m approximately, horizontal and vertical errors were around 1 cm and 2 cm.

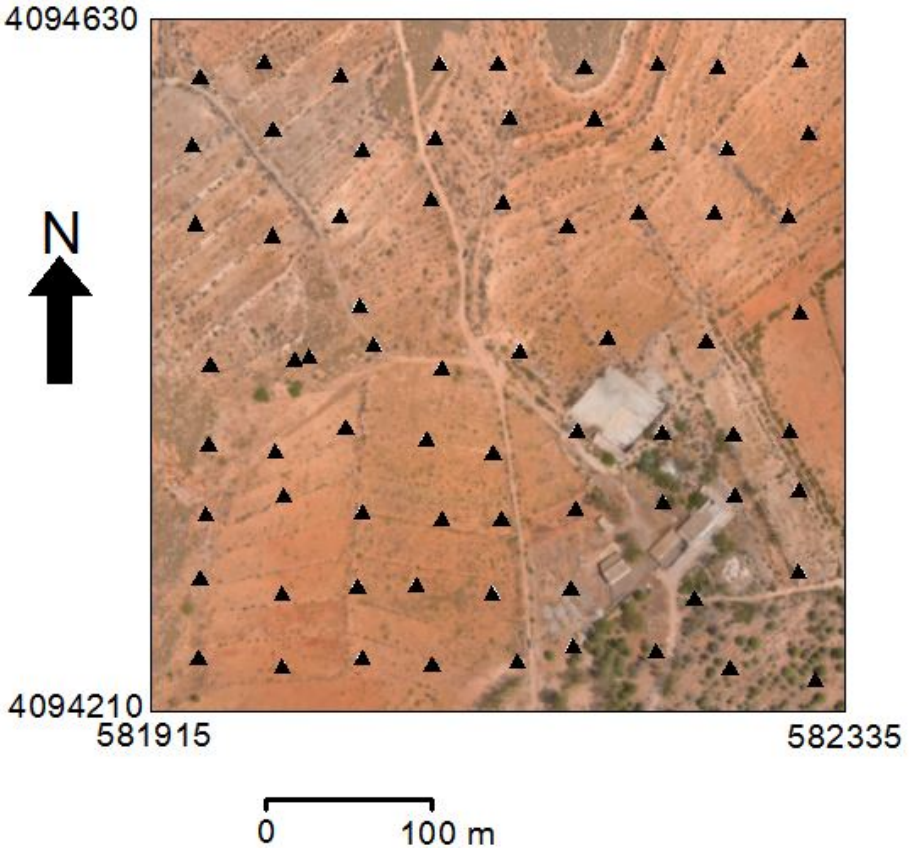

Figure 3. Location of the 72 targets used as GCP or CP. Coordinates are referred to UTM Zone 30N (European Terrestrial Reference System 1989, ETRS89).

2.3 IMAGE PROCESSING

Image processing was performed by the software package Agisoft PhotoScan Professional edition, version 1.0.4 [34]. The SfM procedure of SfM routines incorporated in PhotoScan and commonly used parameters are described in [35]. While carrying out images alignment, this software estimates both internal and external camera orientation parameters, including nonlinear radial distorsion. Only an approximate focal length value is required, which is extracted automatically from the EXIF metadata. The workflow is a three-step process. The first step is the alignment of the images by the feature identification and feature matching. This task was carried out with the PhotoScan accuracy set to high. The result of this step is the camera position corresponding to each picture, the internal calibration parameters and the 3D coordinates of a sparse point cloud of the terrain. In the second step, a densification of the point cloud is achieved using height field method that is based on pair-wise depth map computation. This resulted in a more detailed 3D model that can be used to identify the GCPs and CPs. The third step applies a texture to the mesh obtained in the previous step and the point cloud is referenced to a local coordinate system (ETRS89 and frames in the UTM, in our case). The bundle adjustment can be carry out using three GCPs at least but more accuracy results are obtained if more GCPs are used, being a recommendation to use more of then to obtain optimal accuracy [36]. Attending to this affirmation, this task was repeated in this work using 4, 5, 6, 7, 8, 9, 10, 15 and 20 GCPs uniformly sparse on the terrain. Furthermore, for every number of GCPs, five replications were carried out changing the combination of selected points. Figure 4 shows the GCPs distribution for every studied combination. Finally, the orthophoto is exported and a grid DSM can be generated from the point cloud.

2.4 ACCURACY ASSESSMENT

Taking into account combinations of number of GCPs used for georeferencing and replications, a total of 9 × 5 = 45 photogrammetric projects were carried out.

For every photogrammetric project, the accuracy assessment in Easting (X), Northing (Y), horizontal (XY) and height (Z), was carried out on the surveyed points which have not been used for georeferencing (CPs).

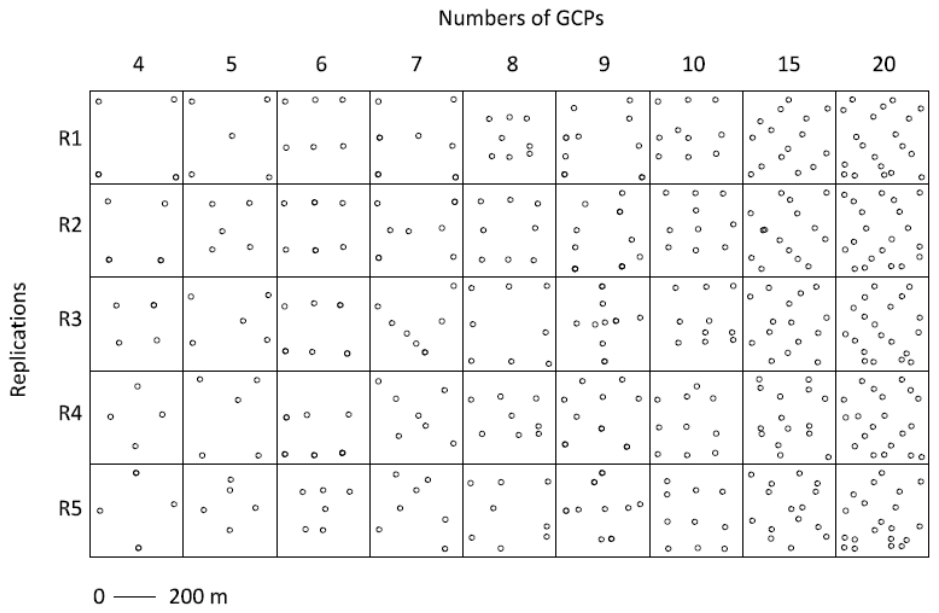

Figure 4. GCPs distribution for every number of GCPs and replication studied.

So, the number of CPs ranged from 52 to 69 depending on the number of GCPs used in the photogrammetric project. These CPs were identified in the orthoimages and their coordinates were compared to the surveyed GPS coordinates, resulting $RMSE_X$, $RMSE_Y$ and $RMSE_{XY}$ horizontal accuracy measures:

$$RMSE_X = \sqrt{\frac{\sum_{i=1}^{n}(X_{Oi}-X_{GPSi})^2}{n}} \quad (1)$$

$$RMSE_Y = \sqrt{\frac{\sum_{i=1}^{n}(Y_{Oi}-Y_{GPSi})^2}{n}} \quad (2)$$

$$RMSE_{XY} = \sqrt{\frac{\sum_{i=1}^{n}[(X_{Oi}-X_{GPSi})^2+(Y_{Oi}-Y_{GPSi})^2]}{n}} \quad (3)$$

where:

n: number of CP tested for this project.

X_{Oi}, Y_{Oi}: X and Y coordinates measured in the orthophoto for the i^{th} CP.

X_{GPSi}, Y_{GPSi}: X and Y coordinates measured with GPS for the i^{th} CP.

Furthermore, the height value was derived from the grid DSM for the X and Y coordinates of the CP on the orthoimage and it was also compared to the GPS observations, producing $RMSE_Z$ accuracy measure for the Z direction:

$$RMSE_Z = \sqrt{\frac{\sum_{i=1}^{n}(Z_{Oi} - Z_{GPSi})^2}{n}} \qquad (4)$$

where:

Z_{Oi} is the height in the i^{th} CP, derived from DSM, taking into account its coordinates X and Y, measured on the orthophoto.

Z_{GPSi}: Z coordinate of the i^{th} CP measured with GPS.

For each photogrammetric project, the orthophoto and DSM were generated at a resolution equal to its own ground sample distance (3.291 cm). DSM was derived from the generated cloud points by using the inverse distance to square power, taking into account the eight nearest points. Then, distance from interpolated grid point to the eight nearest points used for interpolation was less than 15 cm. In this way, the generated DSM fits with the points cloud generated during the photogrammetric process.

3. RESULTS AND DISCUSSION

A total of 160 images were used in every photogrammetric project studied in this work. Figure 5 shows camera location of every picture and indication of the image overlap. In view of this image, it can observe that the whole studied surface was covered by more than nine pictures, which is optimum number for the image matching algorithms used in SfM.

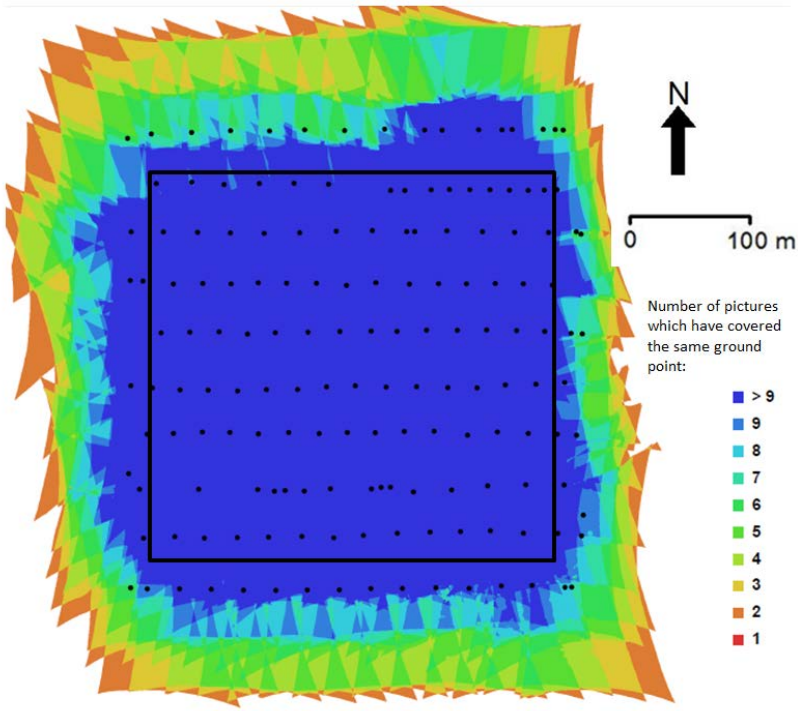

Figure 5. Camera location of every picture and indication of the image overlap (black circles). Color scale indicates the number of pictures which have covered the same ground point. Black square indicates the studied area.

Figure 6 shows the mean value of the five replications of $RMSE_X$, $RMSE_Y$ and $RMSE_{XY}$ (cm) found for every combination of GCPs. In this figure, extrems of the bars indicate mean value plus and minus standard deviation. Based on this figure, it can conclude that $RMSE_X$, $RMSE_Y$ can be agruped in three levels: the first one include 4, 5 and 6 GCPs and yielded values around 6 cm for Easting and Northing components and around 8 cm for $RMSE_{XY}$. The second level includes 7, 8 and 9 GCPs and shows values around 5 cm for Easting and Northing components and around 6 cm for $RMSE_{XY}$, and the third level includes 10, 15 and 20 GCPs, which shows values around 3 cm for Easting and Northing components and around 4 cm for $RMSE_{XY}$. Furthermore, the trend was to reduce the RMSE standar deviation as the GCP increased, finding the lower values for 20 GCPs: 0.346 cm for $RMSE_X$, 0.0218 cm for $RMSE_Y$, and 0.0169 cm for $RMSE_{XY}$. Although mean accuracies found for 10 GCPs were similar to found for 15 and 20 GCPs, standard deviation was several times greater .

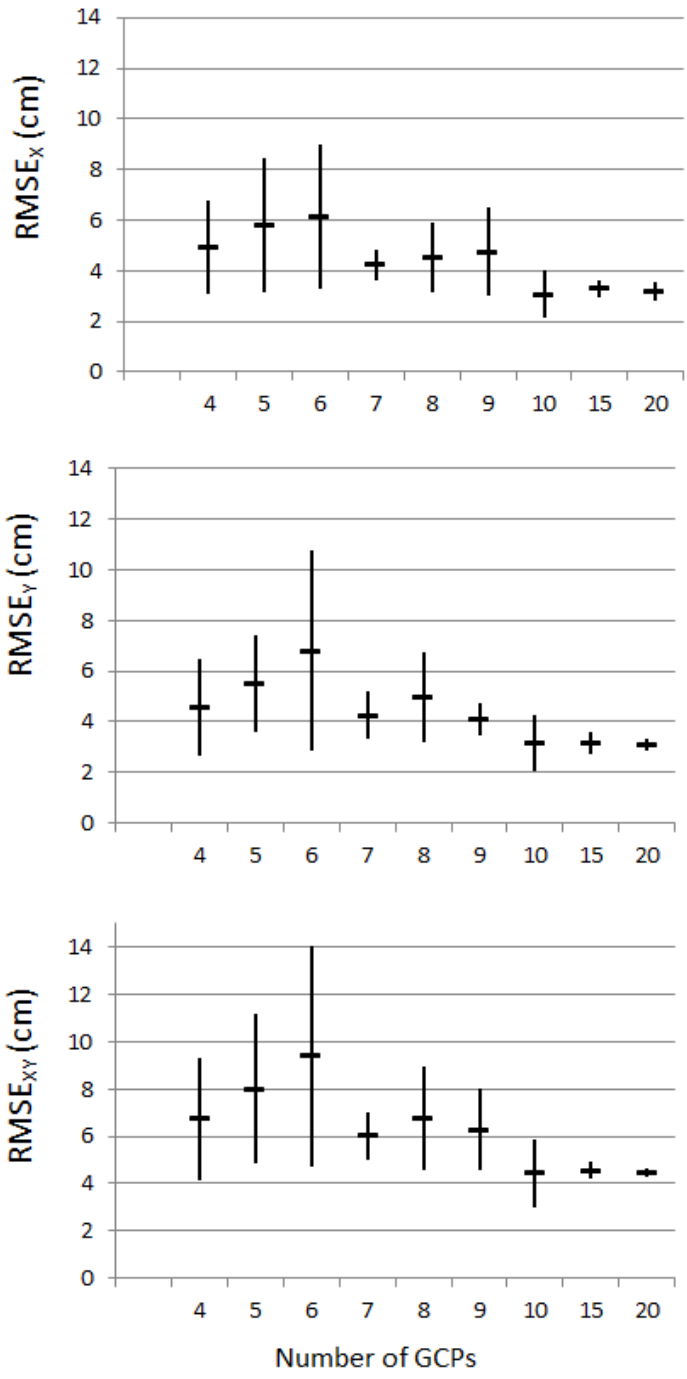

Figure 6. Mean values of RMSE$_X$, RMSE$_Y$ and RMSE$_{XY}$ (cm), vs number of GCP. Extrems of the bars indicate mean value plus and minus standard deviation found in the five replication of every GCP combination.

Figure 7 shows the mean of the five replications values of $RMSE_Z$ (cm) found for every combination of GCPs. In this figure, extrems of the bars indicate mean value plus and minus standard deviation. The trend of mean $RMSE_Z$ and standar deviation values was to decrease as the number of GCPs increased. For 15 and 20 GCPs, mean $RMSE_Z$ ± standard deviation values were 5.8±1.21 cm and 4.7±0.861 cm respectively. Although for 10 GCPs the $RMSE_Z$ was quite similar to those found for 10 and 20 GCPs (6.9 cm), standar deviation was 4.4 cm, aproximately five times greater than those found for 15 and 20 GCPs. The other $RMSE_Z$ values were higher than 10 cm and standar deviations were higher than values found for 15 and 20 GCPs.

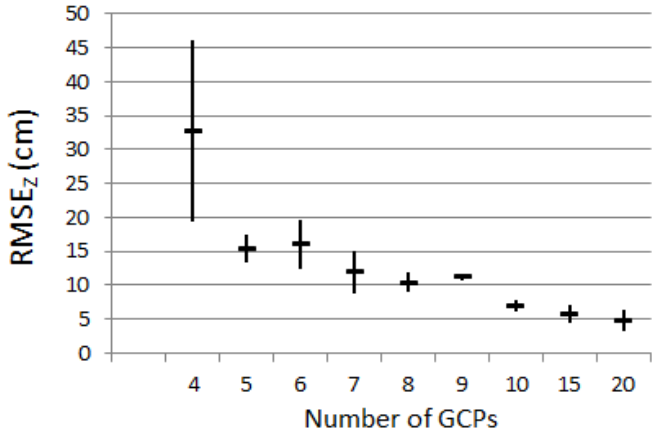

Figure 7. Mean values of $RMSE_Z$ (cm), vs number of GCP. Extrems of the bars indicate mean value plus and minus standard deviation found in the five replication of every GCP combination.

Tahar [37] concluded that different configurations in distribution and number (from 4 to 9) of GCPs contributed different errors in photogrammetric block. The study area consist different slope class which involves undulating area and the elevation range is about 70 m, which is similar to the present work. Furthermore, a high resolution digital camera with 12 megapixel resolution was used. This work concluded that most accuracy results are reached from 8 GCPs. Results of the present study had the same trend, although if higher number of GCPs is taken into account, as in our case, a decrease of RMSE for horizontal components can be observed.

Hugenholtz et al. [2], with a rotatory-wing UAV, 10 GCPs and 100 m flying height, performed two aerial surveys of a stockpile, before and after a portion of this was excavated, and they reported a vertical RMSE of 10.6 cm and 9.7 cm, respectively. They used a 12 megapixel resolution camera and a ground sample distance of 5 cm. Although these results are worse than mean value found in this work for 10 GCPs, standard deviation indicates that we found similar values in the replications. Cryderman et al. [38] study was carried out on a stockpile too, using a fixed-wing UAV, with a flight altitude of 118 m and taking into account 11 GCPs. They yielded values of $RMSE_{XY}$ equal to 3.9 cm, which is quite similar to results observed in this work. Nevertheless, values of $RMSE_Z$ reached in [38] was 4.9c m, while equivalent mean value in this work was 6.9 cm. Uysal et al. [27], reports vertical accuracy of 6.2 cm with a flight altitude of 60 m, using a 18 megapixel resolution camera and 27 GCPs, which is similar to the results presented in this work for 120 m flight altitude and 15 GCPs.

4. CONCLUSIONS

The results obtained in this work conclude that UAV photogrammetry is a methodology which allows data collection and DEM generation for geomatic applications. Compared with traditional platforms (manned airborne or satellite), methodology based on UAV platforms reduces the working time and avoids the risk when the study site is dangerous.

The study shows that both horizontal and vertical accuracy increases as the number of GCPs used increases. Best results for $RMSE_X$ and $RMSE_Y$ mean±standard deviation values are reached for 15 and 20 GCPs: 3.3±0.346 cm and 3.2±0.346 cm for $RMSE_x$ and 3.2±0.441 cm and 3.1±0.218cm for $RMSE_Y$, respectively. Mean $RMSE_{XY}$ and standard deviation values for 15 and 20 GCPs were 4.6±0.340 cm and 4.5±0.169 cm for 15 and 20 GCPs respectively. As regard of vertical accuracy, similar conclusions are derived: lower $RMSE_Z$ mean±standard deviation values are reached for 15 and 20 GCPs: 5.8±1.21 cm and 4.7±0.86 cm respectively.

So, as GCPs must be surveyed using classical technology (GPS or tachymetry), field work can be saved if 15 GCPs are used instead of 20, without accuracy loss.

According to the legacy ASPRS map standard of 1990 [39], and taking into the results yielded in this study for 15 GCPs and 120 m flight altitude, the equivalent map scale will be 1:150 approximately and a contour interval of 15 cm, which is enough to make must of engineering projects.

ACKNOWLEDGMENTS

This work was supported by grant P08-TEP-3870 from CICE-Junta de Andalucía (Spain) and was co-financed with European Union FEDER funds.

REFERENCES

[1] F. Mancini, M. Dubbini, M. Gattelli, F. Stecchi, S. Fabbri, G. Gabbianelli. Using Unmanned Aerial Vehicles (UAV) for High-Resolution Reconstruction of Topography: The Structure from Motion Approach on Coastal Environments, Remote Sensing 5 (2013) 6880-6898.

[2] C.H. Hugenholtz, J. Walker, O. Brown, S. Myshak,. Earthwork volumetrics with an unmanned aerial vehicle and Softcopy Photogrammetry, Journal Surveying Engineering 141 (2015) 06014003-1-06014003-5.

[3] A.S. Laliberte, J.E. Herrick, J.E., A. Rango, C. Winters. Acquisition, Orthorectification, and Object-based Classification of Unmanned Aerial Vehicle (UAV) Imager y for Rangeland Monitoring, Photogrammetric Engineering & Remote Sensing 76 (6) (2010) 661-672.

[4] S. Harwin, A. Lucieer. Assesing the accuracy of georeferenced point clouds produced via multi-view stereopsis from unmanned aerial vehicle (UAV) imagery, Remote Sensing 4 (2012) 1573-1599.

[5] C.H. Hugenholtz, K. Whitehead, O.W. Brown, T.E. Barchyn, B.J. Moorman, A. LeClair, K. Riddell, T. Hamilton. Geomorphological mapping with a small unmanned aircraft system (sUAS): Feature detection and accuracy assessment of a photogrammetrically-derived digital terrain model, Geomorphology 194 (2014) 16-24.

[6] V.W. Immerzeel, P.D.A. Kraaijenbrink, J.M. Shea, A.B. Shrestha, F. Pellicciotti, M.F.P. Bierkens, S.M. de Jong, S.M. High-resolution monitoring of Himalayan glacier dynamics using unmanned aerial vehicles, Remote Sensing of Environment 150 (2014) 93-103.

[7] J.S. Aber, I. Marzolff, J.B. Ries. Small-format aerial photography. Principles, techniques and geoscience applications. Elsevier, Amsterdam, 2010.

[8] K. Lambers, H. Eisenbeiss, M. Sauerbier, D. Kupferschmidt, T. Gaisecker, S. Sotoodeh, T. Hanusch. Combining photogrammetry and laser scanning for the recording and modelling of the Late Intermediate Period site of Pinchango Alto, Palpa, Peru. Journal of Archaeological Science 34 (2007) 1702–1712.

[9] I. Colomina, P. Molina. Unmanned aerial systems for photogrammetry and remote sensing: a review, ISPRS Journal of Photogrammetry and Remote Sensing 92 (2014) 79-97.

[10] P. Liu, A.Y. Chen, H. Yin-Nan, H. Jen-YU, L. Jihn-Sung, K. SHIL-Chung, W. Tzong-Hann, W. Ming-Chang, T. Meng-Han. A review of rotorcraft unmanned aerial vehicle (UAV) developments and applications in civil engineering, Smart Structures and Systems 13 (6) (2014) 1065-1094.

[11] F. Nex, F. Remondino. UAV for 3D mapping application: a review, Applied Geomatics, 6 (2014) 1-15

[12] k. Atkinson. Close *range photogrammetry and machine vision*, Whittles Publishing, Caithness. 1996

[13] R. Hartley, A. Zisserman. Multiple view geometry in computer vision, Cambridge University Press, NewYork. 2003.

[14] J. Fernández, D. González, P. Rodríguez, J. Mancera. Image-based modelling from unmanned aerial vehicle (UAV) photogrammetry: an effective, low-cost tool for archaeological applications, Archaeometry 57(1) (2015) 128-145. DOI: 10.1111/arcm.12078.

[15] N. Snavely, S.M. Seitz, R. Szeliski. Modelling the world from internet photo collections, International Journal of Computer Vision 80 (2007) 189–210.

[16] M.J. Westoby, J. Brasington, N.F. Glasser, M.J. Hambrey, J.M. Reynolds. Structure from Motion photogrammetry: A low cost, effective tool for geoscience applications, Geomorphology 179 (2012) 300-314.

[17] Y. Vasuki, E.J. Holden, P. Kovesi, S. Micklethwaite. Semi-automatic mapping of geological structures using UAV-based photogrammetric data: an image analysis approach, Computers & Geosciences 69 (2014) 22-32.

[18] Y. Furukawa, J. Ponce. Accurate, dense, and robust multi-view stereopsis. In *Proceedings of the 2007 IEEE Conference on Computer Vision and Pattern Recognition,* Minneapolis, MN, USA, 18-23 June 2007 (1), 1-8.

[19] D.G. Lowe. Distinctive image features from scale-invariant keypoints, Int. J. Comput. Vis., 60 (2004) 91-110.

[20] F. Remondino, S. El-Hakim. Image-based 3d modelling: A review, Photogramm. Rec. 21 (2006) 269-291.

[21] L. Juan, O. Gwun. A comparasion of SIFT, PCA-SIFT and SURF, Int. J. Image Process 3 (2009) 143-152.

[22] D. Turner, A. Lucieer, C. Watson. An automated technique for generating georectified mosaics from ultra-high resolution unmanned aerial vehicle (UAV) imagery, based on structure from motion (SfM) point clouds". Remote sensing 4 (5) (2012) 1392-1410.

[23] A. Lucieer, D. Turner, D.H. King, S.A. Robinson. Using an unmanned aerial vehicle (UAV) to capture micro-topography of Antarctic moss beds, International Journal of Applied Earth Observation 27 (part A) (2013) 53-62.

[24] A. Lucieer, S.M. de Jong, D. Turner. Mapping landslide displacements using Structure from Motion (SfM) and image correlation of multi-temporal UAV photography, Progress in Physical Geography, 38 (1) (2014) 97-116.

[25] T.N. Tonkin, N.G. Midgley, D.J. Graham, J.C. Labadz. The potential of small unmanned aircraft systems and structure-from-motion for topographic surveys: A test of emerging integrated approaches at Cwm Idwal, North Wales. Geomorphology 226 (2014) 35-43.

[26] A. Eltner, P. Baumgart, H. Maas, D. Faust. Multi-temporal data for automatic measurement of rill and interrill erosion on losses soil, Earth Surface Processes and Landform 40(6) (2014) 741-755.

[27] Uysal, M., Toprak, A.S., Polat, N., DEM generation with UAV Photogrammetry and accuracy analysis in Sahitler hill. Measurement 73 (2015) 539-543.

[28] F. Agüera-Vega, F. Carvajal-Ramírez and P. Martínez-Carricondo. Accuracy of Digital Surface Models and Orthophotos Derived from Unmanned Aerial Vehicle Photogrammetry. Journal of Surveying Engineering, (2016) http://dx.doi.org/10.1061/(ASCE)SU.1943-5428.0000206.

[29] F.J. Mesas-Carrascosa, J. Torres-Sánchez, I. Clavero-Rumbao, A. García-Ferrer, J.M. Peña, I. Borra-Serrano, and F. López-Granados. Assessing optimal flight parameters for generating accurate multispectral orthomosaicks by UAV to support site-specific crop management. Remote Sensing, 7(10) (2015), 12793-12814.

[30] Ruzgiene, B., Berteska, T., Gecyte, S., Jakubauskiene, E., Aksamitaukas, V. C., The surface modelling base don UAV Photogrammetry and qualitative estimation. Measurements, 73 (2015) 619-627.

[31] F.J. Mesas-Carrascosa, I.C. Rumbao, J.A.B. Berrocal, and A.G.F. Porras. Positional quality assessment of orthophotos obtained from sensors onboard multi-rotor UAV platforms. Sensors, 14(12) (2014), 22394-22407.

[32] MiKrokopter Company. www.mikrokopter.de. (last date accessed: 15 August 2015).

[33] Instituto Geográfico Nacional. Centro Nacional de Información Geográfica. ftp://ftp.geodesia.ign.es/Red_Geodesica/Hoja1046/104639.pdf. (last date accessed: 15 August 2015).

[34] Agisoft Company. www.agisoft.com. (last date accessed: 15 August 2015).

[35] G.J. Verhoeven. Taking computer vision aloft – archaeological three-dimensional reconstructions from aerial photographs with Photoscan, Archaeological Prospection 18 (2011) 67-73.

[36] T. Rosnell, E. Honkavaara. Point cloud generation from aerial image data acquired by a quadracopter type micro unmanned aerial vehicle and a digital still camera. Sensors 12(1) (2012) 453-480.

[37] K.N. Tahar. An evaluation on different number of ground control points in unmanned aerial vehicle photogrammetric block. International Archives of the Photogrammetry, Remote Sensing and Spatial Information Sciences, Vol. XL-2/W2, ISPRS. 8th 3DGeoInfo Conference & WG II/2 Whorkshop, 27-29 November 2013, Istambul, Turkey.

[38] C. Cryderman, S.B. Mah, A. Shufletoski. Evaluation of a UAV photogrammetric accuracy for mapping and earthworks computation, Geomatica 68 (4) (2014) 309-317.

[39] American Society for Photogrammetry and Remote Sensing (ASPRS), 1990. ASPRS Accuracy Standards for Large-Scale Maps, URL: http://www.asprs.org/a/society/committees/standards/1990_ jul_1068-1070.pdf (last date accessed: 22 January 2015)

CONCLUSIONES

CONCLUSIONES

Del **capítulo 1** se derivan dos conclusiones, acorde con los objetivos planteados en el mismo. En primer lugar, y para el contexto de deslizamientos de taludes de desmonte en carreteras, o bien superficies de topografía extrema, donde existen problemas de accesibilidad, se establece la disposición ideal para el mínimo de 3 GCPs necesarios para la georreferenciación absoluta de los proyectos fotogramétricos. Esta distribución ideal aconseja la disposición de dos GCPs en la parte baja del talud y un tercero en la parte alta del talud, bien centrado. Además, el área del triángulo formado por los mismos debe tender a ser máxima.

Respecto a la orientación de las imágenes realizadas por el UAV, el uso de disposiciones con eje perpendicular a la superficie objeto de estudio disminuye el número de fotografías necesarias para ser tratadas con el software fotogramétrico lo que, consecuentemente, reduce la carga de trabajo.

Por último, se puede concluir de los resultados derivados del capítulo 1, que la fotogrametría UAV constituye una técnica útil y adecuada para proyectos de ingeniería relacionados con la reparación y gestión de deslizamientos de taludes de desmonte en carreteras.

En el **capítulo 2** se estudia la incidencia que diferentes parámetros, como la morfología del terreno, la altura de vuelo y el número de GCPs usados para la georreferenciación, tienen en la precisión de los productos obtenidos mediante fotogrametría UAV.

De los resultados se desprende que ni la morfología del terreno, ni la altura de vuelo tienen una incidencia significativa en las precisiones obtenidas en ninguna de las componentes planimétricas. La altura de vuelo tiene muy poca influencia en la precisión horizontal ya que en el rango de vuelo cubierto (50-120 m) el GSD varió de 0.012 m a 0.027 m.

Sin embargo, el número de GCPs tiene una influencia significativa en la precisión obtenida, aumentando ésta conforme aumenta el número de GCPs usado en la georreferenciación.

En cuanto a la precisión altimétrica, se concluye que la morfología del terreno tiene una incidencia significativa solamente cuando las condiciones de vuelo son óptimas, es decir a baja altura (50 m) y aumentando el número de GCPs hasta 10. Bajo estas premisas, se obtienen resultados más precisos para terrenos más planos. Tendencias similares se observan con otras alturas de vuelo, aunque los resultados no son tan evidentes.

En relación a la altura de vuelo, la precisión en Z disminuye conforme aumenta la altura siendo esta consecuencia más notable conforme disminuye el número de GCPs. Si el número de GCPs es alto (valores de 10) la precisión en Z se mantiene prácticamente constante independientemente de la altura de vuelo.

Como conclusión final de este capítulo se observa que la combinación de alturas de vuelo de 50 m, junto con un número elevado de GCPs (10) produce los resultados óptimos en cuanto a precisión se refiere, válidos para crear mapas cartográficos a escala 1:150 según las normas del ASPRS.

En el **capítulo 3** se profundiza expresamente en la influencia que tiene el número de GCPs usado para la georreferenciación en la precisión de los productos resultantes de la fotogrametría UAV.

La conclusión fundamental de este capítulo es que el uso de un número alto de GCPs (15-20) aumenta considerablemente la precisión de los productos obtenidos, tanto en planimetría como en altimetría, permitiendo llegar incluso a alturas de 120 m sin pérdida significativa de precisión, así como la creación de mapas cartográficos a escala 1:150 según las normas del ASPRS.

ANEXOS

ANEXOS

Informe con el factor de impacto y cuartil del Journal Citation Reports de las publicaciones presentadas

REVISTA: JOURNAL OF APPLIED REMOTE SENSING

InCites™ Journal Citation Reports® THOMSON REUTERS

Journal Data Filtered By: Selected JCR Year: 2015 Selected Editions: SCIE Selected Categories: 'IMAGING%20SCIENCE%20%26%20PHOTOGRAPHIC%20TECHNOLOGY' Selected Category Scheme: WoS

Rank	Full Journal Title	Total Cites	Journal Impact Factor	Eigenfactor Score
1	REMOTE SENSING OF ENVIRONMENT	36,252	5.881	0.044990
2	ISPRS JOURNAL OF PHOTOGRAMMETRY AND REMOTE SENSING	5,125	4.188	0.010790
3	IEEE TRANSACTIONS ON MEDICAL IMAGING	13,784	3.756	0.024500
4	IEEE TRANSACTIONS ON GEOSCIENCE AND REMOTE SENSING	26,086	3.360	0.037660
5	SIAM Journal on Imaging Sciences	2,209	2.687	0.010920
6	IEEE Geoscience and Remote Sensing Letters	5,572	2.228	0.016080
7	IEEE Journal of Selected Topics in Applied Earth Observations and Remote Sensing	3,033	2.145	0.010950
8	INTERNATIONAL JOURNAL OF REMOTE SENSING	16,510	1.640	0.016290
9	PHOTOGRAMMETRIC RECORD	649	1.622	0.000840
10	Journal of Real-Time Image Processing	341	1.564	0.000860
11	Remote Sensing Letters	638	1.487	0.002600
12	Geocarto International	564	1.380	0.000990
13	PHOTOGRAMMETRIC ENGINEERING AND REMOTE SENSING	5,570	1.288	0.003230
14	EURASIP Journal on Image and Video Processing	345	1.060	0.001430
15	Journal of Applied Remote Sensing	1,189	0.937	0.002730
16	Signal Image and Video Processing	480	0.872	0.001390
17	JOURNAL OF VISUALIZATION	342	0.720	0.000840
18	JOURNAL OF ELECTRONIC IMAGING	1,307	0.616	0.002750
19	INTERNATIONAL JOURNAL OF IMAGING SYSTEMS AND TECHNOLOGY	549	0.571	0.000970

20	VIRTUAL REALITY	226	0.568	0.000580
21	Photogrammetrie Fernerkundung Geoinformation	172	0.554	0.000480
22	Image Analysis & Stereology	202	0.500	0.000630
23	IMAGING SCIENCE JOURNAL	179	0.454	0.000350
24	JOURNAL OF IMAGING SCIENCE AND TECHNOLOGY	432	0.316	0.000370

REVISTA: JOURNAL OF SURVEYING ENGINEERING

InCites™ Journal Citation Reports® THOMSON REUTERS™

Journal Data Filtered By: Selected JCR Year: 2015 Selected Editions: SCIE Selected Categories: 'ENGINEERING%2C%20CIVIL' Selected Category Scheme: WoS

Rank	Full Journal Title	Total Cites	Journal Impact Factor	Eigenfactor Score
1	COMPUTER-AIDED CIVIL AND INFRASTRUCTURE ENGINEERING	1,935	5.288	0.003670
2	JOURNAL OF HAZARDOUS MATERIALS	69,992	4.836	0.097310
3	TRANSPORTATION RESEARCH PART B-METHODOLOGICAL	7,358	3.769	0.012760
4	BUILDING AND ENVIRONMENT	12,520	3.394	0.019070
5	JOURNAL OF HYDROLOGY	37,044	3.043	0.049610
6	ENERGY AND BUILDINGS	17,211	2.973	0.027970
7	COASTAL ENGINEERING	4,168	2.841	0.007800
8	IEEE TRANSACTIONS ON INTELLIGENT TRANSPORTATION SYSTEMS	4,163	2.534	0.011520
9	JOURNAL OF WATER RESOURCES PLANNING AND MANAGEMENT	3,692	2.521	0.004350
10	JOURNAL OF COMPOSITES FOR CONSTRUCTION	2,846	2.503	0.005290
11	MATERIALS AND STRUCTURES	4,952	2.453	0.008150
12	AUTOMATION IN CONSTRUCTION	3,543	2.442	0.007050
13	WATER RESOURCES MANAGEMENT	6,400	2.437	0.011310
14	COMPUTERS & STRUCTURES	10,168	2.425	0.013290
15	CONSTRUCTION AND BUILDING MATERIALS	18,061	2.421	0.041570
16	EARTHQUAKE SPECTRA	3,068	2.298	0.005070
17	TRANSPORTATION RESEARCH PART E-LOGISTICS AND TRANSPORTATION REVIEW	3,204	2.279	0.007920
18	JOURNAL OF URBAN PLANNING AND DEVELOPMENT	869	2.246	0.001040
19	STOCHASTIC ENVIRONMENTAL RESEARCH AND RISK ASSESSMENT	2,297	2.237	0.005210
20	Archives of Civil and Mechanical Engineering	749	2.194	0.002190
21	EARTHQUAKE ENGINEERING & STRUCTURAL DYNAMICS	6,379	2.127	0.008010
22	STRUCTURAL SAFETY	1,929	2.086	0.003820

23	Structural Control & Health Monitoring	1,294	2.082	0.003150
24	THIN-WALLED STRUCTURES	4,518	2.063	0.008680
25	JOURNAL OF WIND ENGINEERING AND INDUSTRIAL AERODYNAMICS	5,727	2.024	0.006070
26	Journal of Hydro-environment Research	481	1.971	0.001880
27	JOURNAL OF ENERGY ENGINEERING	404	1.895	0.000710
28	ENGINEERING STRUCTURES	11,921	1.893	0.026470
29	JOURNAL OF COMPUTING IN CIVIL ENGINEERING	1,541	1.855	0.003340
30	JOURNAL OF MANAGEMENT IN ENGINEERING	1,138	1.840	0.001330
31	STEEL AND COMPOSITE STRUCTURES	720	1.796	0.001370
32	TUNNELLING AND UNDERGROUND SPACE TECHNOLOGY	2,632	1.741	0.004740
33	MARINE STRUCTURES	1,002	1.729	0.001810
34	JOURNAL OF CONSTRUCTIONAL STEEL RESEARCH	4,987	1.702	0.009790
35	JOURNAL OF STRUCTURAL ENGINEERING	11,091	1.700	0.011290
36	COLD REGIONS SCIENCE AND TECHNOLOGY	2,777	1.693	0.004870
37	IEEE JOURNAL OF OCEANIC ENGINEERING	2,421	1.648	0.002850
38	Road Materials and Pavement Design	871	1.547	0.002320
39	TRANSPORTATION	2,011	1.545	0.003910
40	JOURNAL OF HYDROLOGIC ENGINEERING	3,231	1.530	0.005790
40	Journal of Civil Engineering and Management	776	1.530	0.002030
42	OCEAN ENGINEERING	4,738	1.488	0.009740
43	JOURNAL OF HYDRAULIC RESEARCH	2,515	1.471	0.004720
44	International Journal of Concrete Structures and Materials	197	1.411	0.000750
45	Journal of Analytical Methods in Chemistry	284	1.369	0.000830
46	JOURNAL OF IRRIGATION AND DRAINAGE ENGINEERING	2,910	1.364	0.003080
47	JOURNAL OF WATERWAY PORT COASTAL AND OCEAN ENGINEERING	1,485	1.316	0.001700
48	JOURNAL OF MATERIALS IN CIVIL ENGINEERING	3,948	1.295	0.008380
49	Natural Hazards Review	709	1.293	0.001160
50	JOURNAL OF ADVANCED TRANSPORTATION	538	1.292	0.001430
51	JOURNAL OF HYDRAULIC ENGINEERING	7,275	1.284	0.005900
52	Journal of Infrastructure Systems	890	1.234	0.001570
53	ACI STRUCTURAL JOURNAL	3,918	1.227	0.004080
54	Structure and Infrastructure Engineering	753	1.202	0.002530
55	JOURNAL OF HYDROINFORMATICS	984	1.180	0.002270
56	JOURNAL OF CONSTRUCTION ENGINEERING AND MANAGEMENT	4,261	1.152	0.004270

57	Smart Structures and Systems	761	1.138	0.001920
58	JOURNAL OF ENVIRONMENTAL ENGINEERING	4,506	1.125	0.003580
59	Geomechanics and Engineering	188	1.085	0.000380
60	Journal of Bridge Engineering	1,572	1.069	0.003710
61	WATER INTERNATIONAL	1,093	1.040	0.001040
62	International Journal of Structural Stability and Dynamics	609	1.028	0.001610
63	International Journal of Architectural Heritage	282	1.025	0.000930
64	Structural Concrete	263	1.023	0.000910
65	STRUCTURAL ENGINEERING AND MECHANICS	1,504	1.021	0.002540
66	FIRE SAFETY JOURNAL	1,881	0.936	0.002840
67	JOURNAL OF EARTHQUAKE ENGINEERING	1,347	0.922	0.002690
68	PROCEEDINGS OF THE INSTITUTION OF MECHANICAL ENGINEERS PART F-JOURNAL OF RAIL AND RAPID TRANSIT	710	0.900	0.001730
69	STRUCTURAL DESIGN OF TALL AND SPECIAL BUILDINGS	691	0.898	0.001510
70	Journal of Pipeline Systems Engineering and Practice	110	0.896	0.000560
71	JOURNAL OF PERFORMANCE OF CONSTRUCTED FACILITIES	885	0.893	0.002100
72	CIVIL ENGINEERING AND ENVIRONMENTAL SYSTEMS	265	0.891	0.000580
73	JOURNAL OF SURVEYING ENGINEERING	342	0.884	0.000540
74	International Journal of Pavement Engineering	621	0.877	0.001790
75	Bauingenieur	352	0.866	0.001500
76	Computers and Concrete	399	0.849	0.001140
77	Latin American Journal of Solids and Structures	333	0.830	0.000820
78	JOURNAL OF AEROSPACE ENGINEERING	759	0.815	0.001510
79	Earthquake Engineering and Engineering Vibration	626	0.814	0.001220
80	JOURNAL OF WATER SUPPLY RESEARCH AND TECHNOLOGY-AQUA	823	0.807	0.000840
81	JOURNAL OF TRANSPORTATION ENGINEERING	2,286	0.801	0.003990
82	Earthquakes and Structures	240	0.789	0.000820
83	WIND AND STRUCTURES	460	0.746	0.000660
84	JOURNAL OF COLD REGIONS ENGINEERING	160	0.720	0.000210
85	JOURNAL OF MARINE SCIENCE AND TECHNOLOGY	432	0.709	0.000900
86	COASTAL ENGINEERING JOURNAL	328	0.703	0.000640
87	Proceedings of the Institution of Civil Engineers-Engineering Sustainability	201	0.691	0.000330
88	Ingegneria Sismica	44	0.676	0.000140
89	Journal of Advanced Concrete Technology	588	0.658	0.001030

90	PROCEEDINGS OF THE INSTITUTION OF CIVIL ENGINEERS-WATER MANAGEMENT	550	0.656	0.001630
91	European Journal of Environmental and Civil Engineering	305	0.636	0.001390
92	JOURNAL OF SHIP RESEARCH	642	0.606	0.000470
93	KSCE Journal of Civil Engineering	773	0.600	0.002680
94	CANADIAN JOURNAL OF CIVIL ENGINEERING	2,019	0.586	0.002440
95	ADVANCES IN STRUCTURAL ENGINEERING	765	0.577	0.002230
96	SURVEY REVIEW	282	0.573	0.000490
97	International Journal of Steel Structures	249	0.533	0.000820
98	TRANSPORTATION RESEARCH RECORD	12,833	0.522	0.018940
99	Baltic Journal of Road and Bridge Engineering	162	0.519	0.000450
100	JOURNAL AMERICAN WATER WORKS ASSOCIATION	2,206	0.505	0.001450
101	CHINA OCEAN ENGINEERING	285	0.435	0.000640
102	PROCEEDINGS OF THE INSTITUTION OF CIVIL ENGINEERS-STRUCTURES AND BUILDINGS	504	0.429	0.000970
103	Beton- und Stahlbetonbau	396	0.425	0.001500
104	Journal of Fire Protection Engineering	177	0.417	0.000310
105	Iranian Journal of Science and Technology-Transactions of Civil Engineering	44	0.403	0.000100
106	GEFAHRSTOFFE REINHALTUNG DER LUFT	183	0.394	0.000330
107	International Journal of Civil Engineering	211	0.372	0.000480
108	PROCEEDINGS OF THE INSTITUTION OF CIVIL ENGINEERS-CIVIL ENGINEERING	169	0.348	0.000340
109	Advanced Steel Construction	105	0.346	0.000440
110	INTERNATIONAL JOURNAL OF OFFSHORE AND POLAR ENGINEERING	366	0.341	0.000570
111	PROCEEDINGS OF THE INSTITUTION OF CIVIL ENGINEERS-TRANSPORT	204	0.314	0.000340
112	Structural Engineering International	373	0.299	0.000760
113	Bautechnik	222	0.289	0.001140
114	PROCEEDINGS OF THE INSTITUTION OF CIVIL ENGINEERS-MARITIME ENGINEERING	96	0.281	0.000180
115	PROCEEDINGS OF THE INSTITUTION OF CIVIL ENGINEERS-MUNICIPAL ENGINEER	159	0.275	0.000220
116	Periodica Polytechnica-Civil Engineering	71	0.271	0.000250
117	Stahlbau	321	0.201	0.000880
118	Revista de la Construccion	56	0.185	0.000090
119	ITE JOURNAL-INSTITUTE OF TRANSPORTATION ENGINEERS	221	0.174	0.000370
120	Teknik Dergi	28	0.171	0.000040
121	Gradevinar	100	0.158	0.000170
122	NAVAL ENGINEERS JOURNAL	201	0.157	0.000220

123	CIVIL ENGINEERING	217	0.153	0.000270
124	Journal of the South African Institution of Civil Engineering	59	0.115	0.000190
125	Tecnologia y Ciencias del Agua	17	0.043	0.000080
126	ENGINEERING JOURNAL-AMERICAN INSTITUTE OF STEEL CONSTRUCTION	231	0.033	0.000110

REVISTA: MEASUREMENT

InCites™ Journal Citation Reports® THOMSON REUTERS

Journal Data Filtered By: Selected JCR Year: 2015 Selected Editions: SCIE Selected Categories: 'ENGINEERING%2C%20MULTIDISCIPLINARY' Selected Category Scheme: WoS

Rank	Full Journal Title	Total Cites	Journal Impact Factor	Eigenfactor Score
1	INTEGRATED COMPUTER-AIDED ENGINEERING	533	4.981	0.001240
2	ARCHIVES OF COMPUTATIONAL METHODS IN ENGINEERING	941	4.214	0.003150
3	COMBUSTION AND FLAME	17,512	4.168	0.026250
4	COMPOSITES PART B-ENGINEERING	11,701	3.850	0.026890
5	COMPUTER METHODS IN APPLIED MECHANICS AND ENGINEERING	20,377	3.467	0.033580
6	STRUCTURAL HEALTH MONITORING-AN INTERNATIONAL JOURNAL	1,612	3.193	0.003620
7	INTERNATIONAL JOURNAL OF ENGINEERING SCIENCE	6,048	3.165	0.008350
8	Bioinspiration & Biomimetics	1,285	2.891	0.005950
9	ISA TRANSACTIONS	1,957	2.600	0.004230
10	ENGINEERING APPLICATIONS OF ARTIFICIAL INTELLIGENCE	3,775	2.368	0.008720
11	JOURNAL OF THE FRANKLIN INSTITUTE-ENGINEERING AND APPLIED MATHEMATICS	3,850	2.327	0.009570
12	APPLIED MATHEMATICAL MODELLING	8,836	2.291	0.027130
13	STRUCTURAL AND MULTIDISCIPLINARY OPTIMIZATION	3,896	2.208	0.009480
14	INTERNATIONAL JOURNAL FOR NUMERICAL METHODS IN ENGINEERING	14,432	2.100	0.022660
15	DESIGN STUDIES	1,828	2.070	0.001330
16	ADVANCED ENGINEERING INFORMATICS	1,237	2.000	0.002760
17	JOURNAL OF ENGINEERING DESIGN	844	1.946	0.001280
18	PRECISION ENGINEERING-JOURNAL OF THE INTERNATIONAL SOCIETIES FOR PRECISION ENGINEERING AND NANOTECHNOLOGY	2,216	1.914	0.004240
19	IEEE TRANSACTIONS ON INDUSTRY APPLICATIONS	10,468	1.901	0.017400
20	ENGINEERING ANALYSIS WITH BOUNDARY ELEMENTS	3,287	1.862	0.006230
21	RESEARCH IN ENGINEERING DESIGN	886	1.786	0.000810
22	MEASUREMENT	4,072	1.742	0.010390
23	JOURNAL OF ENGINEERING EDUCATION	1,407	1.739	0.001570

24	ADVANCES IN ENGINEERING SOFTWARE	2,318	1.673	0.005410
25	JOURNAL OF ELASTICITY	2,087	1.656	0.002390
26	MEASUREMENT SCIENCE and TECHNOLOGY	10,298	1.492	0.017280
27	Journal of Bionic Engineering	703	1.466	0.001510
28	QUALITY AND RELIABILITY ENGINEERING INTERNATIONAL	1,394	1.457	0.003180
29	SCIENCE AND ENGINEERING ETHICS	771	1.454	0.001780
30	Science China-Technological Sciences	2,218	1.441	0.008250
31	INTERNATIONAL JOURNAL OF PRESSURE VESSELS AND PIPING	2,618	1.432	0.003760
32	ENGINEERING OPTIMIZATION	1,350	1.380	0.003010
33	International Journal of Critical Infrastructure Protection	158	1.351	0.000380
34	Eksploatacja i Niezawodnosc-Maintenance and Reliability	357	1.248	0.000700
35	ATOMIZATION AND SPRAYS	920	1.235	0.001500
36	COMBUSTION SCIENCE AND TECHNOLOGY	3,966	1.193	0.003980
37	International Journal of Computational Methods	479	1.123	0.001510
38	International Journal for Multiscale Computational Engineering	385	1.103	0.001440
39	Bulletin of the Polish Academy of Sciences-Technical Sciences	698	1.087	0.001270
40	Proceedings of the Institution of Mechanical Engineers Part O-Journal of Risk and Reliability	336	1.073	0.001460
41	Engineering Applications of Computational Fluid Mechanics	334	1.033	0.001030
42	FIRE TECHNOLOGY	804	1.016	0.001510
43	International Journal for Uncertainty Quantification	107	1.000	0.000880
44	Journal of Zhejiang University-SCIENCE A	1,018	0.941	0.001620
45	COMPUTER APPLICATIONS IN ENGINEERING EDUCATION	631	0.935	0.000820
46	INVERSE PROBLEMS IN SCIENCE AND ENGINEERING	525	0.911	0.002110
47	OPTIMIZATION AND ENGINEERING	507	0.900	0.001430
48	AI EDAM-ARTIFICIAL INTELLIGENCE FOR ENGINEERING DESIGN ANALYSIS AND MANUFACTURING	450	0.877	0.000440
49	International Journal of Design	281	0.875	0.000390
50	INTERNATIONAL JOURNAL OF TECHNOLOGY MANAGEMENT	960	0.867	0.000850
51	JOURNAL OF THE AUDIO ENGINEERING SOCIETY	1,047	0.856	0.001240
52	CMES-COMPUTER MODELING IN ENGINEERING & SCIENCES	1,496	0.841	0.003730
53	Journal of Industrial and Management Optimization	409	0.776	0.001430
54	JOURNAL OF FIRE SCIENCES	584	0.758	0.000870
55	ENGINEERING COMPUTATIONS	1,135	0.691	0.001430
56	INTERNATIONAL JOURNAL OF NONLINEAR SCIENCES AND NUMERICAL SIMULATION	567	0.687	0.000870
57	Scientia Iranica	1,266	0.679	0.003890
58	JOURNAL OF ENGINEERING MATHEMATICS	1,358	0.665	0.002110

59	MATHEMATICAL PROBLEMS IN ENGINEERING	4,138	0.644	0.012380
60	COMBUSTION EXPLOSION AND SHOCK WAVES	1,519	0.604	0.001550
61	INTERNATIONAL JOURNAL OF ENGINEERING EDUCATION	916	0.559	0.000920
62	Acta Polytechnica Hungarica	362	0.544	0.000680
63	RUSSIAN JOURNAL OF NUMERICAL ANALYSIS AND MATHEMATICAL MODELLING	177	0.541	0.000510
64	JOURNAL OF PROFESSIONAL ISSUES IN ENGINEERING EDUCATION AND PRACTICE	324	0.538	0.000470
65	JOURNAL OF ENGINEERING TECHNOLOGY	83	0.500	0.000150
66	CMC-Computers Materials & Continua	319	0.475	0.001210
67	ISSUES IN SCIENCE AND TECHNOLOGY	212	0.467	0.000620
68	Tehnicki Vjesnik-Technical Gazette	317	0.464	0.000900
69	INDIAN JOURNAL OF ENGINEERING AND MATERIALS SCIENCES	452	0.456	0.000670
70	Engineering Studies	59	0.417	0.000210
71	JOURNAL OF SCIENTIFIC & INDUSTRIAL RESEARCH	1,538	0.385	0.001270
72	INTERNATIONAL JOURNAL OF TECHNOLOGY AND DESIGN EDUCATION	252	0.355	0.000400
73	INSTRUMENTS AND EXPERIMENTAL TECHNIQUES	816	0.353	0.001160
74	SADHANA-ACADEMY PROCEEDINGS IN ENGINEERING SCIENCES	708	0.349	0.000910
75	SAMPE JOURNAL	166	0.333	0.000120
76	NOISE CONTROL ENGINEERING JOURNAL	337	0.313	0.000830
77	Dyna	88	0.302	0.000170
78	Journal of Marine Science and Technology-Taiwan	371	0.298	0.001000
79	Ingenieria e Investigacion	72	0.278	0.000120
80	FORSCHUNG IM INGENIEURWESEN-ENGINEERING RESEARCH	176	0.250	0.000110
81	JOURNAL OF THE CHINESE INSTITUTE OF ENGINEERS	409	0.246	0.000540
81	MEASUREMENT TECHNIQUES	565	0.246	0.000540
83	Revista Internacional de Metodos Numericos para Calculo y Diseno en Ingenieria	61	0.207	0.000130
84	Journal of Engineering Research	14	0.177	0.000040
85	Journal of the Faculty of Engineering and Architecture of Gazi University	167	0.174	0.000190